High Frame Rate Ultrasonic Imaging of Flowing Blood Cells for Assessment of Cardiovascular Dynamics

PhD Dissertation

High Frame Rate Ultrasonic Imaging of Flowing Blood Cells for Assessment of Cardiovascular Dynamics

(心臓内血流動態可視化のための血球エコーの
高フレームレート超音波イメージング)

Hiroki Takahashi

(Doctoral Program in Biomedical Engineering)

Submitted to the Graduate School of Biomedical Engineering in Partial Fulfillment of the Requirements for the Degree of Philosophy in Biomedical Engineering

at the

Tohoku University

Table of Contents

List of Figures

Abstract

Echocardiography is a predominant modality for the diagnosis of the human heart. The aim of this thesis is to propose a method of high-frame-rate imaging of echoes from blood cells for visualization of complex flow in the cardiac cavity and to examine the feasibility of cardiac blood flow imaging by this proposed method. The proposed method has a potential to visualize real movements of blood within the cardiac lumen owing to high-frame-rate measurement. The consecutive blood echo images would allow the human eyes to perceive complex patterns of cardiac blood flow. Furthermore, an estimator of two dimensional velocity vector of blood flow is studied. The velocity vector field is useful to understand a behavior of blood flow in the cardiac cavity. In this thesis, a basic and *in vivo* experiments of a flow phantom and a healthy volunteer were performed to test the performance of the proposed method.

In the proposed method, high-frame-rate echocardiography using unfocused transmit beam and parallel receive beamforming was used to visualize a fast blood flow with a velocity of up to 1 m/s inside the cardiac cavity. However, the quality of an image composed of echoes from blood cells was low due to the unfocused ultrasound transmission. Therefore, the imaging of blood echoes was improved by means of two weighting techniques; an weighting technique with the coherence of RF echo signals in the direction of frame and the phase coherence weighting with sub-beamforming for echoes from blood cells. The performances of these methods were tested through an *in vivo* measurement.

Speckle tracking method makes it possible to estimate the velocity vector by searching

maximal correlation of echoes between successive frames. However, a stable estimation of the velocity vector of blood flow with this method is difficult because of low signal to noise ratios of echoes from blood cells. Echoes are acquired in a number of frames owing to high-frame-rate echocardiography; therefore, multiple two-dimensional correlation functions can be averaged during a short period to improve the accuracy of velocity vector estimation. The effect of the averaging of two-dimensional correlation functions was examined in a basic experiment with flowing blood-mimicking fluid. First, the number of frames required for improvement of accuracy in estimation of velocity vector was investigated. It was found that the averaging even in a short period of only 2 ms, which corresponds to 12 frames at a frame rate of 6024 Hz, improved the accuracy of estimation of velocity vector significantly. In addition, a limitation of this study, i.e., the angle-dependence of visibility between the major axis of blood flow and the ultrasonic beam, was also verified by comparing the results obtained in the flow experiments at different flow angles.

Finally, blood flows inside the left ventricular cavity of the healthy heart were visualized by the proposed method. The vortex blood flow in the cardiac cavity could be detected in diastole by blood echo images and velocity vector fields. It was shown from the *in vivo* results that visualization of complex blood flow in the cardiac cavity by the proposed method was feasible.

Acknowledgements

I would like to thank **Prof. Hiroshi Kanai** for giving me the the opportunity to carry out this doctoral project in his laboratory. I am deeply grateful for infusing his enthusiasm and visions to me, for letting me learning ethics, belief, techniques, and philosophy of scientist, for being supportive.

I express my gratitude to the Associate Professor **Dr. Hideyuki Hasegawa** for helping this project closely, for giving important ideas and directions of this project, for teaching me everything from signal processing, ultrasound imaging, and so on.

I would like to thank **Prof. Shin-ichiro Umemura** and **Prof. Yoshifumi Saijo** for giving valuable pieces of advice to refine this doctoral thesis. I appreciate Prof. Umemura teaching me his knowledge about blood flow measurement by ultrasound, e.g., clutter suppress filtering. I am also grateful to Prof. Saijo for giving a great deal about cardiac ultrasound.

I appreciate the Specially Appointed Professor **Mr. Yuji Kondo** for teaching me hardware issues, attitudes for system design, and the industrial mind, which would be inaccessible in academic laboratories.

I am grateful to the Associate Professor **Dr. Shin Yoshizawa** for letting me learning a great deal about physical phenomena induced by ultrasound.

I am grateful to the clerical assistants, **Ms Kayo Tominaga** and **Ms Keiko Matsukura** for their assistance and advice about paperwork, for always watching over me with kind eyes.

My gratitude to PhD students **Mr. Ryo Nagaoka**, **Mr. Ryo Takagi**, and **Mr. Jun Yasuda** for introducing experimental systems in Umemura Lab. and Saijo Lab., for discussing together about medical ultrasound, for motivating me by your good works.

My appreciation also goes to **the student members of Kanai Laboratory** who I shared good and bad times with. Especially, **Dr. Nabilah Ibrahim**, I really appreciate your kindness and sincere efforts. I have many people to thank, and I cannot appreciate them enough.

And last but not least by any means, I express my gratitude to my parents for helping my life during a tough time. I have a lot to be thankful for.

Chapter 1

Introduction

1.1 Background

A roll of the heart is to provide enough blood for organs. Cells composing organs can maintain their functions by trading oxygen and nutrient with transported blood. In the cell, the energy is produced by metabolizing glucose with oxygen. At the time, carbon dioxide is also generated, and it has to be released outside the human body through blood flow. Furthermore, blood flow also contributes to transport water, hormone, and glucose over the whole body. As described above, a sufficient blood supply is essential to maintain life; therefore, the heart has one of the most important function for the human body.

Nevertheless, the increase in the number of patients with cardiovascular diseases like heart failure and coronary heart disease is becoming a serious problem in world wide. For instance, cardiovascular diseases accounted for 41% of all deaths in the United States and the direct and indirect costs were estimated to $315.4 billion in total in 2012 [1]. By 2030, the total medical cost of cardiovascular diseases is projected to exceed $1 trillion (real 2008

US$) [2]. Therefore, early diagnosis of cardiovascular diseases significantly contributes to improve quality of life and keep down the medical cost.

The pumping function of the heart is degraded due to cardiovascular diseases. The heart is a pump made up of the myocardium and is driven by changes in pressure and volume of the cardiac cavity generated by changes in force and myocardial length. The cardiac (pumping) efficiency is calculated from external work and oxygen consumption of myocardium [3]. However, the pumping energy cannot be sustained due to cardiovascular diseases: for instance, high blood pressure, valve disease, myocardial infarction, and coronary heart disease. Such diseases lead an imbalance between external work and oxygen consumption and, ultimately, heart failure is developed due to the less pumping efficiency. Therefore, evaluation of the cardiac pumping function is useful for diagnosis of cardiovascular diseases.

The relationship between the pumping function and blood flow is presented as follows. Flowing blood in the cardiac lumen interacts with geometries of the surrounding heart wall and valve. Movements of blood are modified by movements of such boundaries and, thus, can produce a hemodynamic environment comprising pathological abnormality [4]. Because of the chamber geometry, the valves, and wall motion, blood flow inside the cardiac chamber is multi-directional and tend to curl or spin during various phases in the cardiac cycle [4]. It is subject to reveal the influence of such flow structures on the pumping efficiency. Most of the external work done by the heart is expended to eject blood into the aorta and into pulmonary artery from cardiac chambers [3]. Here, let me redefine the pumping efficiency as the amount of ejected blood (external work) divided by required energy (oxygen consumption) to simplify discussion. It has been found that vortex-like blood flow is generated in the cardiac cavity in diastole so that the momentum of blood is

directed to the aorta. Such complex structures of cardiac blood flow is considered to be closely linked with the pumping efficiency as follows: When the momentum of blood in the cardiac chamber direct to the aorta in advance, the blood subsequently can be ejected with the less myocardial energy during ejection phase. Therefore, analyzing blood flow behavior inside the cardiac chamber may provide diagnostic and prognostic information.

Typical blood flow behavior and discussions about the vortex blood flow are introduced in what follows. In recent years, understanding of behavior of blood flow in the cardiac chamber has been progressed because methods for imaging of cardiac flow have been improved increasingly; for instance, color Doppler flow imaging, echocardiographic particle image velocimetry (E-PIV), and phase-contrast magnetic resonance imaging (PC-MRI). Figure 1.1(a) illustrates a cross-sectional view of the human heart. The green-colored arrow roughly represents the typical path of blood flow. Figures 1.1(b) and 1.1(c) show distributions of blood flow velocities inside the left cardiac cavity obtained by Doppler flow imaging in ejection and diastolic phases, respectively. In Figs. 1.1(b) and 1.1(c), the red and blue colors mean directions toward and away from the array transducer, respectively, and their brightness correspond to magnitudes of velocities in terms of that direction. Figures 1.1(b) and 1.1(c) depict blood flowing into and out of the left ventricular cavity, which corresponds to the direction of blood flow in Fig. 1.1(a). In particular, the roll of vortex-like blood flow in the cardiac chamber has been focused strongly. The vortex blood flow has been visualized by E-PIV and PC-MRI mostly. In [4], the vortex pattern of blood flow has been visualized inside the left ventricle of healthy heart using E-PIV and PC-MRI. It is assumed that such vortices contribute to blood smoothly flowing out to the aorta by preserving the momentum of blood in diastolic phase [4]. Various contributions of the vortex have been discussed much more. For instance, some studies suggest that normal vortex flow minimizes the dissipation of the energy of blood flow [6]. It has been

further suggested by several studies that the flow of blood, which trails and circulates on specific flow routes (flow patterns) in the left ventricle, contributes to the efficiency of the pumping function [7–9]. The abnormality of diastolic vortex formation has been reported regarding patients with myocardial infarction [10]. The aforementioned studies mean that the vortex-like behavior of blood enables to eject blood in the chamber with a smaller energy given by myocardium (i.e., better pumping efficiency). Hence, visualization of vortex-like blood flow would be useful for evaluation of cardiac function.

Echocardiography and PC-MRI have been mainly used as a modality for visualization of blood flow patterns in the heart lumen. MRI can produce images with a high contrast with regard to soft biological tissues and a less artifact originated from bone. On the other hand, the spatial distribution of blood velocity vectors can be obtained by PC-MRI (a technique with MRI) [11, 12]. PC-MRI has been also utilized to explain embolism to all brain territories by analyzing retrograde flows from complex plaques of the descending aorta [13]. Recently, the use of PC-MRI has been expanded to visualize three-dimensional blood flow in the cardiac chamber [14, 15]. Several display tools for visualization of complex blood flow were proposed for PC-MRI [16,17]; e.g., velocity vector field, streamline imaging, and time-resolved particle tracing.

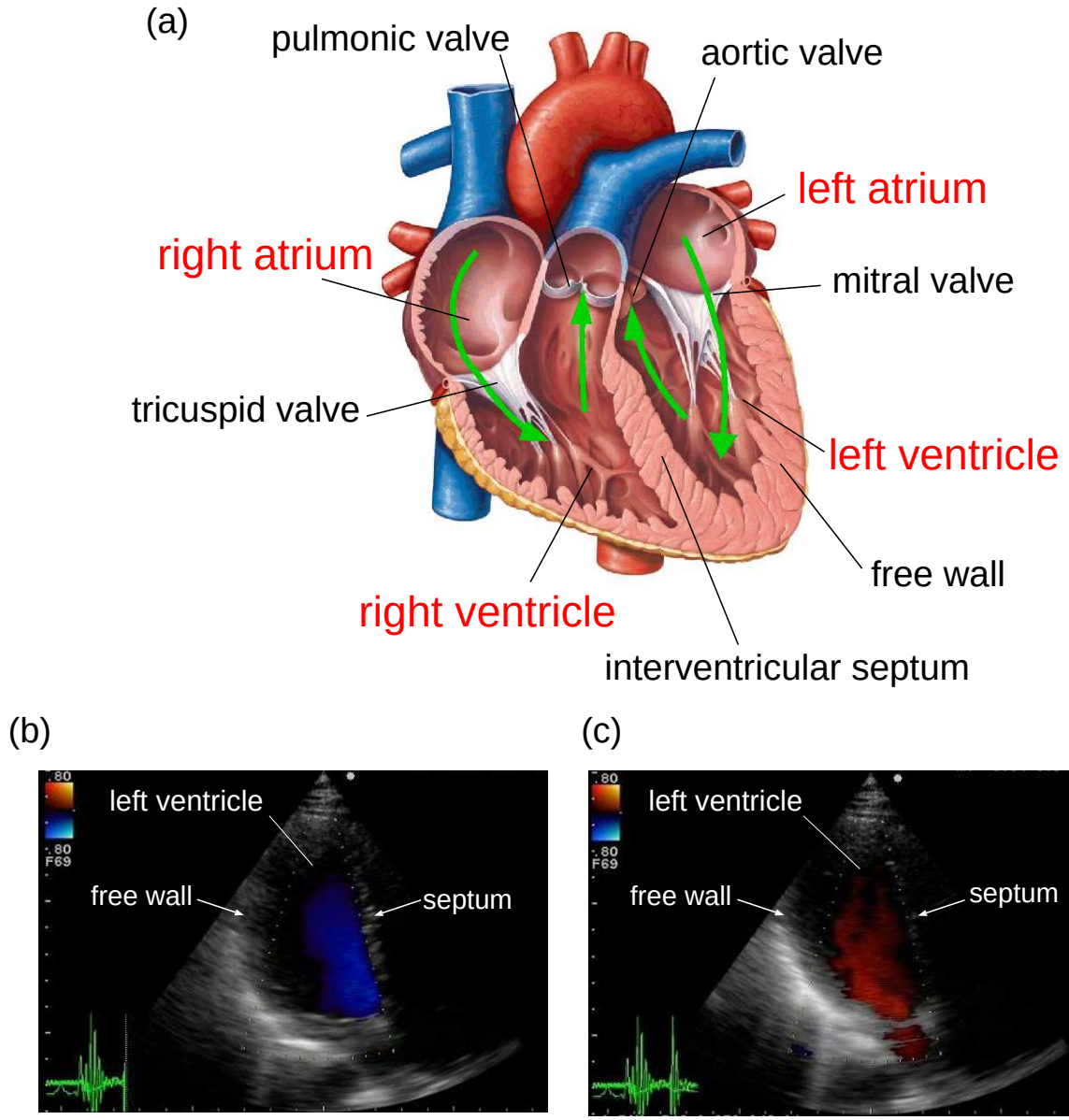

Figure 1.1: (a) Typical paths of cardiac blood flow illustrated on cross-sectional view of the human heart (partial modification of [5]). The green-colored arrows roughly represent the typical paths of blood flow. Spatial distributions of blood flow obtained by color Doppler flow imaging in (b) ejection and (c) diastolic phases. The red and blue colors mean directions toward and away from the array transducer located above the apex.

1.2 Conventional methods for measurement of cardiac blood flow

As described previously, studies with PC-MRI have progressed toward understanding of complex structures of blood flow. However, it takes long time to scan the heart because the temporal resolution is much worse than echocardiography; for instance, using current PC-MRI, cardiac blood flow can be measured with a spatial resolution of 3 mm^3 and a temporal resolution of 50 ms in approximately 20 min [4]. Additionally a PC-MRI scanner is expensive. Under such conditions, throughput of MRI for measurement of cardiac blood flow is relatively low.

On the other hand, echocardiography provides a cross-sectional image noninvasively in real-time; therefore, a method for visualization of cardiac blood flow with echocardiography is quite valuable. In this study, echocardiography was employed as a modality for imaging of cardiac blood flow with a high throughput. In ultrasonography, several methods for measuring blood flow have been developed, and some of them were enabled on commercial systems. Features and problematic points of such ultrasound methods are discussed to determine the direction of this study in the following part.

Ultrasound Doppler measurement

Ultrasound Doppler measurement is a method of measuring the axial component (i.e., the direction parallel to the ultrasonic beam) of the tissue velocity by analyzing echo signals from a specific spatial point in the temporal direction. Doppler measurement has been fallen into two main categories, i.e., spectral Doppler method and color Doppler

method, according to the methodology of measuring the axial velocity. Spectral Doppler method displays the spectrum of Doppler shifts of echoes. The Doppler shift is computed using echoes obtained by transmission of pulsed wave or continuous wave ultrasound. The Doppler spectrum obtained by transmission of continuous wave include axial velocities of all reflectors placed along the ultrasonic beam; therefore, continuous Doppler measurement give no spatial information. As for pulsed wave Doppler method, axial velocities inside a manually assigned region are obtained. However, these spectral Doppler methods cannot provide the spatial distribution of blood flow because only the echoes from a specific spatial region were analyzed. Color Doppler method is a major diagnostic modality to visualize cardiac blood flow. In color Doppler method, the spatial distribution of the axial velocity of blood flow can be obtained by utilizing the auto-correlation technique [18].

Methodologies for improving Doppler measurement have been studied in a long while. For a stable estimation of Doppler shifts by the auto-correlation technique, a theoretical signal model was assumed and an estimator using the model was proposed [19]. Biases in estimation of the velocity and the velocity spread were reduced by improving characteristics of conventional clutter (rejection) filters which effects on estimation of the axial velocity by the auto-correlation technique [20]. Variances in the measurement of Doppler spectrum have been suppressed by using multiple Doppler spectra simultaneously obtained in the surrounding region [21].

These Doppler methods have contributed for visualization of abnormal blood flow: e.g., an analysis of the jet flow caused by aortic valve stenosis and a detection of the back flow caused by valvular regurgitation. However, as a general problem of Doppler measurement, the major direction of blood flow cannot be shown because the Doppler measurement reveals only the axial velocity [22–24]. Although several methods of angle compensation

in conventional Doppler measurement is currently developed, these are inadequate for visualization of complex flow [25].

Vector Doppler method

Many researchers have studied to estimate the transverse component (perpendicular to the ultrasonic beam) of blood flow velocity. A technique with two crossed transmit/receive beams utilizing Doppler spectral broadening effect has been proposed to estimate the transverse velocity component in a specific spatial point [28, 29]. On the other hand, a methodology for measurement of the velocity vector of blood flow by combining Doppler measurement from two directions was proposed (called vector Doppler method) [26, 27]. Recently, an imaging method of the blood velocity vector estimated by the vector Doppler technique with transmissions of crossed plane waves has been developed [30,31]. It has been shown that a better estimation of velocity vectors was achieved by combining the vector Doppler approach with speckle tracking (described in detail in the following section) using plane wave transmissions [32]. As another approach, a velocity vector estimator using transmissions of diverging waves with different apertures and a least squares fitting with the velocities in the different directions was proposed [33] and, moreover, time-resolved flow paths of blood flow in the carotid vessel has been visualized by utilizing blood velocity vectors obtained by the least squares fitting with multi transmissions of steered plane waves [34]. These vector Doppler-like techniques, however, require a relatively large beam steering angle. As a result, a linear-array transducer with a large aperture is used in ongoing studies, and its application is limited to blood flow in a shallow region like carotid blood flow. Hence, the vector Doppler technique is not suitable for the normal cardiac measurement with a phased-array transducer.

Vector flow mapping

A different approach for estimation of the transverse component of the blood flow velocity has been developed, which is called vector flow mapping [35]. With vector flow mapping, the transverse flow velocity is mathematically calculated from the two-dimensional (2D) distribution of the axial velocity measured by color Doppler method on the basis of hydro-kinetic assumptions. An another method of estimation of the transverse velocity from the 2D distribution of the axial velocity has been proposed, which utilizes velocities of surrounding heart walls estimated by speckle tracking to obtain more accurate boundary conditions for continuity equation [36]. Recently, a technique to detect and quantify intraventricular vortices using the 2D field of the axial velocity has been developed [37], which mainly targets special patterns of axial velocities in a specific region. It has been shown that vortex-like blood flow inside the cardiac lumen can be depicted by vector flow mapping in [36]. However, real flows of blood cannot be visualized by such assumptive methods.

Echo movement tracing

An another technique for estimation of the direction of blood flow was developed, which traces the inter-frame movement of echoes by searching the maximal correlation of the echoes between successive frames (called speckle tracking) [38, 39]. This correlation-based motion estimator has been also used for evaluation of mechanical properties of various tissues like myocardium [40, 41] and artery wall [42–44] by many researchers. For estimation by speckle tracking, continuous motions of echoes from a target need to be measured. Methods for imaging of dynamic motions of echoes from blood cells are discussed below.

Løvstakken *et al.* proposed a method for imaging of the blood flow direction by visualizing motions of echoes from blood cells with customized sweeping of focused transmit beam [45]. This method, however, has the critical issue of an insufficient frame rate because multiple transmissions in a direction is required for visualization of echoes from blood particles. As a result, estimation of the 2D blood velocity vector by speckle tracking was not attempted due to insufficient continuity of movements of echoes between consecutive frames as described in [45]. A method for visualization of blood flow, called B-flow, has been proposed and reached clinical use [46]. In this method, coded excitation was used to obtain a high sensitivity with keeping the spatial resolution. However, the acquisition frame rate is not enough compared to motions of blood cells likewise.

It has been found that a high frame rate is desired to capture dynamic motions of echoes from blood cells as described previously. The frame rate of ultrasound imaging is defined as the pulse repetition frequency divided by the number of transmissions per frame; therefore, decreasing the number of transmissions per frame is effective for the high-frame-rate measurement. However, many transmissions are required with sweeping a focused beam to cover a wide region (i.e., to realize a large field of view). To obtain echo signals from a broad region with fewer transmissions, parallel receive beamforming was proposed [47]. Parallel receive beamforming with plane wave transmissions has been intensively used in transient elastography with a linear array transducer [48]. Recently, its applications has been broadened to the monitoring of the treated area for ultrasonic therapy [49].

Parallel receive beamforming is useful in terms of even blood flow imaging. In recent years, speckle tracking with high-frame-rate measurement by transmissions of plane waves and parallel receive beamforming has shown to be feasible for an imaging of the 2D velocity

vector of carotid blood flow [50, 51]. At nearly the same time, the artery-wall strain and the axial velocity of carotid blood flow were simultaneously visualized at a frame rate of 3500 Hz by plane wave transmissions and parallel beamforming [52]. Movements of echoes from flowing blood cells in the carotid lumen was also visualized using high-frame-rate measurement [53]. More recently, an imaging of the 2D blood velocity vector estimated in the frequency domain with plane wave imaging was demonstrated [54]. An estimation of the axial blood velocity using echoes in a number of frames obtained by plane wave imaging has been introduced [55]. Many studies using parallel receive beamforming coupled with transmissions of plane waves has been performed for blood flow imaging. However, the width of the region illuminated by a plane wave is limited by the size of the aperture of the transducer. In echocardiography, a phased-array transducer with a small aperture is used because the heart needs to be insonified from a narrow acoustic window between ribs. This means that the use of transmissions of plane waves requires many transmissions per frame to cover the heart and it limits the frame rate in echocardiography. Plane wave imaging, therefore, would not be suitable for visualization of cardiac blood flow requiring a high frame rate.

On the other hand, echoes from blood are enhanced by contrast agents blended in the blood pool in E-PIV [56–58]. Although the intravenous injection of contrast agent is required, motions of enhanced echoes from blood can be visualized in the cardiac lumen with a high contrast. However, it has been reported that the frame rate of current E-PIV is not sufficient to visualize blood flow in the cardiac lumen because blood particles move so fast up to 1 m/s and its movement is complex [59].

1.3 Objective of the research project

Section 1.2 is summarized as follows: Color Doppler flow imaging cannot show the major direction of blood flow. Vector Doppler measurement has been implemented using a linear-array transducer with a large aperture in ongoing studies, but, this technique is not suitable for the normal cardiac measurement with a phased-array transducer. Vector flow mapping cannot visualize the real flow of blood. Echo movement tracing requires high-frame-rate measurement of echoes from the heart with a phased array transducer.

In this study, a method referable to echo movement tracing was employed to visualize real blood flow in the cardiac lumen. Flowing blood inside the cardiac cavity exhibits complex flow patterns like vortex pattern. Furthermore, blood cells (scatterers) can flow at a velocity of over 1 m/s in the human heart. High-frame-rate measurement with parallel receive beamforming, therefore, would be of value for visualization of such blood flow patterns. To do that, an ultrasound wave for insonifying the cardiac cavity from a narrow acoustic window between ribs is required to be coupled with parallel receive beamforming. Hasegawa and Kanai have developed high-frame-rate echocardiography with transmissions of spherically diverging waves and parallel receive beamforming [60–62]. In this thesis, a method of imaging of echoes from blood cells with high-frame-rate echocardiography is proposed for visualization of complex blood flow in the cardiac cavity [63,64]. Furthermore, in the herein presented method, 2D blood velocity vectors of the cardiac blood flow are estimated by speckle tracking. Note that the result of our work can also be applied to studies of E-PIV with high-frame-rate echocardiography.

In recent medical ultrasound, an array-type probe equipped with multiple transducers has been used normally. In the conventional beamforming with the array probe, both

transmit and receive beams are electronically focused by activating transducer elements with delay times determined according to the focal position. As compared to the conventional beamforming, the spatial resolution and the sidelobe characteristics of high-frame-rate echocardiography are significantly degraded due to transmissions of unfocused beams. As described in [60], [65], and [66], two different methods have been proposed to improve the quality of the B-mode image of high-frame-rate measurement as follows: One is the spatial compounding, and another is the phase coherence weighting. It was shown that improvement of the image-quality of B-mode is feasible by these methods. On the other hand, blood echo images are constructed using echoes from blood cells measured with high-frame-rate echocardiography in this study; therefore, the image-contrast and the spatial resolution for blood echo imaging are also desirable to be improved. Although the quality of B-mode image become better owing to these techniques, their effects on echoes from blood cells have not been examined.

Speckle tracking makes it possible to estimate the blood velocity vector without depending on the angle between an ultrasonic beam and flowing blood. In this study, to capture fast movements of blood cells in the cardiac chamber, echoes from blood cells are measured at a high-frame-rate of several kilohertz (conventionally, several tens Hertz). Nevertheless, an accurate estimation of the blood velocity vector would be still hard because signal-to-noise ratios (SNRs) of echoes from tiny blood particles are low.

For aforementioned reasons, objectives of this research project are described as follows; consideration of a procedure for blood echo imaging with a better image-quality, improvement of the accuracy of estimation of the 2D blood velocity vector, and validation of the feasibility of cardiac blood flow imaging by the proposed method through an *in vivo* experiment.

1.4 Thesis structure

In Chapter 1, background, conventional methods, and objective of our study are presented. The subsequent part of this thesis is organized in what follows. At first, a method for high-frame-rate measurement of ultrasonic echoes from the human heart is presented. Subsequently, it is presented how echoes from blood cells are visualized. After that, an accurate estimator of the blood velocity vector is presented and its effect is examined through a basic experiment with a flowing blood-mimicking fluid. Finally, the feasibility of visualization of complex cardiac blood flow by the proposed methods is evaluated in an *in vivo* experiment. The chapters' substances are described below.

Chapter 2 shows a strategy for high-frame-rate imaging of movements of echoes from blood cells. Methods for blood echo imaging with high contrast and spatial resolution are described. In the proposed procedure, echoes from tissues except for blood are suppressed by the moving target indicator (MTI) filtering, namely, clutter suppression filtering. The MTI filtering with adaptive selection of the cutoff frequency is also presented.

In Chapter 3, a technique for improvement of the accuracy in estimation of the blood velocity vector with speckle tracking is described. In this method, 2D correlation functions are temporally averaged for a fine estimation of the blood velocity vector. The effect of the averaging of 2D correlation functions is examined through a steady flow measurement using a phantom.

In Chapter 4, visualization of blood flow in the cardiac chamber is tested by the proposed method through an *in vivo* experiment of a healthy volunteer.

Chapter 5 reports overall conclusions of this thesis.

Chapter 2

Methodology for blood echo imaging

2.1 Overview

Red blood cell is a scatter in blood and its diameter is as small as almost 8 μm. To obtain a sufficient range resolution for distinguishing individual blood cell, an ultrasonic frequency higher than 96 MHz is required at a sound velocity of 1530 m/s. On the other hand, the full width half maximum FWHM in the azimuth amplitude profile of an ultrasonic beam from a disk aperture is given by [67]

$$FWHM = 2\sin^{-1}\left(\frac{0.51\lambda}{L}\right), \tag{2.1}$$

where L, λ, and z denote the aperture diameter, the wavelength, and the axial distance. The aperture size required for distinguishing blood cells at a depth of 5 cm and a frequency of 96 MHz is estimated to almost 10 cm. If such a high transmit frequency is used, the degradation of sensitivity cannot be negligible because the attenuation factor

is proportional to the frequency and the propagation distance. Such requirements of the transmit frequency and the aperture size are unrealistic for echocardiography.

Figure 2.1 illustrates an echo from a blood pool filled with blood cells (scatterers). In Fig. 2.1, the transmit wavelength is assumed to be almost 400 μm at a sound velocity of 1530 m/s and a transmit frequency of 3.75 MHz. An ultrasound image of blood has a speckle-like texture because the constructive and destructive interferences occur among echoes from many scatterers, which are much smaller than the wavelength of transmitted ultrasound, in the focal point. Because the speckle echo generated by interferences among echoes contains information on tissue structures, many researchers have studied methods utilizing the speckled echo for an estimation of blood flow vector [38, 39], a quantitative evaluation of liver fibrosis [68, 69], and the shear wave velocity measurement for imaging of tissue elasticity [70, 71].

The variation of speckle patterns arising from blood echoes between successive frames is considered as follows: When blood cells move without changing their relative positions, the speckle texture generated from the echoes is translated without transformation. This means that the direction of blood flow can be identified using motions of speckle echoes from blood cells although a location of each blood cell is not visualized. The dynamic textures produced by strong scattering from aggregated blood cells inside the left atrium has been used for calculation of its velocity vector in transesophageal echocardiography [72]. However, the speckle texture frequently transmutes during a short time because blood cells flow at a velocity of up to 1 m/s in the left ventricular cavity. Hence, a higher frame rate would be desirable to visualize motions of echoes from blood cells in the cardiac lumen. Our group has developed high-frame-rate echocardiography with transmission of spherically diverging wave and parallel receive beamforming [60–62]. However, the spatial

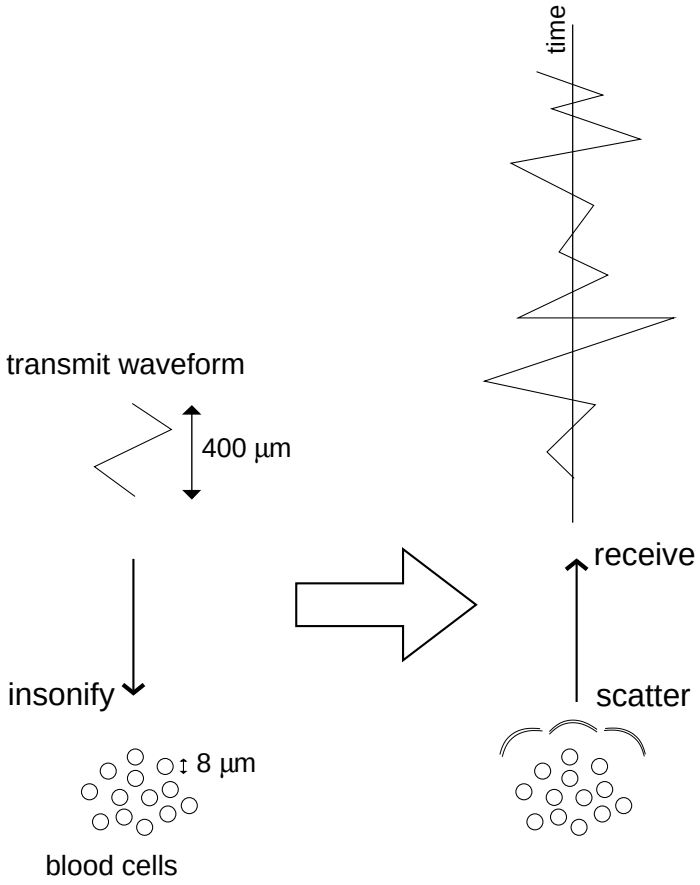

Figure 2.1: Illustration of echoes from blood including many blood cells (scatterers).

resolution and the sidelobe characteristics are seriously degraded due to transmission of unfocused beam.

In this chapter, a strategy for high frame rate imaging of echoes from blood cells with a better image quality is presented. Let me start to describe the procedure for high-frame-rate measurement of echoes from the heart. A frame rate required for imaging of a fast blood flow in the cardiac cavity is investigated. Then, methods for improvement of the image quality are proposed and tested through a measurement of a human heart. Furthermore, an adaptive MTI filtering is presented.

2.2 High-frame-rate echocardiography

The frame rate of ultrasonic imaging is defined as a pulse repetition frequency divided by the number of transmission per frame. Figures 2.2(a) and 2.2(b) show illustrations of transmit/receive beams in the conventional imaging and high-frame-rate echocardiography. As shown in Fig. 2.2(a), a focused ultrasound is transmitted and receive beams are created at each spatial point inside the insonified region. To visualize the whole cardiac lumen, the transmit beam is swept (steered) by changing the time delay applied to transducer elements. The large number of transmissions with sweeping the focused transmit beam is required to cover the cardiac lumen; therefore, the frame rate becomes low necessarily. In high-frame-rate echocardiography, transmission of diverging beam and parallel receive beamforming are implemented [60, 61]. The spherical diverging wave do not limit the illuminated region by the size of the aperture and enables the acquisition of echoes with higher SNRs than the synthetic aperture ultrasound [73, 74], which uses one or small number of elements in transmission. As shown in Fig. 2.2(b), the receive focusing can be performed at spatial points in a wide region by single transmission of a diverging beam. Hence, the frame rate in measurement of echo signals is drastically increased by decreasing the number of transmission per frame. In the present study, the transmit wave was diverged from a virtual point source placed at a distance r_f of 30 mm behind the array surface and its diverging angle Θ was 35.5 degree.

The side lobe level increases due to the unfocused transmission in comparison with conventional beamforming with focusing both in transmit and receive. A weighting technique using the phase coherence factor with sub-aperture beamforming (PCF-SB) has been developed to reduce the side lobe characteristics [65]. PCF evaluates the diversity among phases of echoes received by transducer elements after the application of delay compensa-

tion, in which the time delay becomes large with the distance from a focal point. Echoes originated from side lobes can be suppressed by weighting the PCF-SB to the amplitude of echoes. In this study, the PCF-SB was computed using individual echo signals received by transducer elements before receive beamforming, and the B-mode image was created using beamformed RF signals weighted by the PCF-SBs.

In the present study, a modified diagnostic ultrasound system (Hitachi-Aloka Medical α-10) with a commercial 3.75 MHz phased array transducer was used to acquire ultrasonic RF echo signals from 96 transducer elements. RF signals received by individual elements were sampled at 15 MHz for off-line processing by a personal computer.

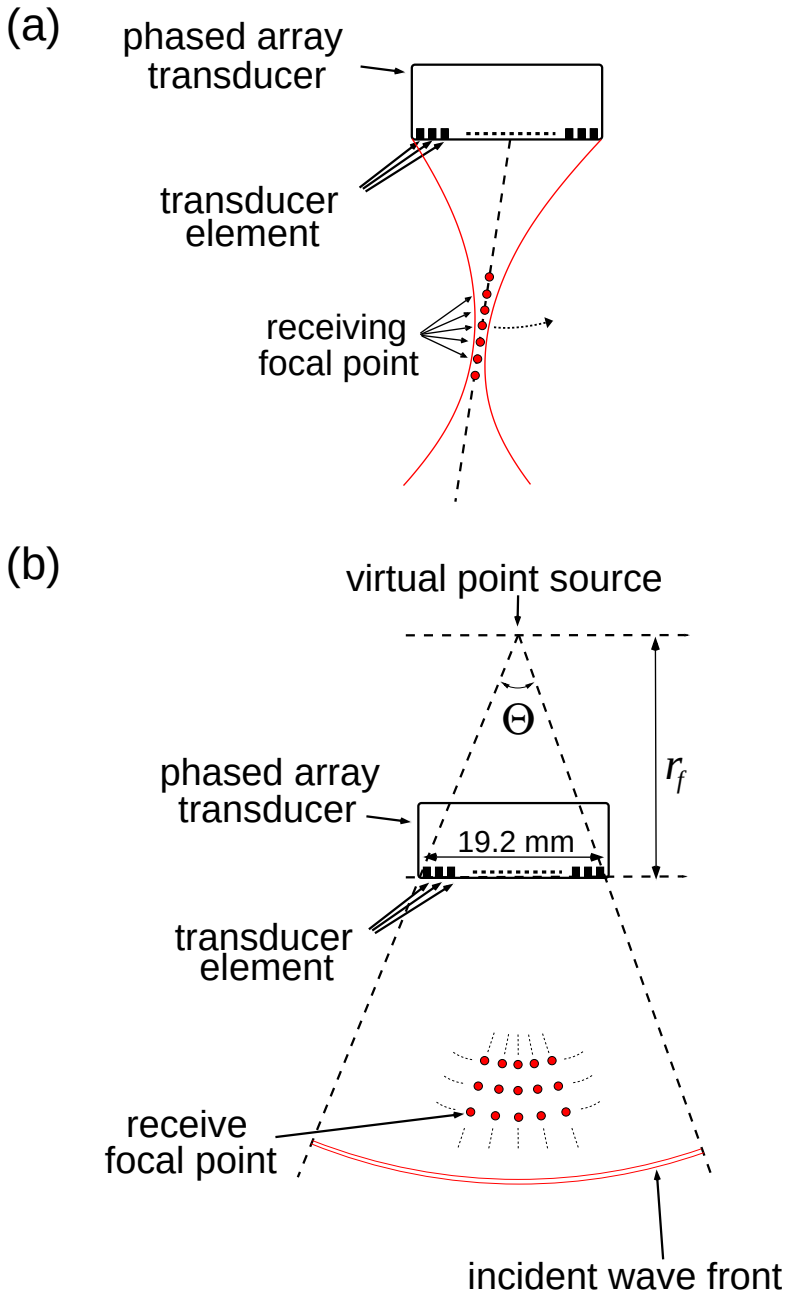

Figure 2.2: Illustration of transmission of spherically diverging beam and parallel receive beams.

2.2.1 Frame rate for blood echo imaging

The frame rate required for visualization of the cardiac blood flow was examined through a steady flow experiment. Echoes from a blood mimicking fluid steadily flowing in a cylindrical flow path (diameter of 8 mm) surrounded by tissue-mimicking rubber were measured. The angle between the transducer surface and the flow axis was set at 56 degrees. The transducer surface was placed at a distance of 7 cm from the outer surface of the flow path. The flow rate, which corresponds to the mean flow velocity, was measured by a mass flow meter connecting to the flow path. The echo data was acquired at the frame-rate of 6024 Hz with the single transmission of a non-steered diverging beam per frame at a flow rate of 0.6 L/min (mean flow velocity: 0.2 m/s, Reynolds number: 960).

In this measurement, the accuracy of velocity estimation was evaluated in different frame rates at a constant Reynolds number of 960. RF echo signals of different frame rates (1506, 2008, 3012, and 6024 Hz) at a mean flow velocity of 0.6 m/s were simulated by changing the frame interval, i.e., twice, triple, and quadruple of the original frame interval. The velocity vector was estimated by speckle tracking with a temporal averaging of 2D correlation functions for 12 frames (see Section 3.2 for details). Figure 1 shows mean flow velocities computed using velocity vectors as follows:

$$\bar{V} = \frac{1}{A} \sum_{j=0}^{N_j-1} (\pi r_j \Delta r)\, \mathbf{v}_j \cdot \mathbf{n}, \tag{2.2}$$

where $\mathbf{v}_j$, r_j, Δr, A, and $\mathbf{n}$ are the velocity vector estimated at the j-th spatial point, the distance from the center of flow path to the j-th spatial point, the interval between the j-th and the $(j+1)$-th spatial point, the cross-sectional area of the flow path, and the unit vector parallel to the flow direction, respectively. The interval between the j-th and the $(j+1)$-th spatial points was set at 0.4 mm.

As can be seen in Fig. 2.3, the accuracy in estimation of 2D velocity vector is improved with the frame rate. It was found that a high frame rate of 6 kHz was required to measure the fast blood flow. It is highly likely that such fast blood flow occurs in the cardiac lumen. The number of transmission is allowable to be once per frame to achieve such a high frame rate. However, the transmit ultrasound need to be widely diffused to cover the heart by the single transmission; therefore, the spatial resolution and the sidelobe characteristics are much low in the obtained blood echo image. In [60] and [66], a compounding technique of RF signals, which are obtained by transmissions toward different directions, has been proposed to improve the spatial resolution and the side lobe characteristics. Although the frame rate is decreased due to the larger number of transmissions, the high image-quality can be obtained by this compounding technique. However, this procedure is considered to be unsuited for the blood echo imaging because it compensates echoes from flowing blood cells (see Appendix A). This means that the blood echo imaging with a better image quality cannot be achieved even if measurement of a fast blood flow is compromised for the compounding effect.

In the present study, ultrahigh-frame-rate measurement was performed with the single transmission of the diverging beam per frame. The improvement of the spatial resolution and the sidelobe characteristics is an important subject for this study. The techniques required for improving the image quality are presented and tested in the subsequent sections.

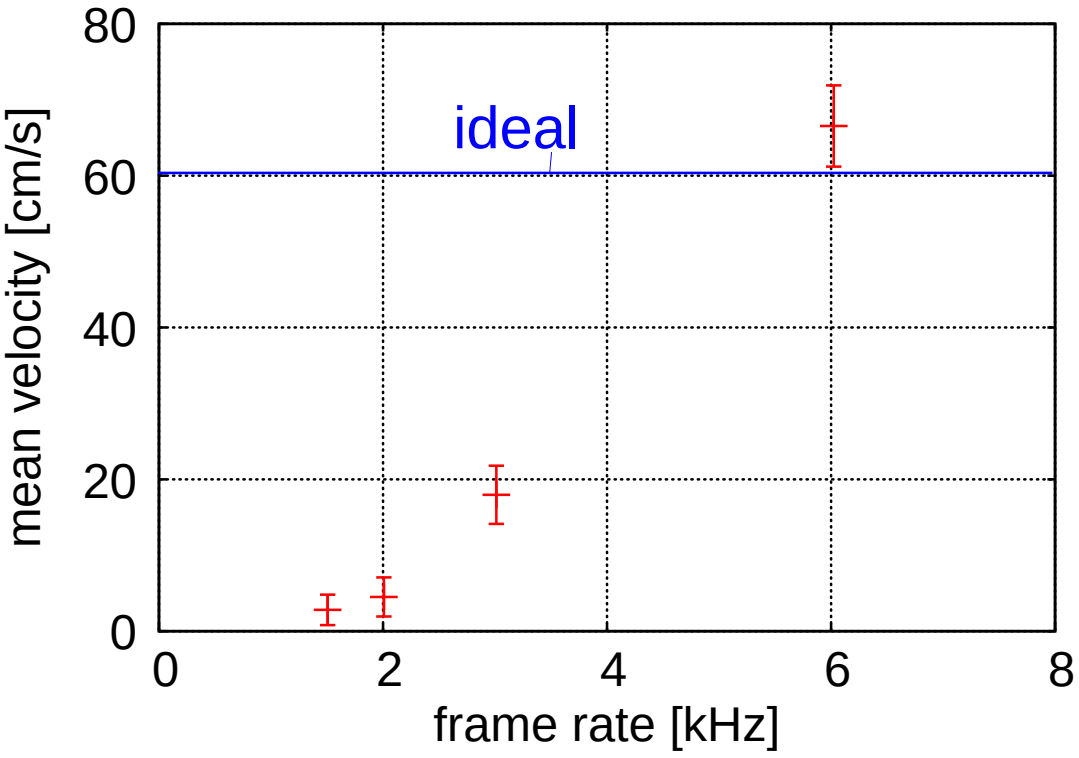

Figure 2.3: Mean flow velocities estimated at different frame rates in steady flow measurements. The standard deviations were computed from 50 frames.

2.3 Algorithm for imaging of echoes from blood cells

The amplitude of a scattered echo depends on the size of the scatterer, the reflection coefficient of the surface of the scatterer, and the frequency of the insonified ultrasound [75]. Because of the small size of blood cells and the small reflection coefficient between blood cells and blood plasma, the amplitudes of echoes from a blood pool are much smaller than those from the heart wall and ribs. Therefore, echoes from blood cells placed in the direction of the main lobe are contaminated even by sidelobe echoes from clutter sources

such like ribs and the heart wall. To suppress such undesirable echoes, the difference in velocities between the heart wall and blood flow has been utilized. The maximal velocity of the heart wall is almost 0.1 m/s, while that of the cardiac blood flow reaches over 1 m/s. The velocity can be defined as the ultrasound wavelength multiplied by the frequency of RF echo signals from a specific position in the direction of frame; therefore, the frequency of echo signals in the direction of frame increases with the velocity of an echo source. Hence, echoes from the heart wall and ribs can be suppressed by the high-pass filtering in the direction of frame (namely, the MTI filtering).

The proposed sequence of successive procedures is shown in Fig. 2.4. In the proposed method, blood echo images were created using envelopes of MTI-filtered echo signals. The MTI filtering was applied to individual echo signals received by transducer elements. Two weighting techniques were used to improve the image-quality of blood echo image as follows; PCF-SBs with MTI filtering described in Section 2.4 and the coherence in the direction of frame, i.e., the variance of temporal changes of phases in RF signals described in Section 2.5. The cutoff frequency of MTI filtering was adaptively changed using echo signals before the application of MTI filter as described in Section 2.6. Blood velocity vectors were estimated by applying speckle tracking to envelope signals given by the weighting techniques as shown in Section 3.2. Finally, the blood echo image (or the distribution of velocity vectors) was visualized with the B-mode image to simultaneously provide information of both flowing blood cells and the heart walls. In this study, the intensities of envelope signals in the B-mode image and in the blood echo image were coded according to gray scale and hot scale, respectively.

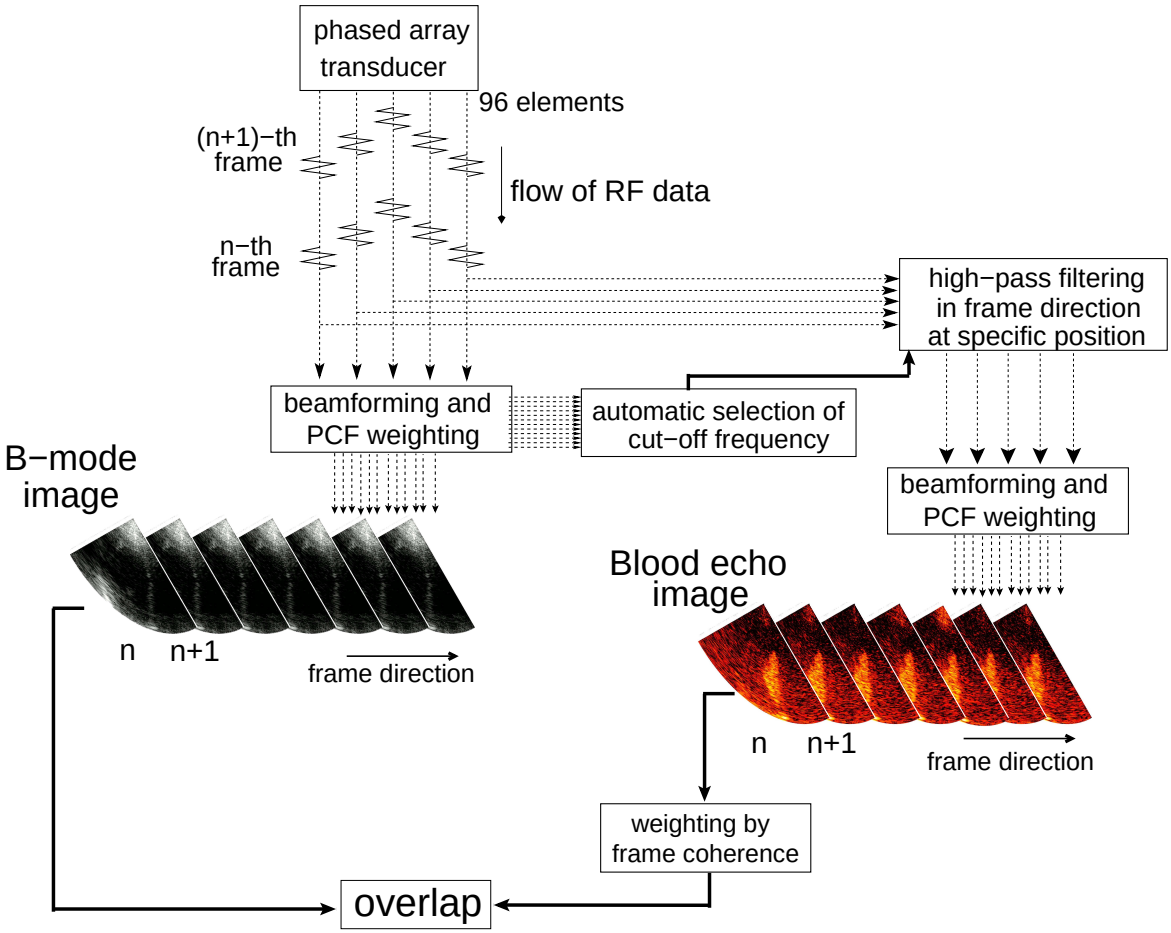

Figure 2.4: Schematic of proposed procedure for imaging of echoes from blood particles.

2.4 Improvement of fineness of blood echo image with array coherence

The PCF-SB improves the side-lobe characteristics and the spatial resolution by utilizing the diversity of echo signals received by transducer elements. One of the technical merits is to improve such imaging factors without decreasing the frame rate unlike the compounding

technique. Through phantom and *in vivo* experiments, the strategy of the PCF-SB has shown to be effective for improving the quality of B-mode image [65]. In this section, an algorithm for computing PCF-SBs for echoes from blood cells is presented, and it is examined that the improvement of blood echo imaging using the proposed algorithm is feasible.

In the beginning, to obtain PCF-SBs for blood flow images, the MTI filtering was applied to individual echo signals received by transducer elements. Then, the PCF-SB for the blood echo image was computed from MTI-filtered element signals. As in the phase coherence B-mode imaging, beamformed signals after the MTI filtering were weighted using the PCF-SB for blood echo imaging. Figure 2.5 shows blood echo images (hot-scaled) without and with weighting by the PCF-SBs with B-mode images (gray-scaled) of a healthy heart, respectively. As shown in Fig. 2.5, speckle echoes from blood cells became sharper by improving the sidelobe characteristics and the spatial resolution of MTI-filtered echoes. It was shown that the PCF-SB was effective even for the blood echo imaging.

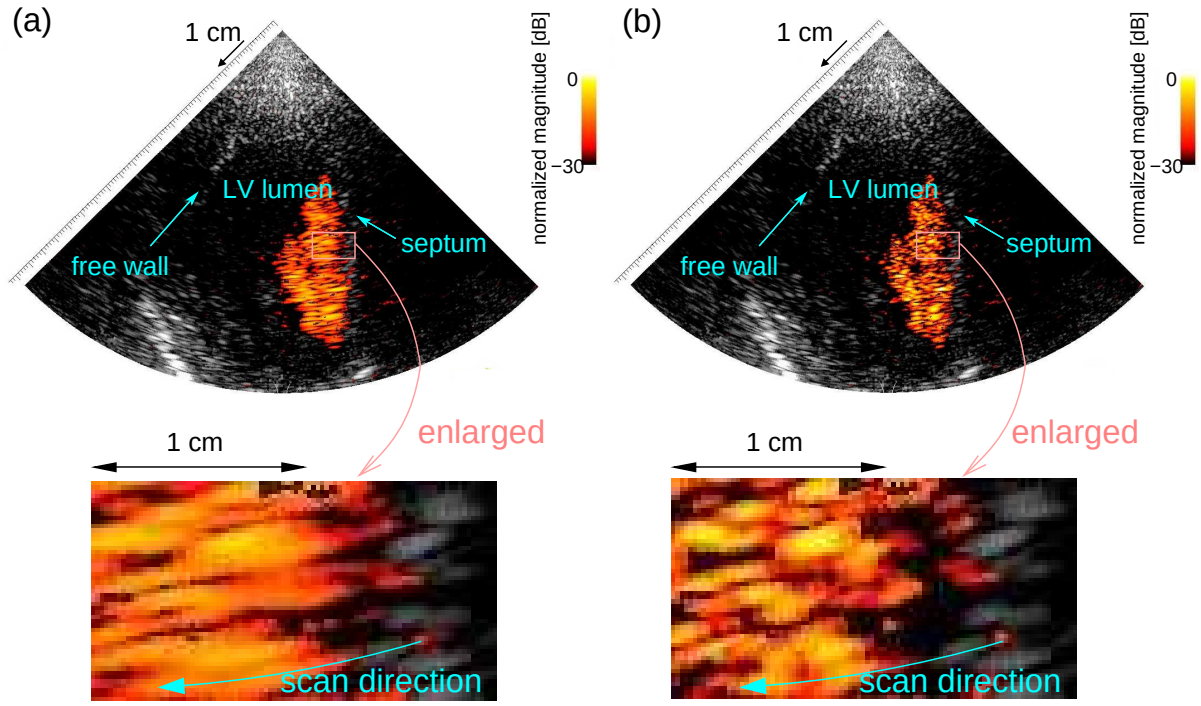

Figure 2.5: Enlarged blood echo images in *in vivo* experiment of a healthy volunteer (a) without and (b) with weighting by PCF-SB.

2.5 Improvement of image-contrast with frame coherence

A noise component generated by electronic devices cannot be rejected by the MTI filtering because the powers of noise signals are dispersed over all frequencies. Hence, the undesirable noise component still remains in MTI-filtered echoes as a high frequency component in the direction of frame. The suppression of the remaining noise is efficient for imaging of echoes from blood cells with a better contrast because such noise component

contaminates visualization of weak echoes from blood cells.

The temporal changes in phases of the signal components (corresponding to the echo from an object) would be spatially constant during a pulse duration. In addition, the temporal change in phase of the signal component of an echo from a specific depth was assumed to be also constant during a short period (small number of frames). On the other hand, the temporal changes in phase of the noise component would be random in terms of time and space. Therefore, in the present study, the random noise remaining after the MTI filtering was suppressed by weighting using the ratio of the coherent (signal) component to the total signal. The coherent component was obtained by minimizing the noise component using the least square method applied to quadrature demodulated signals. Let us define the complex demodulated signal at the frame number i and the sampled point number n, which corresponds to time $t = nT$ (T: sampling interval) as $x_i(n)$. The normalized mean square error (corresponding to the ratio of the noise component to the total signal) α among complex RF signals $\{x_i(n)\}$ for a few sampled points N_d and frames N_f was expressed as follows:

$$\alpha = \frac{\mathrm{E}_k\left[\mathrm{E}_m\left[\left|x_{i+m}\left(n+k\right) - z \cdot x_{i+m-1}\left(n+k\right)\right|^2\right]\right]}{\mathrm{E}_k\left[\mathrm{E}_m\left[\left|x_{i+m}\left(n+k\right)\right|^2\right]\right]}, \tag{2.3}$$

where z, $\mathrm{E}_k\left[\cdot\right]$, and $\mathrm{E}_m\left[\cdot\right]$ denote the transfer function from $\{x_{i-1}(n)\}$ to $\{x_i(n)\}$ and the averaging procedures with respect to depth and frame, respectively. The averaging numbers of $\mathrm{E}_k\left[\cdot\right]$ and $\mathrm{E}_m\left[\cdot\right]$ are defined by N_f and N_d, respectively. The estimated $\hat{z}$, which minimizes α, can be estimated by the least square method using Eq. (2.3). By substituting $\hat{z}$ into Eq. (2.3), the minimum mean square error $\alpha_{\min}$ is obtained by

$$\alpha_{\min} = 1 - \frac{\left|\mathrm{E}_k\left[\mathrm{E}_m\left[x^*_{i+m-1}\left(n+k\right)x_{i+m}\left(n+k\right)\right]\right]\right|^2}{\mathrm{E}_k\left[\mathrm{E}_m\left[\left|x_{i+m-1}\left(n+k\right)\right|^2\right]\right]\mathrm{E}_k\left[\mathrm{E}_m\left[\left|x_{i+m}\left(n+k\right)\right|^2\right]\right]}. \tag{2.4}$$

The achieved minimum error $\alpha_{\min}$ corresponds to the normalized residual noise component in the signal $\{x_i(n)\}$, which cannot be predicted by $\{x_{i-1}(n)\}$. Hence, the instantaneous intensity of the coherent component at the n-th depth point in the i-th frame is obtained as (1 - $\alpha_{\min}$), and the estimate $\hat{S}_i\,(n)$ of the amplitude of echo from blood cells was obtained by weighting the instantaneous signal amplitude $|x_i(n)|$ with the coherency $\sqrt{1-\alpha_{\min}}$ as follows:

$$\hat{S}_i\,(n) = |x_i(n)|\,\sqrt{(1-\alpha_{\min})}. \tag{2.5}$$

In the present study, the lengths for averaging in the frame and depth directions, N_f and N_d, were set to 6 and 8 (corresponding to about 2 ms and 0.5 μs), respectively. The number of frames used for computation of the frame coherence was determined so that echoes from almost same scatterers were used during the period. Here, let me estimate the elapsed time in which blood cells pass through the ultrasonic beam transversely. The width at half-maximum of the lateral profile of an echo from a fine wire (i.e., spatial resolution) is almost 1.9 mm. On the assumption that the maximum transverse velocity (perpendicular to the ultrasonic beam) of blood flow was 1 m/s, a blood cell was estimated to slip from the ultrasonic beam during 11 frames at a frame rate of 6024 Hz. In the present study, the number of frames for the coherence estimation was set at neighboring 6 frames to fill this necessary condition (less than 11 frames) for the use of echoes from same scatterers.

Figures 2.6(a) and 2.6(b) show the blood echo images without and with the proposed weighting by coherence in the direction of frame. As shown in Figs. 2.6(a) and 2.6(b), the noisy regions surrounding the cardiac lumen were reduced using the weighting by the frame coherence. Therefore, it was shown that the suppression of the random noise contained in MTI-filtered echo signals was feasible by the proposed weighting technique.

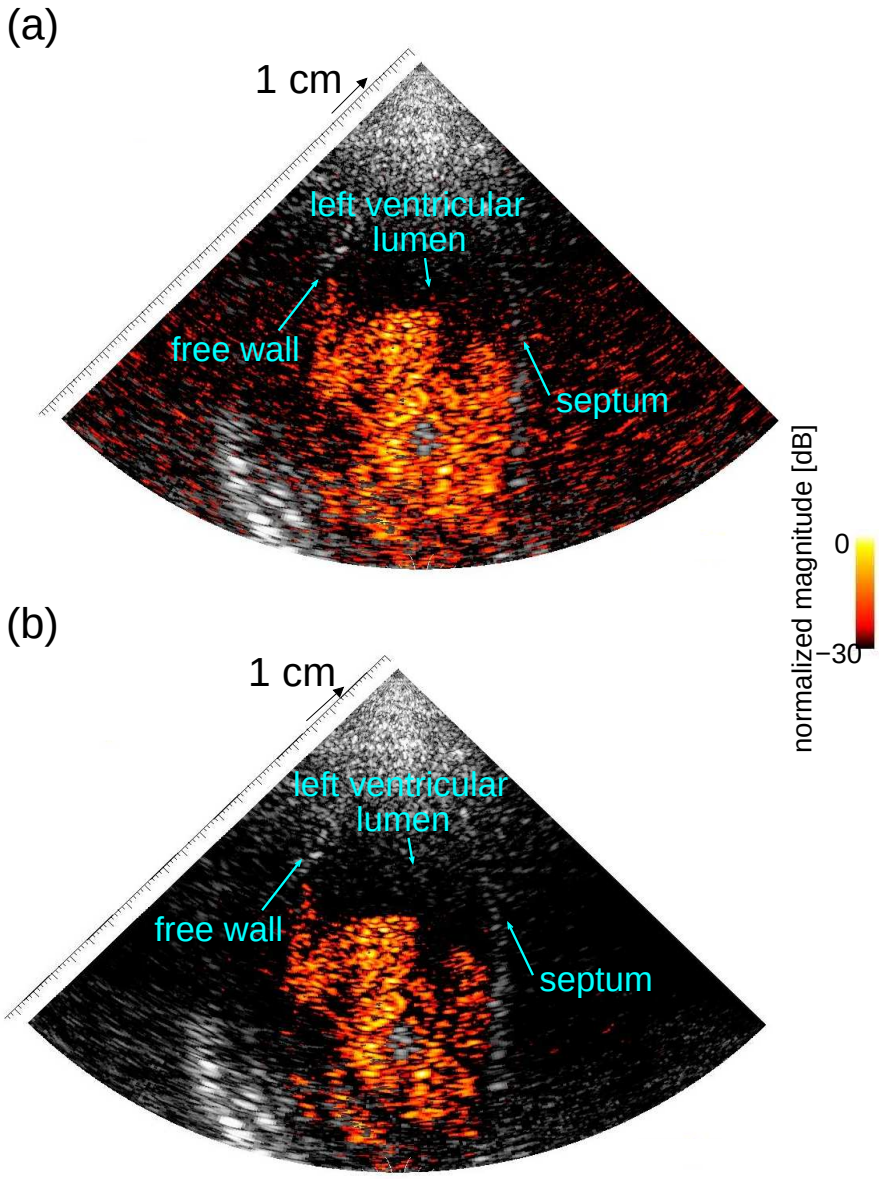

Figure 2.6: Blood echo images (a) without and (b) with weighting by coherence in direction of frame.

2.6 Adaptive MTI filtering

The amplitude of echoes from blood cells in a slow flow is decreased by the MTI filtering and, therefore, it is desirable that the cutoff frequency of the MTI filter is set as low as possible. However, the velocity of the heart wall (clutter source) changes over time. This means that the desirable cutoff frequency of the MTI filter is different depending on the cardiac phase. For instance, in early diastolic phase, the cutoff frequency of the MTI filter needs to be high because the heart wall can move very fast at a velocity of over 10 cm/s. On the other hand, in mid and end diastolic phases, the cutoff frequency of the MTI filter is allowed to be comparatively low.

In this study, the brightness in a blood echo image corresponds to the intensity of MTI-filtered echo signals. The magnitude of clutter echoes is intensified at a low cutoff frequency of the MTI filter. On the other hand, the detectability of a slow blood flow is degraded when the cutoff frequency of the MTI filter is high. As for the blood echo image obtained with unfocused transmission, the serious artifact is generated by sidelobe echoes from clutter sources due to the high sidelobe level when the cutoff frequency of the MTI filter is low. Figure 2.7 shows the blood echo image (hot-scaled) with the B-mode image (gray-scaled) in early diastole. The green-colored arrows indicate belt-like artifacts originated from side lobes. As shown in Fig. 2.7, the artifacts interfered with echoes from blood particles in the cardiac lumen.

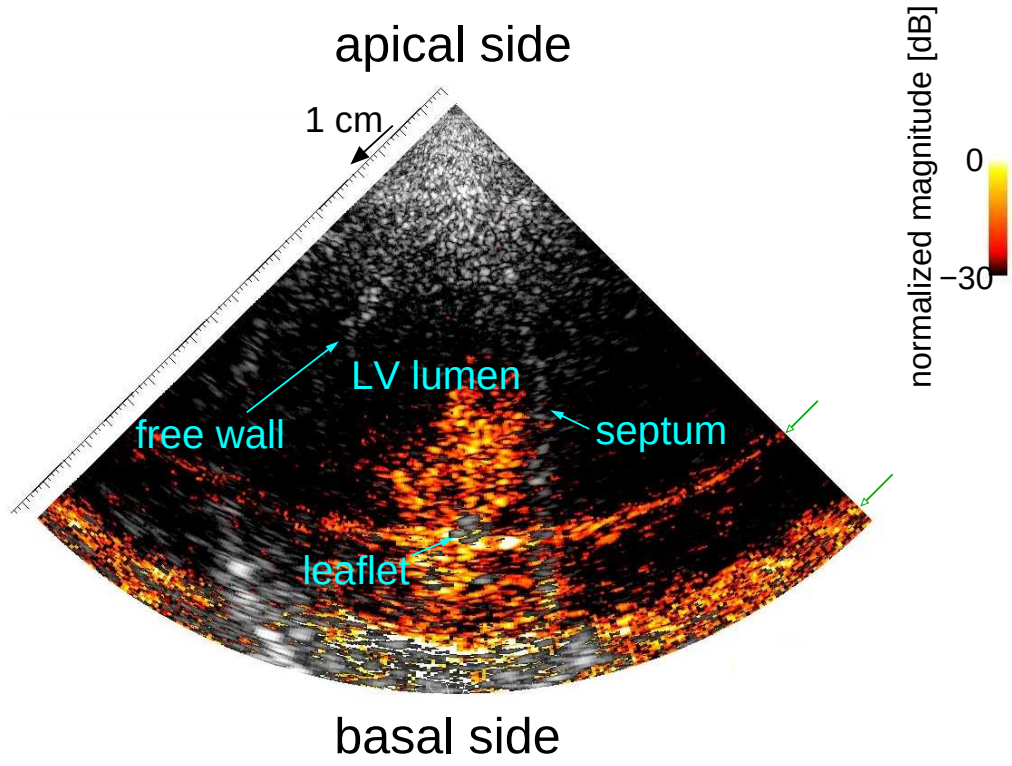

Figure 2.7: Sidelobe artifact captured in early diastole in *in vivo* experiment of a healthy volunteer. The green-colored arrows indicate the sidelobe artifacts. The cutoff frequency of the MTI filter was set at 650 Hz.

A manual control of the cutoff frequency in the MTI filtering in every frame is so time-consuming because a number of frames are acquired owing to ultrahigh-frame-rate measurement with a frame rate of over several thousand hertz. Therefore, the automatic selection of the appropriate cutoff frequency is desirable for stably producing fine blood echo images.

To solve the problem, a procedure for the adaptive MTI filtering was proposed. In this method, the cutoff frequency of the MTI filter was changed over time as a function of the velocity of the heart wall adaptively. First, echo signals from the heart wall and

ribs (clutter sources) were identified (labeled) on the basis of the amplitudes of echoes using the k-means clustering technique [76]. In the k-means technique, means of features belonging to respective groups are updated repeatedly while all points are discerned so that the distance between the mean feature of the group and the feature of each point is small. Then, as for labeled echoes from clutter sources, the mean of the frequency of the echo signal μ and the standard deviation σ in terms of frame were estimated by the auto-correlation technique [18]. Because the velocity of the heart wall fluctuates spatially and temporally, the deviation of the frequency of echoes in the direction of frame should be considered for determination of the cutoff frequency. In this study, we defined the cutoff frequency as $f_{cut} = \mu + n\sigma$ where n is an integer. For evaluation of the difference in myocardial velocities between spatial positions, the spatial average μ_f^{Π} and its standard deviation σ_f^{Π} were estimated using f_{cut} in each position labeled as the heart wall. Finally, the cutoff frequency in the frame $f_{cut.sp}$ was set to $\mu_f^{\Pi} + 3\sigma_f^{\Pi}$. Note that echo signals with a very slow variation in the direction of frame were omitted in this analysis. The ribcage is almost static in entire cardiac cycle; therefore, the cutoff frequency can be underestimated if echoes from ribs are used in the computing of μ_f^{Π} and σ_f^{Π}. In the present study, echoes from tissues with a velocity below 0.2 mm/s were excluded for computing μ_f^{Π} and σ_f^{Π}, which were assumed to be originated from ribs. Figures 2.8(a) and 2.8(b) show the B-mode image and points labeled as the heart wall (red) and ribs (green) by the k-means clustering.Estimated cutoff frequencies $\{f_{cut.sp}\}$ were temporally averaged in the direction of frame to prevent a drastic variation of the cutoff frequency in near frames. In the present study, the MTI filter's impulse response was generated by a 60-th order sinc function multiplied with the Kaiser widow function, and the cutoff frequency was automatically determined in each frame.

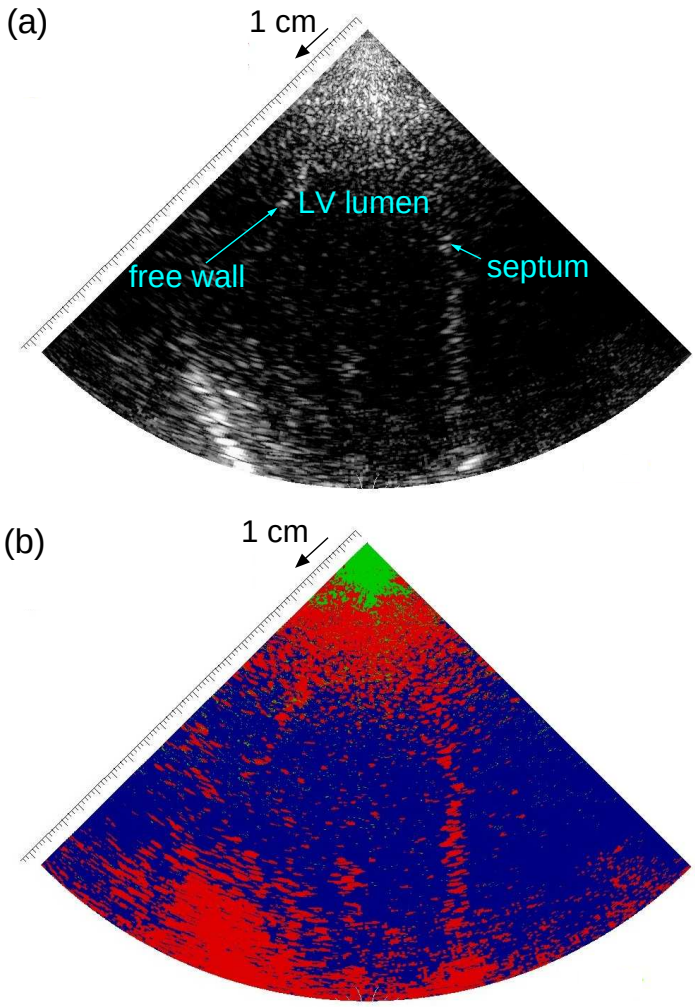

Figure 2.8: (a) B-mode image and (b) distribution of points labeled as the heart wall (red) and ribs (green) by the k-means clustering.

2.7 Conclusion

In this chapter, the strategy for high-frame-rate imaging of motions of echoes from blood cells in the cardiac cavity was presented. First, the frame rate required for imaging of a fast blood flow was investigated. It was verified that a high frame rate strongly

contributes to estimate 2D velocity vector of fast blood flow and, also, it enables the human eye to perceive such fast movements of bloody echoes as well. Therefore, ultrahigh-frame-rate measurement with parallel beamforming and transmission of a single diverging wave was implemented for our study. Subsequently, a procedure for blood echo imaging with acquired RF signals was shown. In the proposed method, two different weighting techniques were adopted to improve the image quality of a blood echo image: PCF-SBs with MTI filtering and the coherence in the direction of frame, i.e., the variance of changes in phases of RF signals regarding the direction of frame. The MTI filtering with adaptively changing the cutoff frequency was described. The cutoff frequency was changed depending on velocities of heart walls (i.e, clutter (echo) sources).

In the next chapter, a method of estimation of 2D blood velocity vector using motions of echoes from blood cells is presented.

Chapter 3

Estimation of blood velocity vector

3.1 Overview

In Chapter 2, a method for high-frame-rate imaging of motions of echoes from blood cells in the cardiac cavity was presented. This method enables the human eyes to perceive the direction of blood flow based on dynamic motions of echoes from flowing blood cells (i.e., qualitative information). To assess the behavior of cardiac blood flow quantitatively, the spatial distribution of 2D blood velocity vectors is valuable.

Speckle tracking using 2D correlation function makes it possible to estimate the blood velocity vector without depending on the angle between an ultrasonic beam and the flowing blood. Because echoes from blood cells are measured at a high frame rate of several kilo-hertz (conventional: several tens-hertz) owing to high frame rate echocardiography, faster movements of blood cells would be traced much more continuously. Nevertheless, it can be challenging to accurately estimate the blood velocity vector because of low SNRs of

echoes from blood cells.

In this chapter, a method of stable estimation of 2D blood velocity vector with speckle tracking is presented. The averaging of 2D correlation functions in speckle tracking is employed for a stable estimation of the 2D blood velocity vector. Although wrong peak of 2D correlation functions would be suppressed, the temporal resolution is degraded with increasing the number of 2D correlation functions for this averaging process. The following issues of the proposed estimator are investigated mainly; (1) the number of frames for averaging necessary for improvement of the accuracy, (2) the difference in behavior of velocity vector estimation due to the angle of flow axis. For such investigations, a steady flow experiment with a flow phantom is conducted and the obtained results are discussed.

3.2 Blood flow vector estimation with temporal averaging of correlation functions

By applying speckle tracking to estimation of inter-frame movements of echoes from blood cells, 2D blood velocity vectors of the cardiac blood flow can be estimated. In speckle tracking, the similarities of echo signals in a region of interest (called kernel) between successive frames are evaluated with sliding the kernel in space in the post frame. The map of similarity can be expressed as a function of the slid distances in the lateral and axial directions, respectively. The velocity can be estimated as the inter-frame displacement, which gives the maximal similarity, divided by the frame interval. In this study, the 2D correlation function was acquired for evaluation of the similarity of envelope signals in a

kernel as follows:

$$
\begin{aligned}
C(d_{\mathrm{la}}, d_{\mathrm{ax}}, n) &= \frac{\sum_{m=-N_i}^{N_i} \sum_{k=-N_j}^{N_j} D_{\mathrm{pre}} D_{\mathrm{post}}}{\sqrt{\left\{ \sum_{m=-N_i}^{N_i} \sum_{k=-N_j}^{N_j} (D_{\mathrm{pre}})^2 \right\} \left\{ \sum_{m=-N_i}^{N_i} \sum_{k=-N_j}^{N_j} (D_{\mathrm{post}})^2 \right\}}}, \\
D_{\mathrm{pre}} &= S_n(i+m, j+k) - \bar{S}_n(i,j), \\
D_{\mathrm{post}} &= S_{n+1}(i+d_{\mathrm{la}}+m, j+d_{\mathrm{ax}}+k) - \bar{S}_{n+1}(i+d_{\mathrm{la}}, j+d_{\mathrm{ax}}), \qquad (3.1)
\end{aligned}
$$

where $S_n(i,j)$ is the envelope signal at the i-th axial point and the j-th scan line, respectively, in the n-th frame, and $\bar{S}_n(i,j)$ represents the averaged envelope signal within the kernel. The kernel sizes in the axial and lateral directions correspond $(2N_i+1)$ and $(2N_j+1)$, respectively, and these were set at 8.2 mm and 9 degree in the actual dimensions. The envelope signals in the kernel were weighted by the 2D Tukey window function. $C(d_{\mathrm{la}}, d_{\mathrm{ax}}, n)$ denotes normalized 2D correlation function of lateral and axial lags of d_i and d_j, respectively, between n-th and $(n+1)$-th frames.

Blood cell is small and acoustic outputs of defocused ultrasonic beams employed for high-frame-rate measurement are low. Under such conditions, SNRs of echoes from blood cells are low; therefore, it is hard to accurately estimate the blood velocity vector. Because the correlation coefficient involuntarily increases/decreases due to low SNRs, the peak at the wrong position can be derived. In our proposed method, echoes in many frames obtained by high-frame-rate echocardiography in a short period were used to recover the true peak in the 2D correlation functions. The correlation coefficient at the true position is considered to be high averagely during a short duration. On the other hand, the deviation of correlation caused by noise component in echoes can be assumed to be random even in a short period. The undesirable rise of the correlation coefficient would be suppressed by the averaging operation of 2D correlation functions for the short period and, thus, the

maximal correlation at the true position is produced, i.e, a stable estimation of blood velocity vector becomes possible.

These are several different operations for averaging of 2D correlation functions in multiple frames: (i) averaging of velocity vectors computed in each frame; (ii) averaging of unnormalized 2D correlation functions; (iii) averaging of 2D correlation functions normalized by the variance. As for the averaging of velocity vectors, the information of 2D correlation function cannot be utilized. In the present study, the averaging operation of the normalized 2D correlation function was used to emphasize the temporal change in phase of echoes in each frame.

Normalized 2D correlation functions between two consecutive frames at a spatial point were temporally averaged in N_{cf} (the number of frame intervals) as follows:

$$\bar{C}(d_{\mathrm{la}}, d_{\mathrm{ax}}, n) = \frac{1}{N_{\mathrm{cf}}} \sum_{k=-N_{\mathrm{cf}}/2}^{N_{\mathrm{cf}}/2-1} C(d_{\mathrm{la}}, d_{\mathrm{ax}}, n+k). \tag{3.2}$$

Figure 3.1 illustrates the proposed averaging process. After the averaging process, the averaged 2D correlation function was up-sampled with a reconstructive interpolation [77] to estimate the small displacement between consecutive frames below the sampling interval.

3.3 Evaluation of accuracy by steady flow measurement

The aim of this experiment was to examine the effect of the averaging process of 2D correlation functions. While the estimation of the 2D correlation function is stable, the temporal resolution in estimation of velocity vectors is degraded with increasing the number

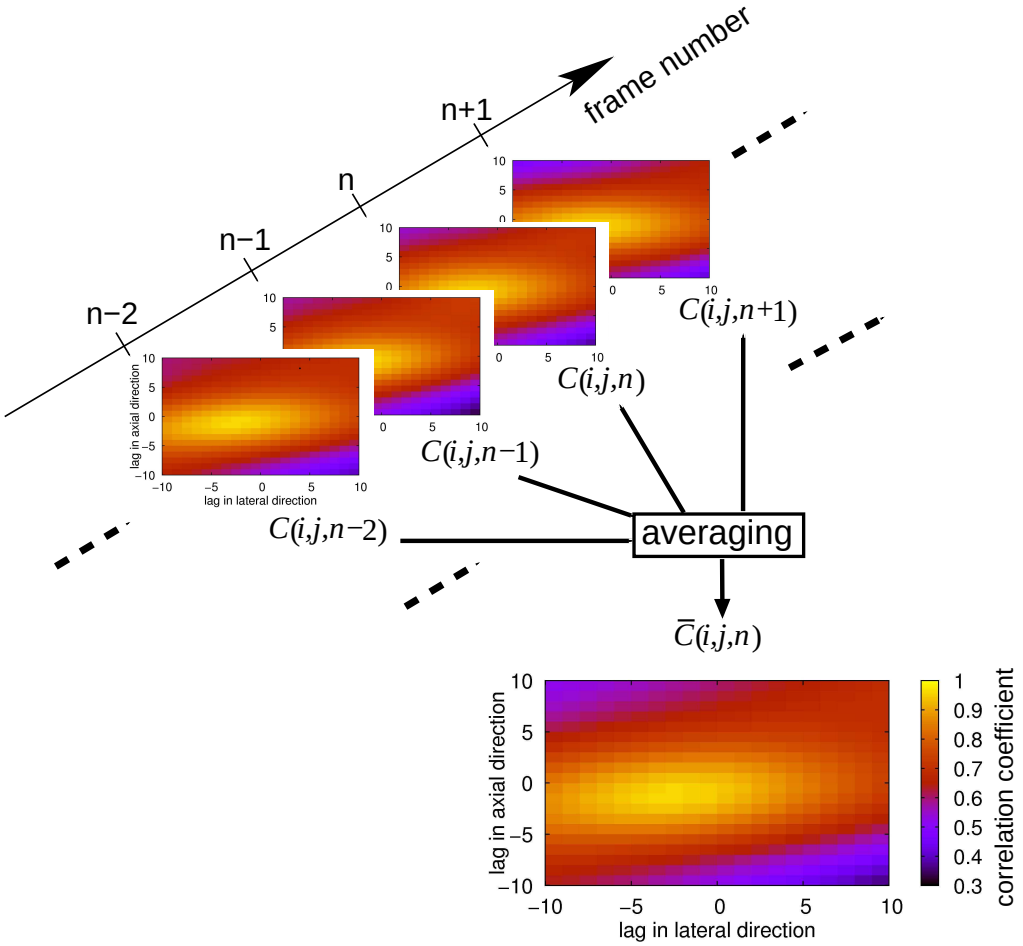

Figure 3.1: Schematic illustration of temporal averaging of normalized 2D correlation functions.

of 2D correlation functions for this averaging process. First, to investigate the averaging duration required for a stable estimation of flow velocity vector, the accuracies of vector estimates were evaluated at different numbers of frames for averaging of 2D correlation functions. From experimental results, the averaging duration was determined. In addition, blood flows in various directions inside the cardiac cavity. Therefore, the behavior of the proposed estimator in different angles of flow axis was also evaluated. A steady flow experiment with blood-mimicking fluid was conducted for such investigations.

3.3.1 Experimental setup

Figure 3.2 shows the experimental system for the steady flow measurement. This experimental system was also used to investigate the effect of the frame rate on the accuracy in estimation of velocity vectors in Section 2.2.1. A blood mimicking fluid was steadily flowed in a cylindrical flow path (diameter of 8 mm) surrounded by tissue-mimicking rubber, and echoes from this flow phantom was measured. The flow rate, which corresponds to the mean flow velocity, was measured by a mass flow meter connecting to the flow path. The non-steered diverging ultrasound was transmitted once per frame so that a frame rate of 6024 Hz was achieved. In the experiments described in this Chapter 3, the cutoff frequency of the MTI filter was constant at 500 Hz corresponding to a axial velocity of 10 cm/s. Figure 3.3 shows a subset of estimated velocity vectors of blood mimicking particles with the blood echo image. Using these estimated vectors, the performance of estimation

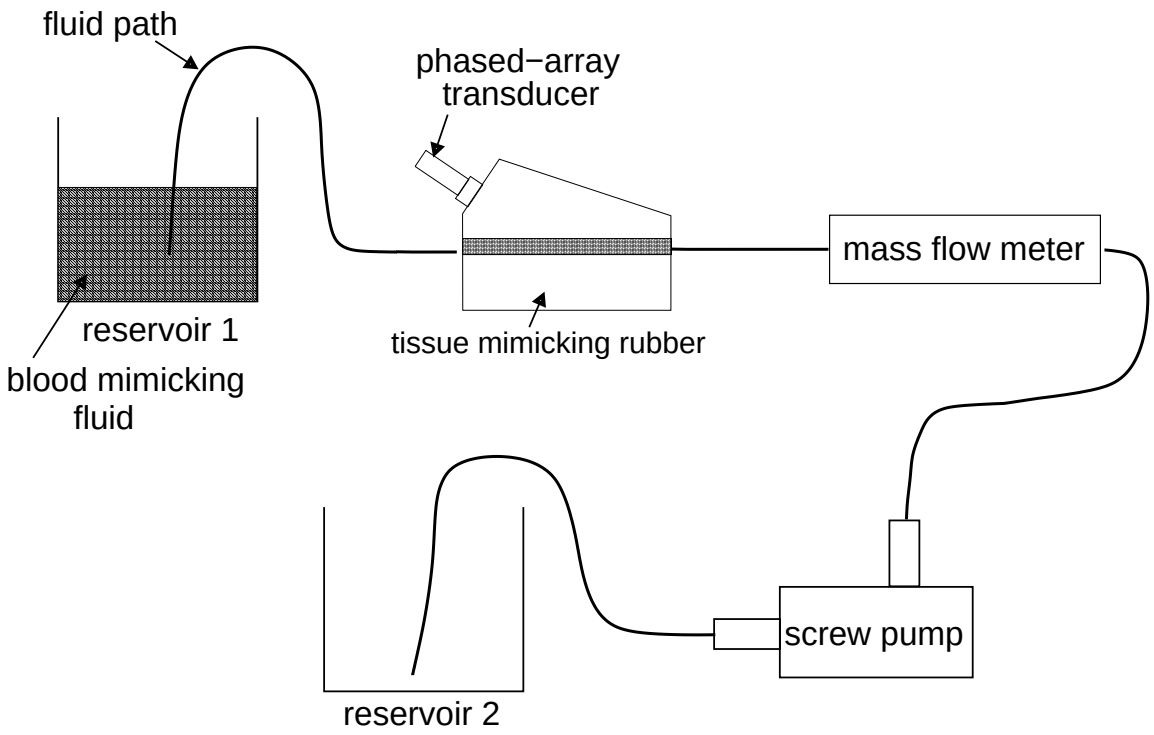

Figure 3.2: Illustration of experimental environment.

of 2D velocity vector was evaluated.

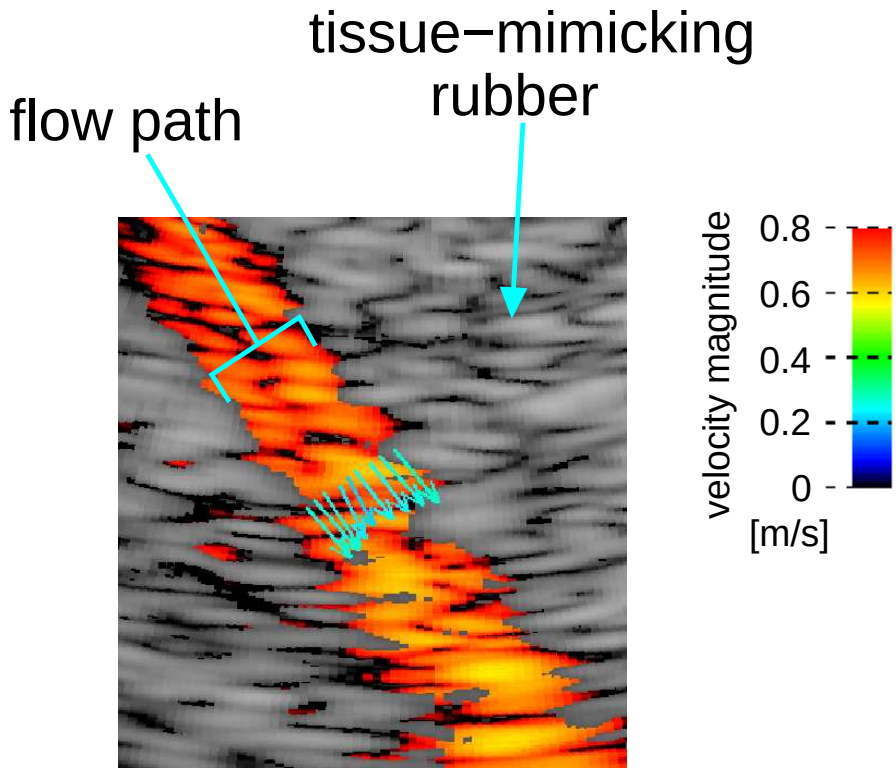

Figure 3.3: Velocity vectors of blood mimicking particles with blood echo image. A subset of estimated velocity vectors along the direction perpendicular to the flow axis was visualized.

3.3.2 Effect of averaging of correlation functions

To investigate the averaging number necessary for improvement of the accuracy, effects of the averaging process of 2D correlation functions on estimation of 2D velocity vector were examined through a steady flow measurement. The transducer surface was placed at a distance of 7 cm from the outer surface of the flow path, and the angle between the transducer surface and the flow path was set at 56 degrees. RF echo signals from the flow phantom were measured at a flow rate of 0.6 L/min (mean flow velocity: 0.2 m/s, Reynolds

number: 960). To simulate the steady flow experiment with a higher flow velocity with keeping the Reynolds number, the flow velocity was increased apparently by changing the frame interval of the original echo data. Simulated flow velocities were 0.4 and 0.6 m/s while the Reynolds number of 960 was hold. Figure 3.4 shows directional errors E_{dir} of estimated 2D velocity vectors at different numbers of 2D correlation functions for averaging

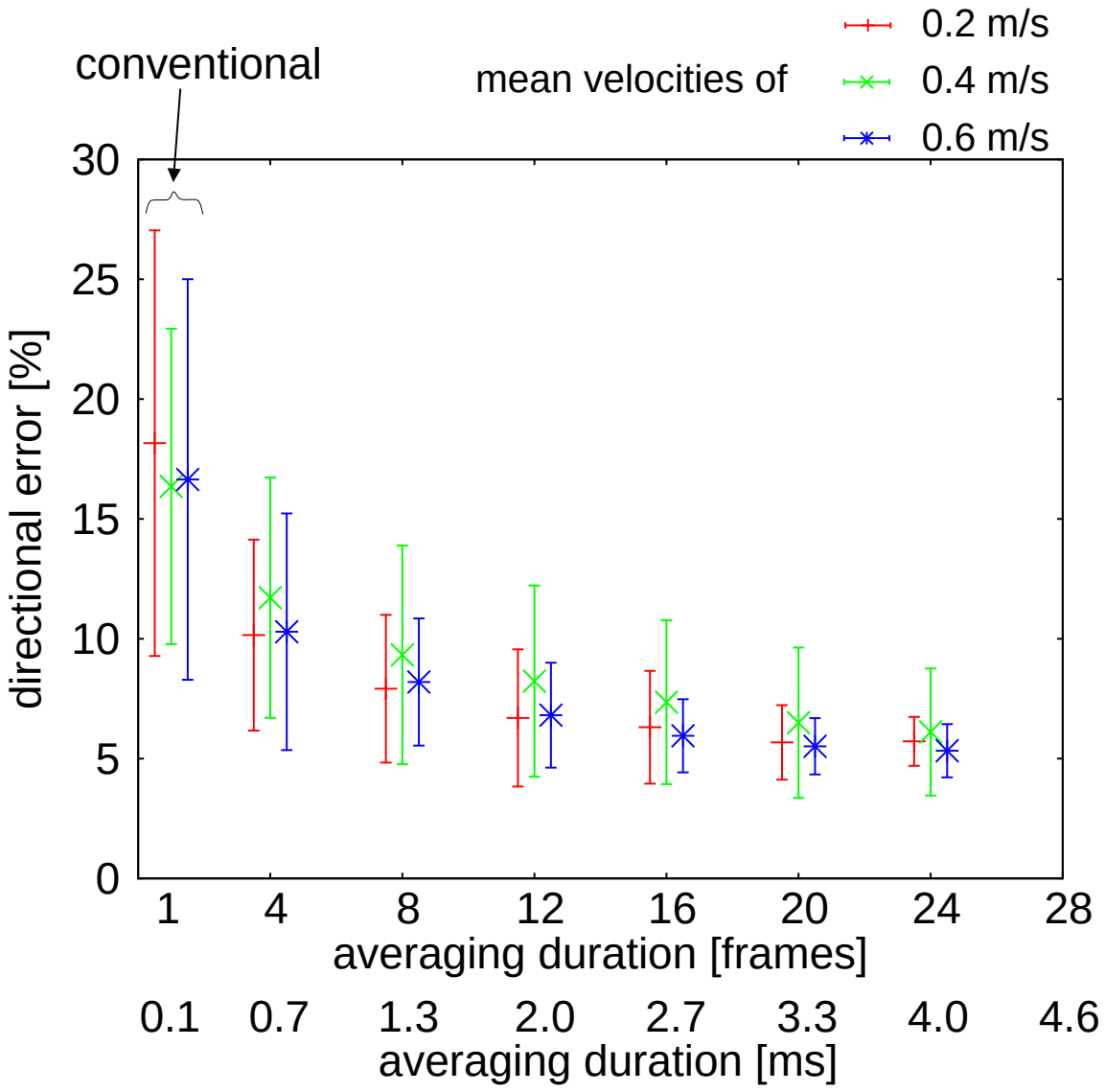

Figure 3.4: Directional errors of estimated 2D velocity vectors at different number of 2D correlation functions at different flow velocities of 0.2, 0.4, and 0.6 m/s.

at different flow velocities of 0.2, 0.4, and 0.6 m/s, which were defined as follows:

$$E_{dir} = \frac{1}{\pi}\sqrt{\frac{1}{N_j}\sum_{j=0}^{N_j-1}\left\{\cos^{-1}\left(\frac{\mathbf{v}_j \cdot \mathbf{n}}{|\mathbf{v}_j|\,|\mathbf{n}|}\right)\right\}^2}, \tag{3.3}$$

where $\mathbf{v}_j$ and $\mathbf{n}$ represent the velocity vector estimated at the j-th spatial point and the unit vector parallel to the flow direction, respectively. The standard deviations were computed from 50 frames. As for all of flows at different velocities, it can be seen that the directional errors decreased and converged with the averaging number of 2D correlation functions. Using the averaging method for 2D correlation functions, the deviation of directional errors in the vector estimation was reduced to almost half of the conventional speckle tracking (i.e, non-averaging of 2D correlation functions) at an averaging duration of over 8 frames. To prioritize the temporal resolution in the velocity vector estimation, N_{cf} was set to 12 corresponding to mere 2 ms.

Figures 3.5 and 3.6 show mean flow velocities $\bar{V}$ and directional errors E_{dir} obtained without and with the averaging of 2D correlation functions during 12 frames. The mean flow velocity was evaluated by Eq. (2.2). The standard deviations were computed from 50 frames. It was shown that the error of estimation of the velocity component along the flow axis was also reduced owing to the temporal averaging of 2D correlation functions.

3.3.3 Dependence on angle of flow axis

The blood flow structure in the cardiac lumen is very complex unlike the unidirectional flow in the common carotid artery. As a major example, it has been reported that the vortex flow is generated with flow streams from the mitral valve toward the arterial valve through the apex in the left ventricular lumen. Such vortex flows are considered to enhance

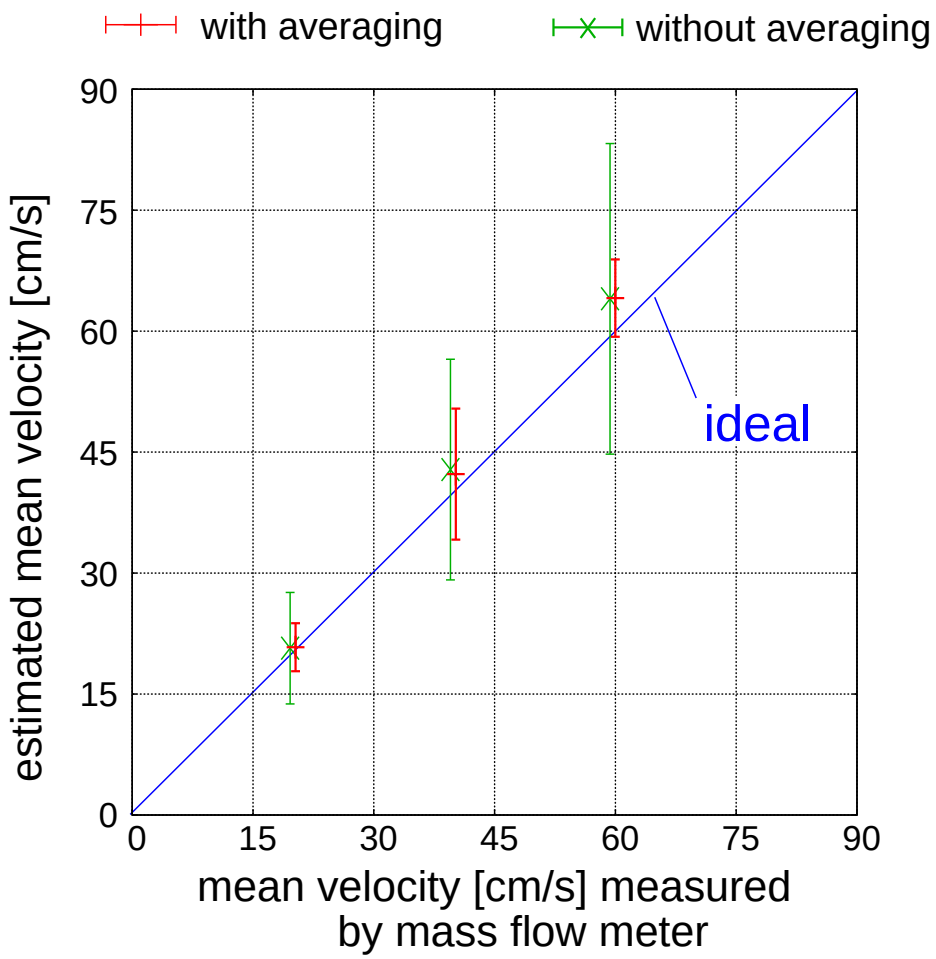

Figure 3.5: Mean flow velocity estimated by speckle tracking with and without averaging 2D correlation functions through steady flow experiment at different mean flow velocities.

the cardiac pumping efficiency by preserving the momentum of blood in diastolic phase; therefore, visualization of vortex flow is valuable.

On the other hand, the MTI filtering suppresses an echo from an object moving below the cutoff velocity with respect to the axial direction (parallel to the ultrasonic beam). The diastolic vortex flow in the cardiac lumen is ultrasonically measured from a narrow acoustic window between ribs. This means that the flow velocity along the direction of beam is much variable depending on the position within the vortex. Therefore, a diversity of accuracy depending on the angle between the flow axis and the beam direction is considerable. To

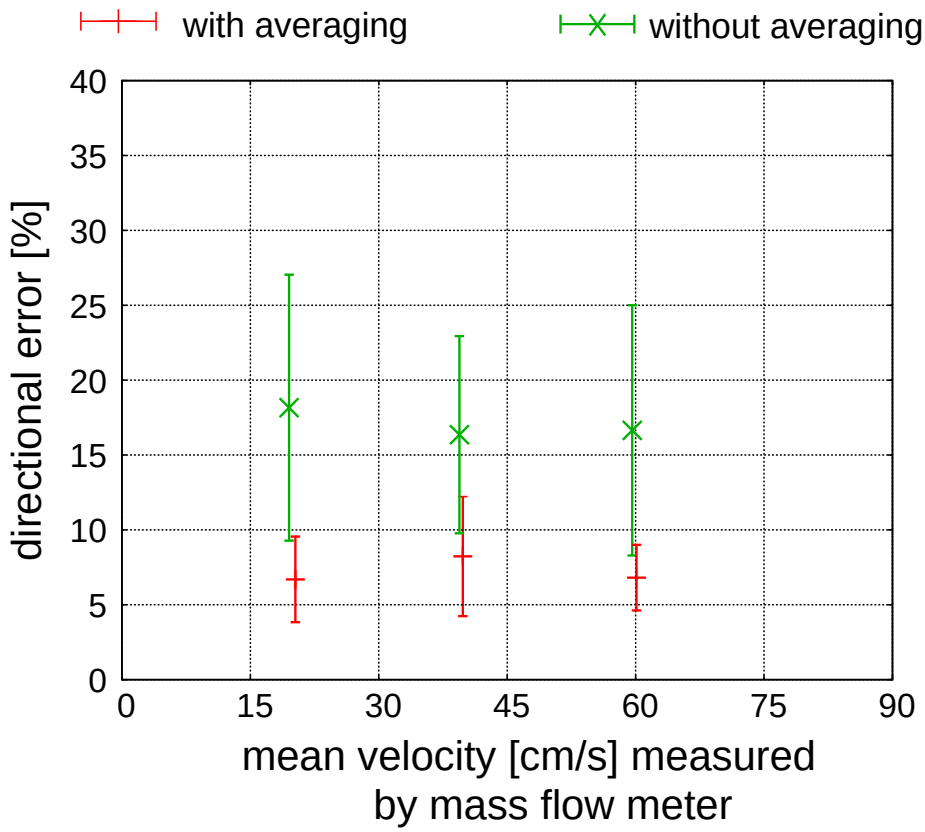

Figure 3.6: Directional error in velocity vectors estimated by speckle tracking with and without averaging 2D correlation functions through steady flow experiment at different mean flow velocities.

examine such effect, the accuracy of velocity vector estimation at different flow angles of 18 and 56 degrees to the array surface was compared.

The transducer surface was placed at distances of 5 cm (at 18 degree) or 7 cm (at 56 degree) from the outer surface of the flow path. The echo data was acquired at a flow rate of 0.12 L/min (mean flow velocity: 0.04 m/s, Reynolds number: 192). By changing the frame interval of the original data, faster flows with mean velocities of 0.08, 0.12, 0.16, and 0.2 m/s were simulated with keeping the Reynolds number of 192. Figures 3.7(a) and 3.7(b) show mean flow velocities and directional errors computed by following Eqs. (2.2) and (3.3). The standard deviations were computed from 50 frames. The difference

in accuracy depending on the angle between the flow axis and the ultrasonic beam can be seen in Figs. 3.7(a) and 3.7(b).

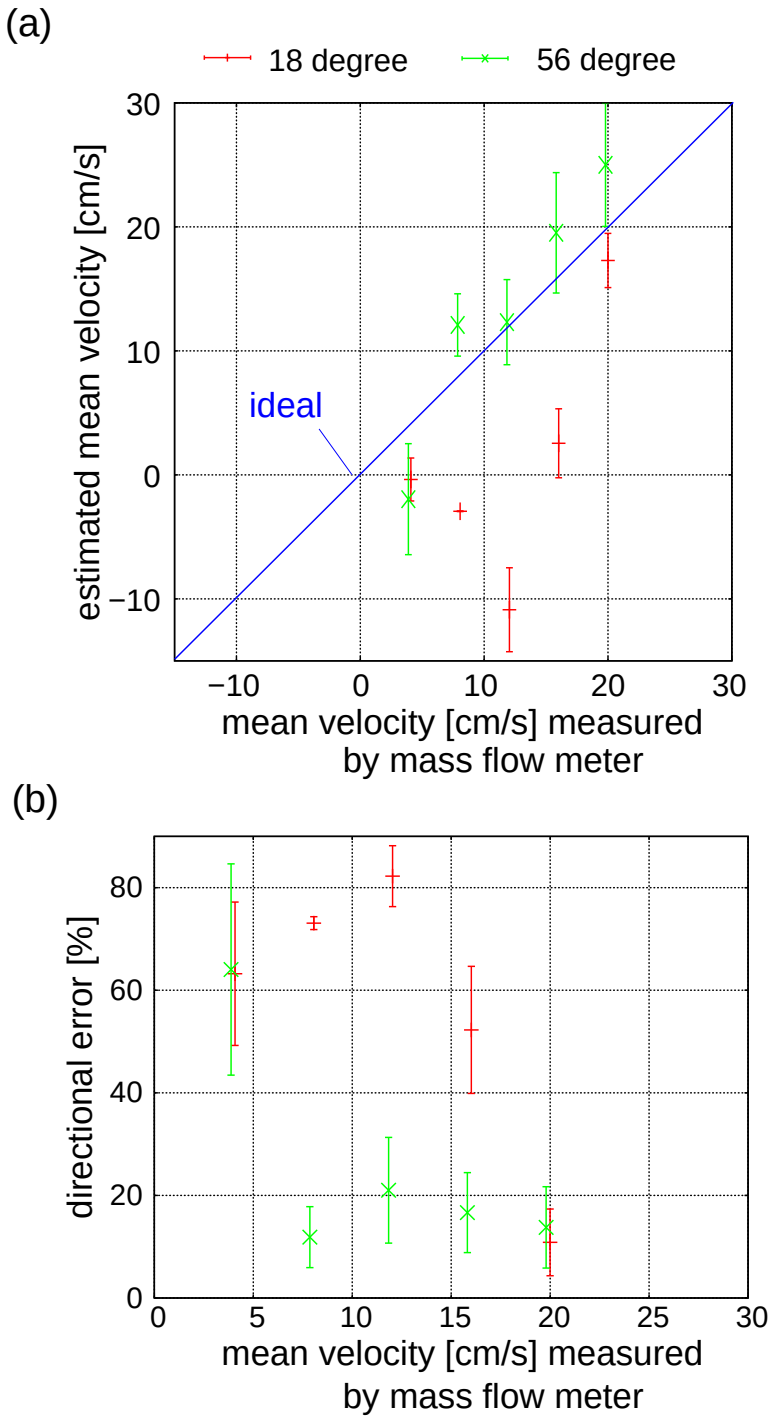

Figure 3.7: (a) Mean flow velocities and (b) directional errors computed with 2D velocity vectors at different flow angles of 18 and 56 degree to the array surface.

3.3.4 Evaluation of total error in velocity vector estimation

The error of direction of 2D velocity vector was evaluated in the previous sections. The magnitude of 2D velocity vector (i.e., velocity in major direction) has not been included in the evaluations. In this subsection, the accuracy of estimation of velocity vector was evaluated in terms of both the magnitude and the direction of 2D velocity vector.

Garcia *et al.* evaluated an error in estimation of velocity vector in a phantom experiment with a flowing blood mimicking liquid inside a mimicked cardiac cavity and an *in vivo* experiment [36]. In their experiment, the velocity vector field within the cavity was measured by particle image velocimetry (PIV). Using the measured velocities, another velocity vector map was reconstructed based on the vector flow mapping technique. The reconstructed velocity vectors and the original velocity vectors measured by PIV were compared by the error of velocity vector estimates as

$$E_{\mathrm{tot}} = \frac{\int_{\mathrm{LV}} \left| \vec{V}_{\mathrm{PIV}} - \vec{V}_{\mathrm{REC}} \right| dS}{\int_{\mathrm{LV}} \left| \vec{V}_{\mathrm{PIV}} \right| dS}, \tag{3.4}$$

where LV, $\vec{V}_{PIV}$, and $\vec{V}_{REC}$ denote the region of acquisition of velocity vector map inside the cavity, the velocity vector measured by PIV, and the reconstructed velocity vector by vector flow mapping, respectively. The total error E_{tot} evaluated both the magnitude and the direction of 2D velocity vector in total. The formula in Eq. (3.4) means the error relative to the velocity vectors measured by PIV.

The accuracy including the magnitude and the direction of 2D velocity vector in the proposed estimator was evaluated with reference to Garcia's study. The total error of velocity vector estimates was evaluated with the steady flow measurement as described in the previous sections. First, the reference flow velocity of our flow experiment was exam-

ined. Hypothesizing Hagen-Poiseuille flow inside the flow path, the velocity distribution was expressed as follows:

$$v(r) = v_{\max}\left(1 - \frac{r^2}{R^2}\right), \tag{3.5}$$

where $v(r)$, $v_{\max}$, r, and R represent the velocity, the maximal velocity, the distance from the center axis of the flow path, and the radius of the flow path, respectively. Here, two conditions were considered: (1) the flow path was measured by ultrasound in a 2D plane traversing in the direction of the long axis and (2) the path diameter of 8 mm was similar to the size of the kernel (lateral: 9 degree, axial: 8.2 mm) for speckle tracking. Under such conditions, the comparison of the average velocity along a line traversing the cross-sectional plane of the flow path would be adequate. The average velocity on the transverse line $\bar{v}_{\text{line}}$ was given by a line integral as follows:

$$\begin{aligned} \bar{v}_{\text{line}} &= \frac{\int_{-R}^{R} v(r)dr}{\int_{-R}^{R} dr}, \\ &= \frac{\int_{-R}^{R} v_{\max}\left(1 - \frac{r^2}{R^2}\right) dr}{2R}, \\ &= \frac{2}{3} v_{\max}. \end{aligned} \tag{3.6}$$

The mean fluid velocity can be estimated using the flow rate measured by the mass flow meter in this experiment as used previously. v_{max} is twice as high as the mean fluid velocity corresponding to a surface integral of Eq. (3.5) divided by the cross sectional area. Therefore, $\bar{v}_{\text{line}}$ can be computed by following Eq. (3.6). Using the reference velocity $\bar{v}_{\text{line}}$, let us define the total error for our experiment as follows:

$$E'_{\text{tot}} = \frac{|E_j\left[v_j\right] - \bar{v}_{\text{line}}|}{|\bar{v}_{\text{line}}|}, \tag{3.7}$$

$E_j\left[\cdot\right]$ denotes the averaging process in spatial points aligned along the transverse line.

Figure 3.8 shows total errors in Eq. (3.7) at different mean flow velocities. The number of 2D correlation functions for averaging was set at 12 frames.

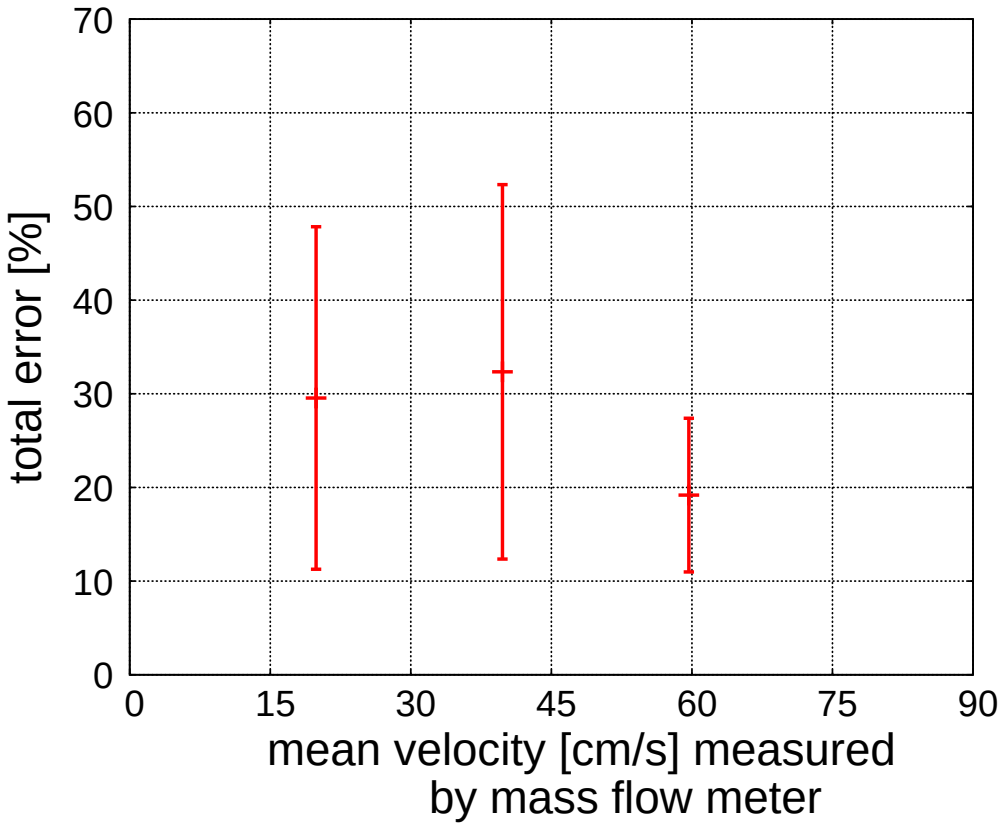

Figure 3.8: Total error of vector estimates with averaging of 2D correlation functions in 12 frames at different mean flow velocities.

3.4 Discussions

With respect to the cardiac blood flow imaging, the visualization of complex flow, such like vortex flow, has become important and blood particles in such complex flow travel in various directions. Hence, it is considerable if the direction of blood flow is successfully

estimated. The temporal averaging of 2D correlation functions in speckle tracking was proposed for a stable estimation of the 2D blood velocity vector. Owing to high-frame-rate echocardiography, 2D correlation functions between a very short frame interval (a couple of hundred microseconds) could be obtained. As can be seen in Fig. 3.4, the directional error of velocity vector estimates decreases with increasing the averaging duration of 2D correlation functions. Although the averaging duration was mere 2 ms, the directional error could be reduced significantly from 18.2% to 6.7% at a mean velocity of 0.2 m/s. Although the averaging technique with multiple 2D correlation functions is computationally intensive, it is of great value to visualize the cardiac vortex flow.

It was also shown that the fine estimation of blood velocity vector with the high temporal resolution of 2 ms is possible by the proposed averaging technique. The typical frame rate of conventional color Doppler method are several tens hertz, which corresponds to the temporal resolution of several tens milliseconds. If the temporal resolution equal to color Doppler method is permitted, 2D velocity vector would be estimated more correctly by the proposed method because 2D correlation functions of over 50 frames can be averaged. The temporal averaging process of 2D correlation functions with high-frame-rate echocardiography has a great potential for a stable estimation of 2D velocity vectors.

As shown in Fig. 3.7, the accuracy of estimation of flow velocity at a flow angle of 56 degree is worse below 0.04 m/s, but, that with a a flow angle of 18 degree further degraded below 0.2 m/s. The cutoff velocity of the MTI filtering indicates the velocity component in the axial direction (i.e, direction parallel to ultrasonic beam) of an object dominantly. The axial velocity decreases with increasing the angular difference between the blood flow and the ultrasonic beam; therefore, the proposed method has an angle-dependence of visibility between the flow major axis and the ultrasonic beam. The proposed blood flow imaging

should be worked under such limitation.

The average total errors of velocity vector estimates were 29.5, 32.3, and 19.2%, at the mean fluid velocities of 0.2, 0.4, and 0.6 m/s, respectively, as shown in Fig. 3.8. In Garcia's basic experimental study, those were 20% in systole and 15% in diastole. The differences of experimental situations between these studies should be considered. The experimental material was different between our study and Garcia's study. A complex flow inside a mimicked cardiac chamber was used in Garcia's study. Hence, errors in estimation of flows toward all directions were involved in the results obtained by their experiment. In addition, the total error would decrease with the magnitude of the reference velocity vector because the formula in Eqs. (3.4) and (3.7) evaluated the errors relative to the reference velocity; therefore, the difference of the flow velocity in the experiment leads to a biased evaluation. Although the obtained total errors could not be rigorously compared between the studies due to the significant differences described above, there is not a major difference in the accuracies of velocity vector estimates between them. However, our proposed method enables to visualize the real movements of flowing blood cells uniquely.

Furthermore, it was also found that the overall accuracy in estimation of velocity vectors was significantly low as compared to the estimation of only the axial direction based on the Doppler method. In our basic experiment, blood mimicking particles moved toward the outlet of the phantom along the flow axis. On the other hand, the velocities along the flow axis were different depending on the distance from the center of the flow path as can be found in Eq. (3.5). This means that the flow velocities were inhomogeneous while the flow directions were uniform inside the kernel. Therefore, the error of estimation of the velocity magnitude was relatively high in this experiment, which led to high total errors of velocity vector estimates. This can be considered to indicate the vulnerability of the

present estimator of blood velocity vector to inhomogeneous motions of scatterers inside the kernel.

3.5 Conclusion

In this chapter, a method for estimation of 2D blood velocity vector with speckle tracking was presented and its accuracy was evaluated. The accuracy of estimation of the 2D blood velocity tends to degrade due to weak echoes from blood cells. Although the temporal averaging of 2D correlation functions is effective to improve the accuracy of speckle tracking, the temporal resolution is degraded with increasing the averaging duration. Therefore, the duration for averaging of 2D correlation functions required for improving the accuracy was investigated under mean flow velocities of 0.2, 0.4, and 0.6 m/s. Although the averaging duration was only 2 ms, the directional error in the estimation of 2D blood velocity vector with speckle tracking was significantly improved from 18.2% to 6.7% at a flow velocity of 0.2 m/s.

On the other hand, it was found that the accuracy was influenced by the angle between the flow axis and the beam direction. The proposed method should be used with understanding of such limitation. Furthermore, the total errors of vector estimates with both the magnitude and the direction of 2D velocity vector was evaluated. The average total errors were 29.5, 32.3, and 19.2% at the mean fluid velocities of 0.2, 0.4, and 0.6 m/s, respectively.

In the next chapter, the feasibility of cardiac blood flow imaging by the proposed method was examined through an *in vivo* measurement of the left ventricle of the healthy heart.

Chapter 4

In vivo experimental study

4.1 Overview

The blood flow structure inside the left ventricular lumen apparently alters depending on the cardiac phase. In ejection phase, the blood is ejected to the aortic valve owing to the myocardial contraction. In diastole, the blood flows into the left ventricular lumen from the left atrium throughout the mitral valve. Then, the vortex-like flow is grown up and centered in the left ventricular lumen with decreasing the inflow velocity of the blood. In this chapter, the feasibility of the cardiac blood flow imaging by the proposed method was examined by visualizing such blood flow patterns through an *in vivo* measurement of the left ventricle of a healthy human heart.

RF echo signals from the left ventricle were measured at a frame rate of 6024 Hz in a transthoracic three-chamber view of a 27-year-old healthy volunteer. Figure 4.1 illustrates the measured 2D plane. In the corresponding image view, the left ventricular lumen was

surrounded by the septum and the free wall.

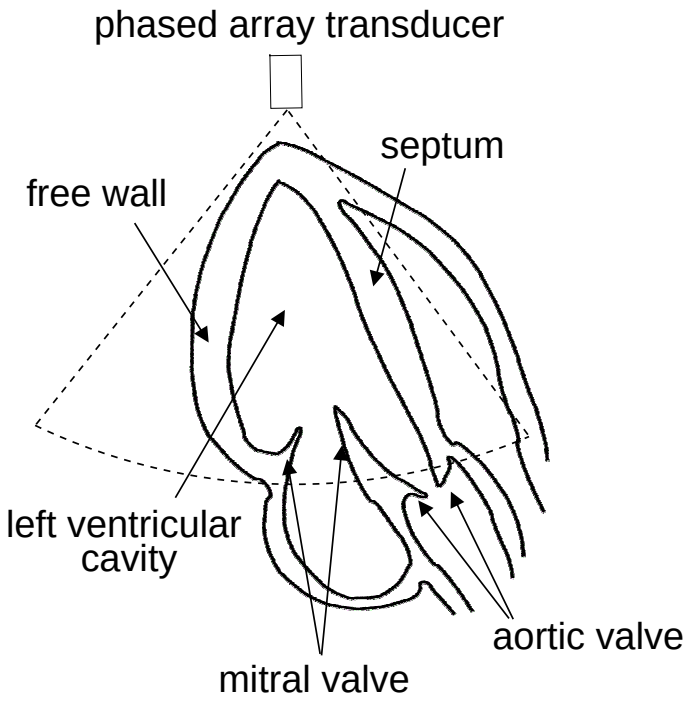

Figure 4.1: Illustration of region in the heart measured by high-frame-rate echocardiography.

4.2 Effect of adaptive clutter filtering

Figure 4.2 shows the cutoff frequency automatically-determined at an integer of $n = 3$. Figure 4.3 shows blood echo images obtained at the integers of $n = 1$, 2, and 3 in the frame indicated by the blue-colored dash line in Fig. 4.2 (when the cutoff frequency was minimum in diastole). In Fig. 4.3, the B-mode images were not superimposed. Echoes from the heart wall contaminated those from blood particles significantly at $n = 1$ in Fig. 4.3(a), and echoes from the free wall surrounded by the cyan-colored dash line remained at $n = 2$

in Fig. 4.3(b). Therefore, the cutoff frequency was defined as $f_{cut} = \mu + 3\sigma$ in the present study. Figure 4.4(1) shows blood echo images with the B-mode images in the frame during early diastole which was indicated as (1) in Fig. 4.2. In Figs. 4.4(a-1), (b-1), and (c-1), blood echo images were obtained using MTI filters with different cutoff frequencies of 300, 650, which were constant in the entire cardiac cycle, and 1059 Hz which was estimated by the proposed method, respectively. Figure 4.4(2) shows blood echo images obtained in the frame during mid diastole, which was indicated as (2) in Fig. 4.2, at different cutoff frequencies of 300, 650, and 410 Hz (the proposed method).

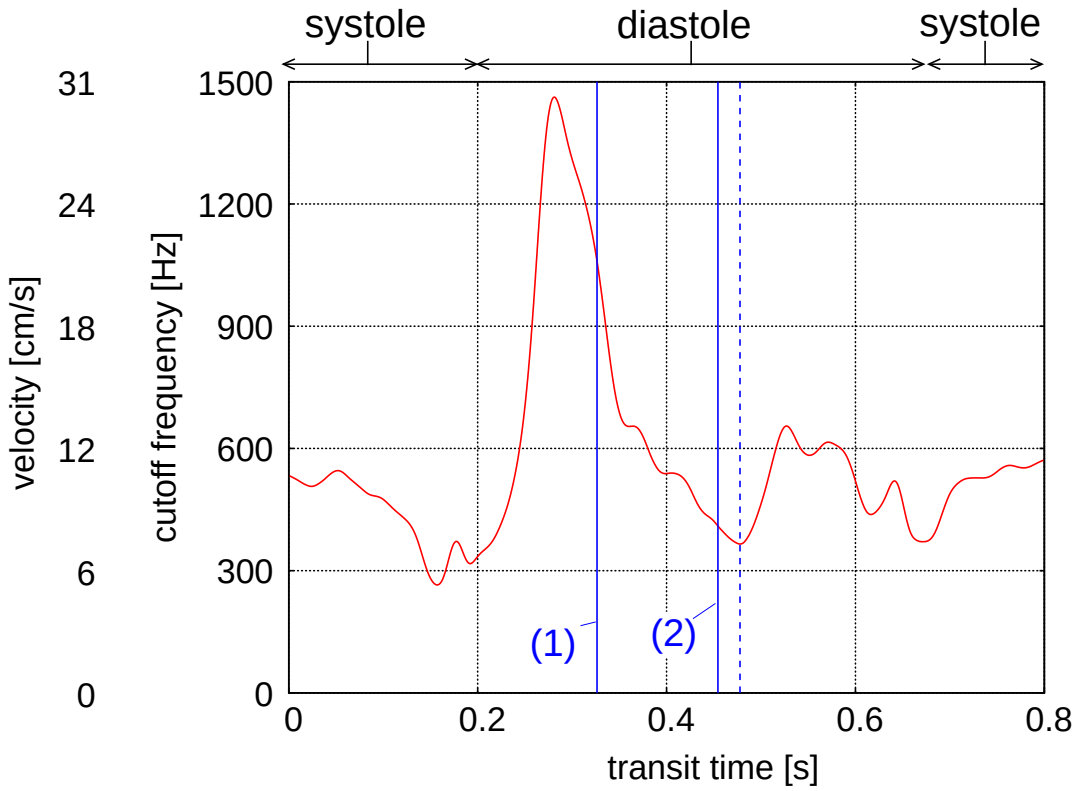

Figure 4.2: Cutoff frequencies $\{f_{cut.sp}\}$ automatically-determined at $f_{cut} = \mu + 3\sigma$ in entire cardiac cycle.

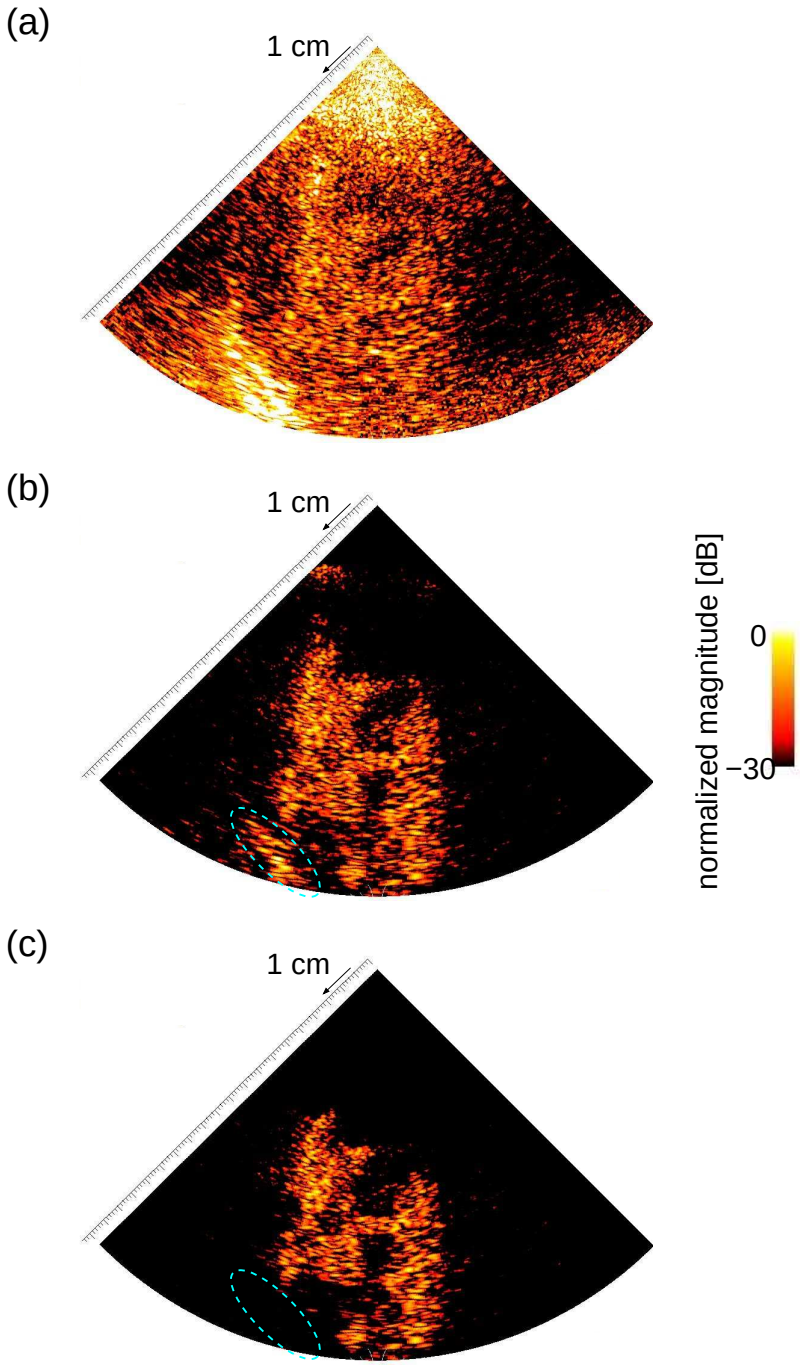

Figure 4.3: Blood echo images obtained by determining the cutoff frequency f_{cut} as (a) $f_{cut} = \mu + \sigma$, (b) $\mu + 2\sigma$, and (c) $\mu + 3\sigma$, respectively, in the frame indicated by the blue-colored dash line in Fig. 4.2.

As shown in Figs. 4.4(a-1) and 4.4(a-2), echoes from blood cells were visualized in a wider region in mid diastole using the low cutoff frequency of 300 Hz, but more clutter echoes were seen in early diastole. Using the MTI filter with the cutoff frequency of 650 Hz, echoes from blood cells flowing into the cardiac lumen could be visible with suppressing clutter echoes in early diastole as shown in Fig. 4.4(b-1). However, as shown in Fig. 4.4(b-2), the visible echoes from blood cells decreased as compared to Fig. 4.4(a-2) in mid diastole. As shown in Fig. 4.4(c-2) obtained by our proposed method, although visible echoes from blood cells slightly decreases as compared to Fig. 4.4(a-2), echoes from blood cells within the vortex flow could be visualized over a wider field in mid-diastole while clutter echoes were rejected in early-diastole.

4.3 Imaging of blood velocity vector

Figures 4.5(a) and 4.5(b) show 2D velocity vectors of blood flow estimated by speckle tracking with temporally-averaged 2D correlation functions in systole and diastole, respectively. The spatial points, at which 2D velocity vectors were estimated, were manually assigned at a regular interval inside the cardiac lumen. The kernel sizes in the lateral and axial directions were set to 9 degrees and 8.2 mm, respectively. The number of 2D correlation functions used for the temporal averaging was 12 corresponding to almost 2 ms. The averaged 2D correlation function was up-sampled by a reconstructive interpolation [77] in order to measure the small movement of echoes between successive frames. Velocity vector magnitudes at all pixels were obtained using a reconstructive interpolation [77] of the distribution of 2D vector velocities measured by speckle tracking. The cyan-colored arrow and the hot color-coded intensity indicate the direction and the magnitude of the

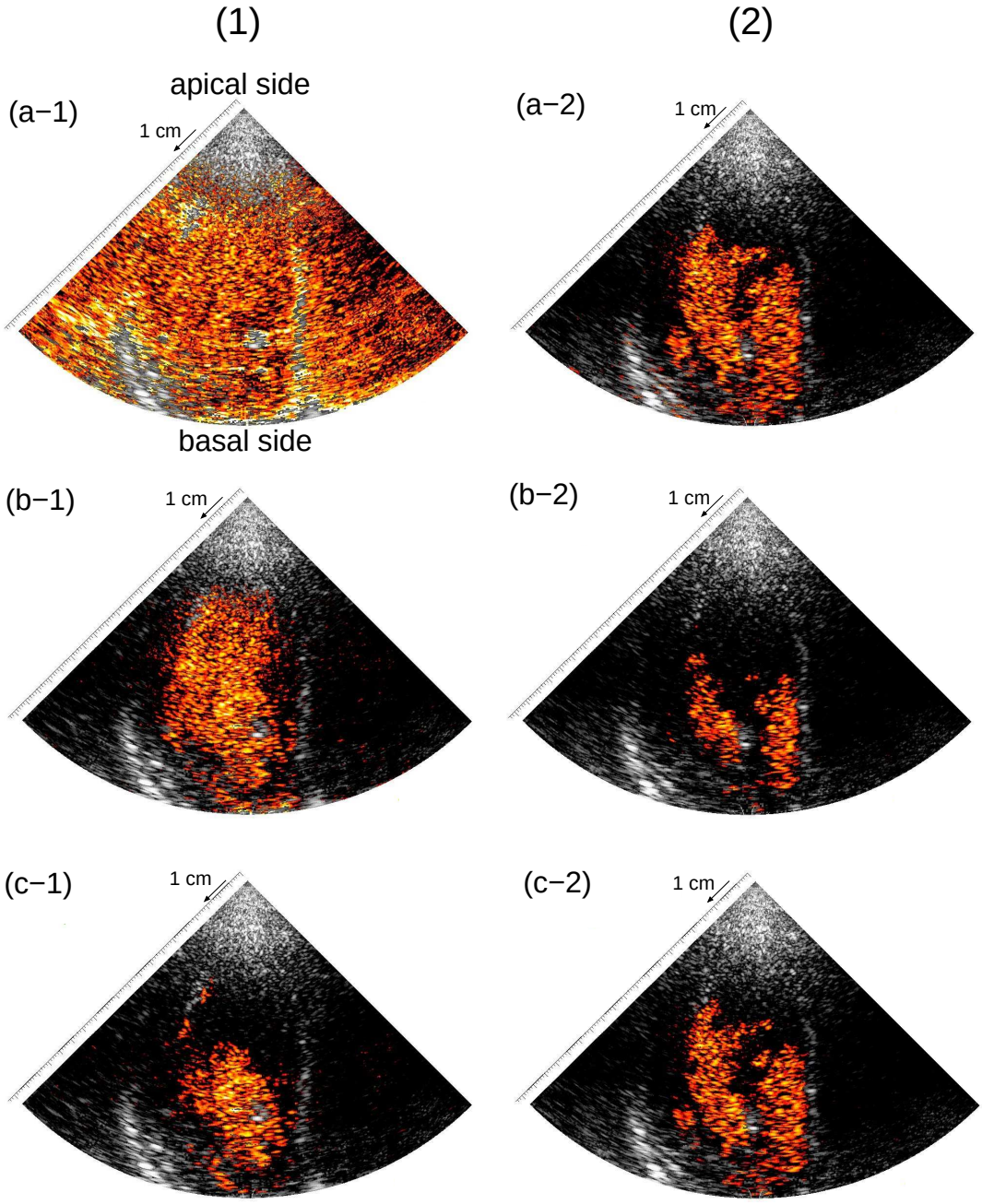

Figure 4.4: Blood echo images obtained in frames in (1) early diastole and (2) mid diastole: (a) by the MTI filtering with a cutoff frequency of 300 Hz, (b) by the MTI filtering with a cutoff frequency of 650 Hz, and (c) by the MTI filtering with cutoff frequencies of 1059 Hz in (1) and 410 Hz in (2) estimated by our proposed method.

2D velocity vector, respectively. As shown in Figs. 4.5(a) and 4.5(b), the blood flowing into and out of the cardiac cavity could be visualized by mapping 2D velocity vectors. Figure 4.6 shows the left ventricular blood velocity vector in mid diastole. The flux rotating in clockwise direction was revealed by 2D blood velocity vector.

The effect of the cutoff frequency of the MTI filter on visualization of vortex blood flow by the 2D velocity vector was investigated. Figure 4.7 shows the 2D velocity vector field of blood flow obtained by the proposed method in the frame during mid diastole at cutoff frequencies of 650, 300, and 410 Hz (the proposed method) in the same frame as Fig. 4.4(2). The flux rotating in clockwise direction was revealed by 2D blood velocity vectors in Fig. 4.7. In Fig. 4.7(a), the discontinuous distribution of velocity vector can be found in the green-colored circle due to low detectivity of echoes from blood particles in the slow flow. The peak values of 2D correlation functions averaged for all velocity vectors were 0.77 in Fig. 4.7(a), 0.86 in Fig. 4.7(b), and 0.85 in Fig. 4.7(c).

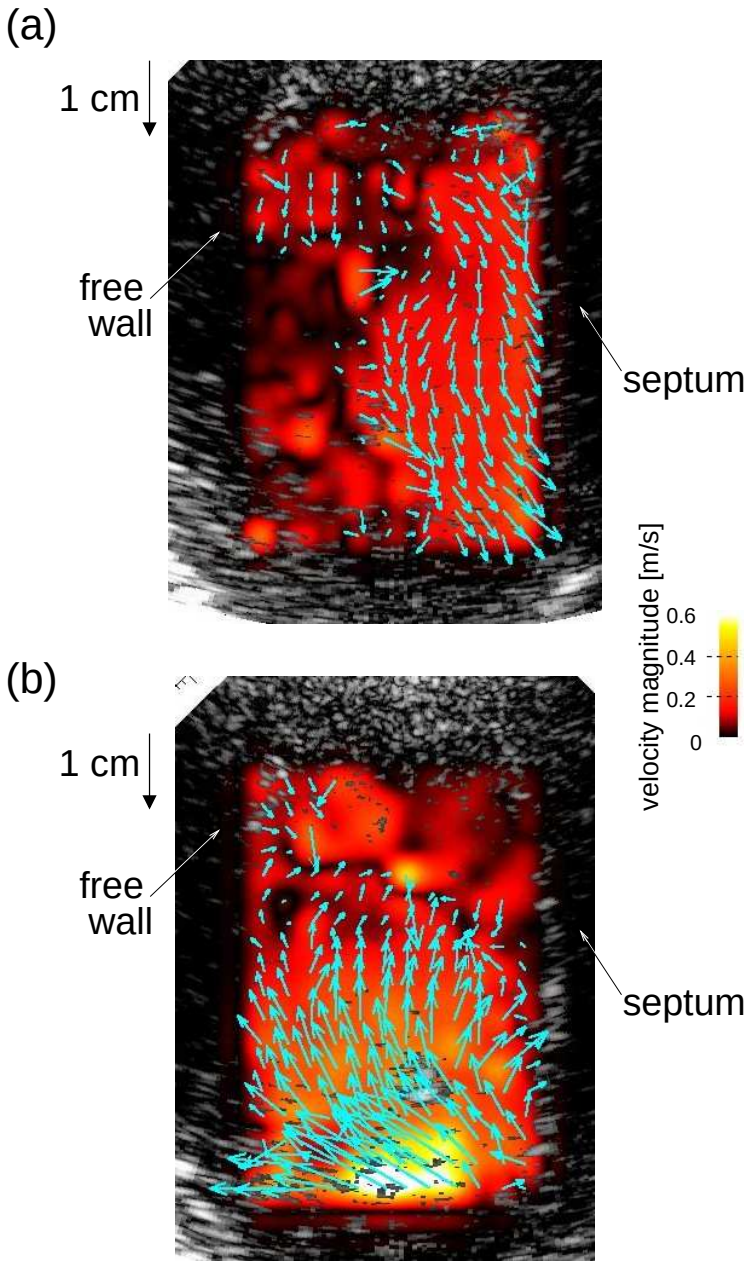

Figure 4.5: 2D velocity vectors of blood flow estimated by speckle tracking with temporally-averaged 2D correlation function in the frames during (a) systole and (b) diastole, respectively. The cyan-colored arrow and the hot color-coded intensity indicate the direction and the magnitude of 2D velocity vector, respectively.

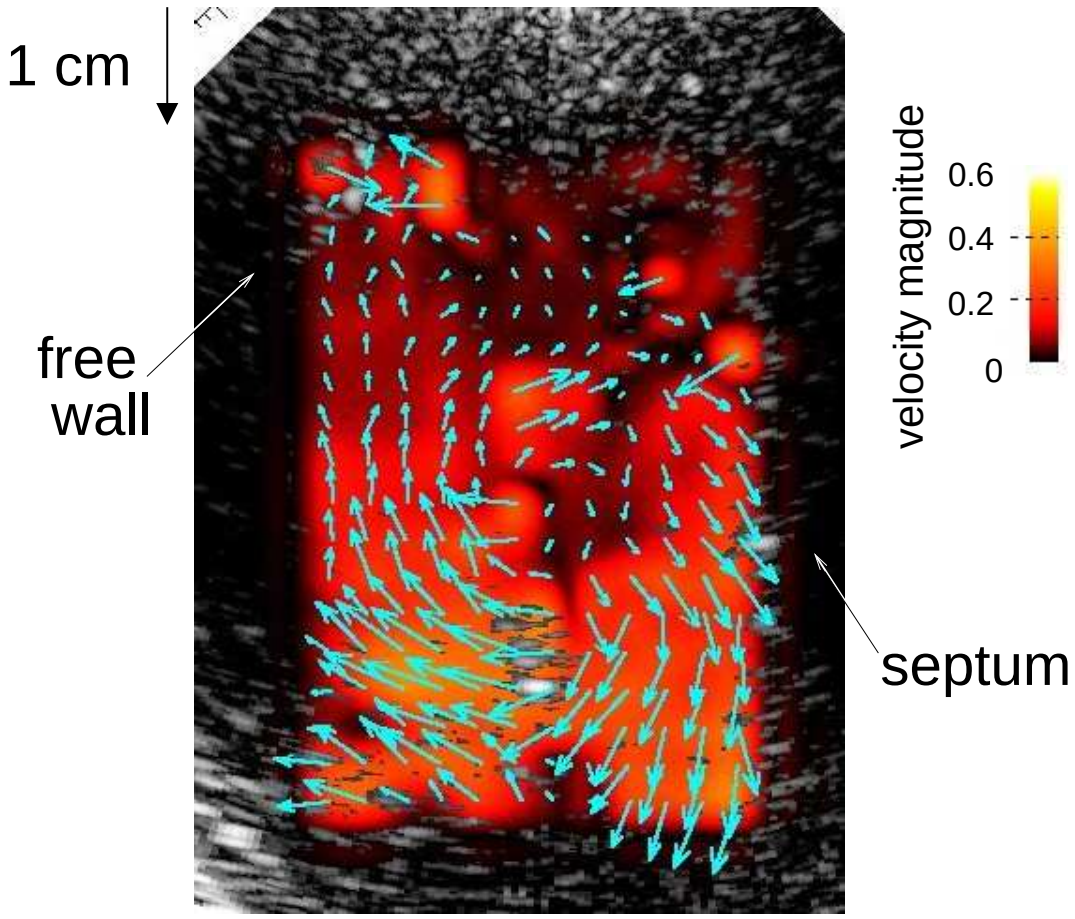

Figure 4.6: Vortex-like blood flow visualized by 2D blood velocity field in the frame during mid diastole.

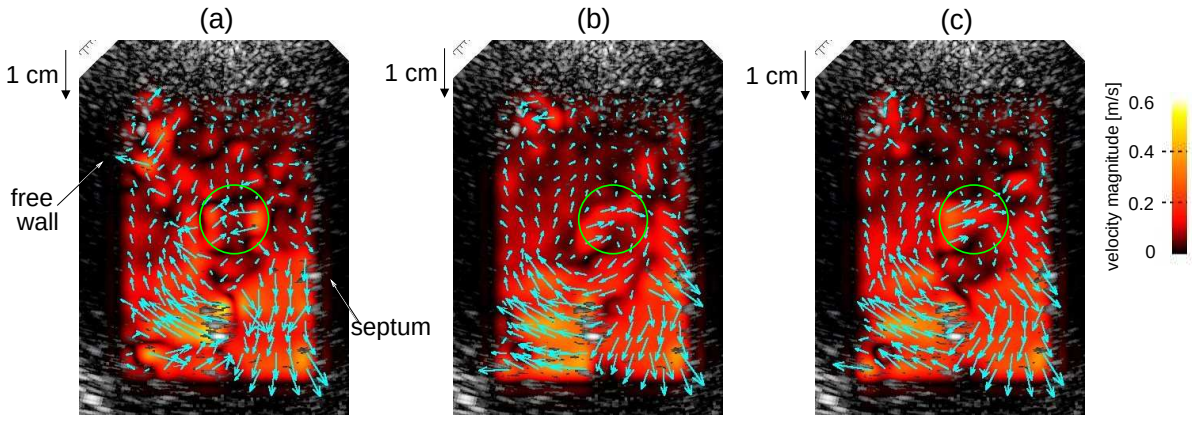

Figure 4.7: 2D velocity vectors of blood flow obtained at fixed cutoff frequencies of (a) 650 Hz, (b) 300 Hz, and at cutoff frequency of (c) 410 Hz determined by our proposed method in mid diastole.

4.4 Discussions

4.4.1 Effectiveness of identification of the heart walls with coherence

In the present study, a method for automatic selection of the cutoff frequency in the MTI filtering was proposed. The aim of this method is to visualize echoes from blood cells in a wider region as possible while clutter echoes from tissues except for blood are suppressed. To estimate the desirable cutoff frequency of the MTI filter, echoes from the heart wall was identified using the k-means clustering method on the basis of the amplitude of echo signals. On the other hand, an alternative method for identification of echoes from

the heart wall using echo amplitude and coherence in the direction of frame has been also proposed by our group [78, 79]. Figures 4.8(a) and 4.8(b) show the distribution of the frame coherence and the region identified as the heart wall by the k-means clustering method using the frame coherence. The regions except for the septum and the free wall were misclassified as the heart wall in Fig. 4.8(b) because the coherence in such region is high.

The reason for such a high coherence in the cardiac lumen was considered to be that echoes from blood cells inside the cardiac lumen was contaminated by sidelobe echoes originated from the surrounding heart wall. In the previous studies in our group [78, 79], parallel receive beamforming with transmission of plane waves in 5 or 7 directions was performed, and the coherence in the direction of frame at each spatial point was estimated using echo signals compounded in different transmissions. Figure 4.9 shows the lateral profile of amplitude of an echo from a wire obtained by the single diverging beam transmission used in the present study and by compounding 7 transmissions of the plane wave with an angular interval of 6 degrees. The wire was placed in water at a range distance of 7 cm from the transducer surface. Ratios of the echo magnitude averaged in lateral angle θ of $-45^\circ < \theta < -4.5^\circ$ and $4.5^\circ < \theta < 45^\circ$ to the peak magnitude were evaluated to be -38.8 dB at the transmission of the single diverging beam and -45.3 dB at the transmission of 7 plane waves. Hence, the echoes originated from side lobes in the case of the compounding of echoes obtained by plane wave transmissions in 7 directions was smaller than in the case of the single diverging beam transmission. As described previously, the number of transmission per frame should be one in order to prioritize increasing the frame rate for visualization of the cardiac blood flow. Under such conditions, the use of the frame coherence is not suitable for identification of the heart wall in ultrahigh-frame-rate measurement. Therefore, echoes from the heart wall was identified only using the echo

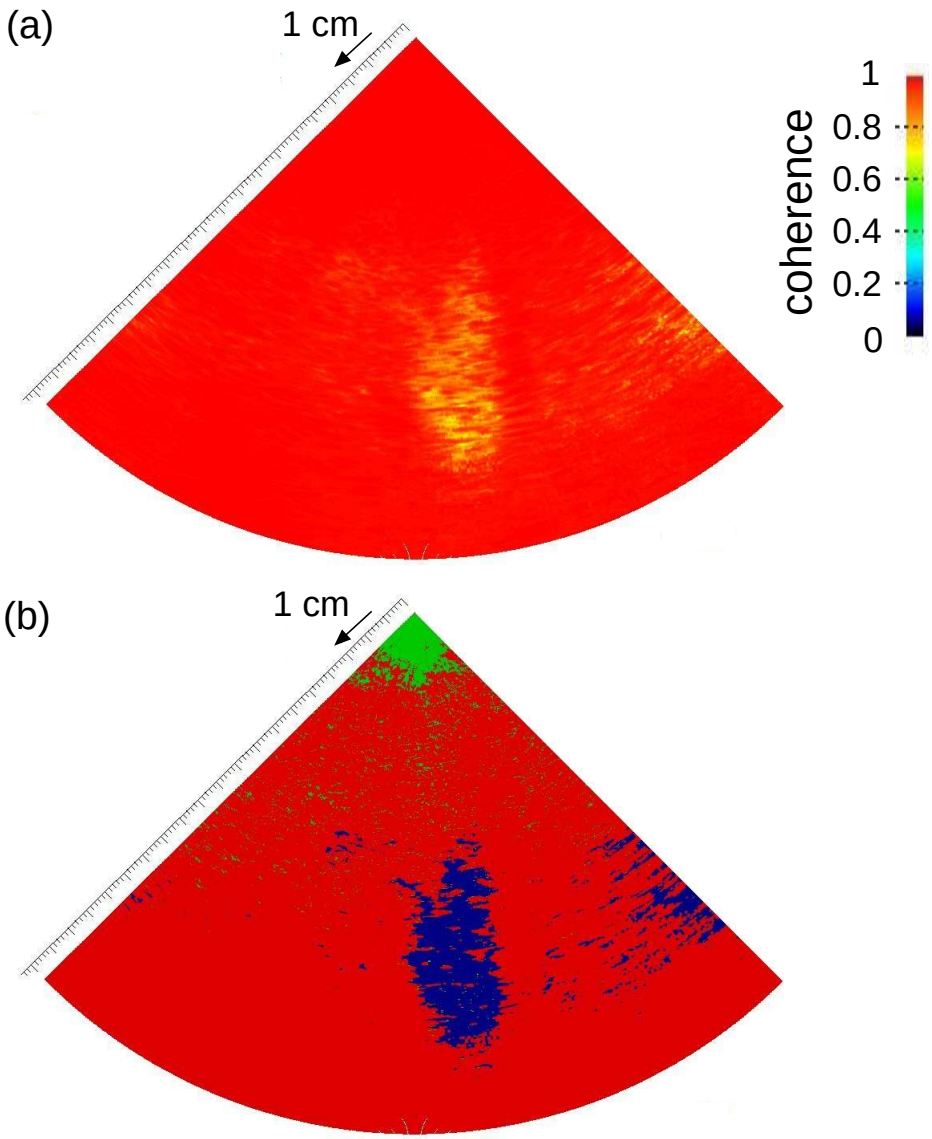

Figure 4.8: (a) Distribution of coherence in direction of frame and (b) distribution of points labeled as the heart wall (red) and ribs (green) by the k-means clustering in the same frame to Fig. 2.8. The coherence was coded according to the right color bar.

amplitude for estimation of the cutoff frequency of the MTI filter in the present study.

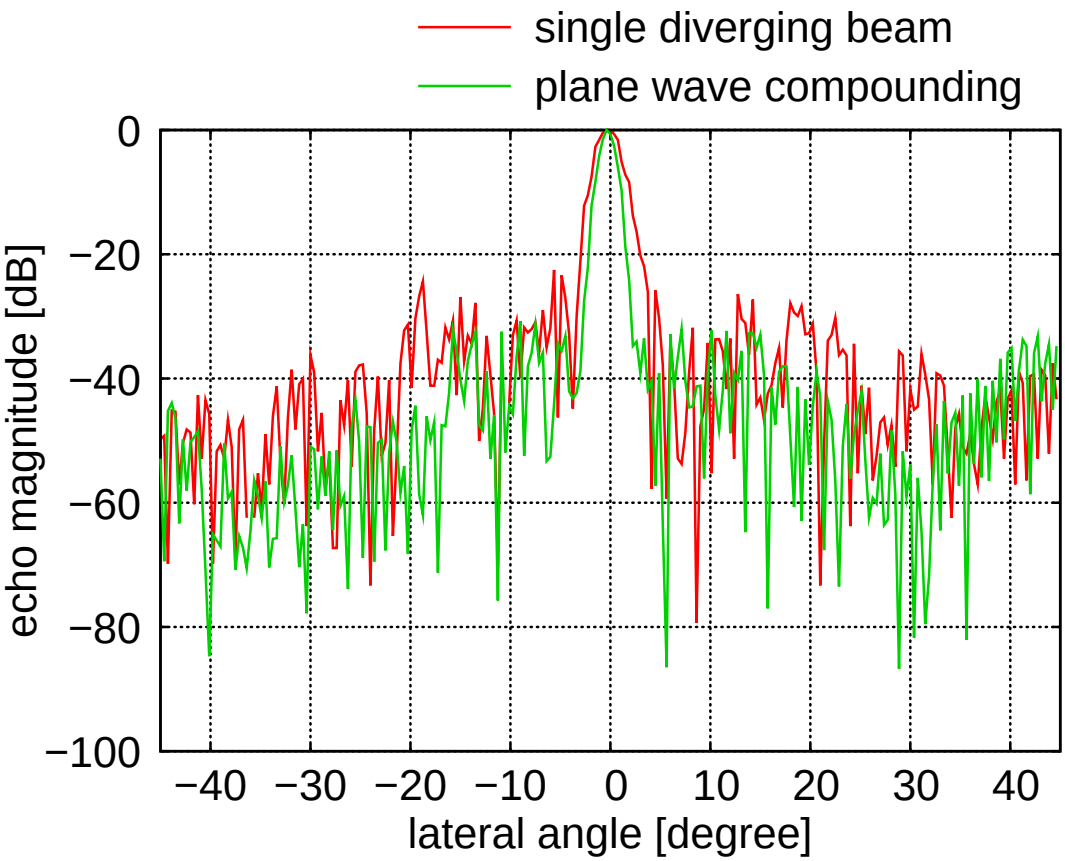

Figure 4.9: Lateral profiles of amplitude of an echo from a wire placed in water at range distance of 7 cm. Amplitude profiles were obtained (a) by the single diverging transmission in the present study (no-compounding) and (b) by compounding with transmissions of plane waves in 7 directions.

4.4.2 Determination of cutoff frequency depending on location

Echoes from blood particles in the apical side were more visualized in the blood echo image in Fig. 4.4(b-1) with a fixed cutoff frequency of 650 Hz as compared to that in Fig. 4.4(c-1) obtained by our proposed method. This means that the blood flow in the

apical side of the cardiac lumen was slow relative to the basal side, and echoes from such region were suppressed by the MTI filtering with the estimated cutoff frequency of 1059 Hz. In early diastole, the leaflets of mitral valve, which is one of clutter sources, independently move very fast due to the inertial force of the blood flowing into the left ventricular chamber. In the proposed method, the spatial variation of the mean frequency in the direction of frame was used for estimation of the desirable cutoff frequency. Therefore, in early diastole, it was considered that the determined cutoff frequency was higher than the desirable one due to the large diversity of velocities in clutter sources.

One of radical solutions for this problem is to determine the cutoff frequency of the MTI filter at each depth by expanding our proposed method. As shown in Fig. 2.7, in high-frame-rate echocardiography with diverging beam transmission, the artifact echoes originated from side lobes are generated in the lateral direction along the wave front of the diverging beam across a clutter source. Here, the cutoff frequency of the MTI filter was over-estimated due to the large diversity of velocities in clutter sources. Hence, it can be effective that the cutoff frequency of the MTI filter is adaptively changed at each depth according to the velocity of the clutter source such like ribs, the heart wall, and the cardiac valve. For consideration of the feasibility of this method, mean frequencies of echoes from the heart wall and the leaflet in the direction of frame were obtained using echoes from the corresponding regions in the same frame as Fig. 4.4(1). Echoes from the regions filled in red in Fig. 4.10(a) were used for evaluation of the mean frequencies. Using the auto-correlation technique, the mean frequencies $\{\mu\}$ of the regions on the apical side of the septum and the leaflet of the mitral valve were evaluated to be 230 Hz and 409 Hz, respectively. Then, for evaluation of the effect of the MTI filtering adaptively changed depending on location, the cutoff frequency of the MTI filter over the whole region was determined as $f_{cut.sp} = \mu + 3\sigma$ using the mean frequency μ and the standard deviation

σ in the direction of frame obtained with echoes from either the septum or the leaflet. Figures 4.10(b) and 4.10(c) show the blood echo images obtained by the cutoff frequencies of 665 Hz and 548 Hz determined with echoes from the regions on the leaflet and the septum indicated in Fig. 4.10(a), respectively. The cyan-colored lines indicate a region on the apical side of the left ventricular lumen. Echoes from blood particles in this apical region in Fig. 4.10(c) were stronger than those in Fig. 4.10(b). Therefore, the MTI filtering adaptively changed depending on location would be effective to increase the detectivity of blood flow.

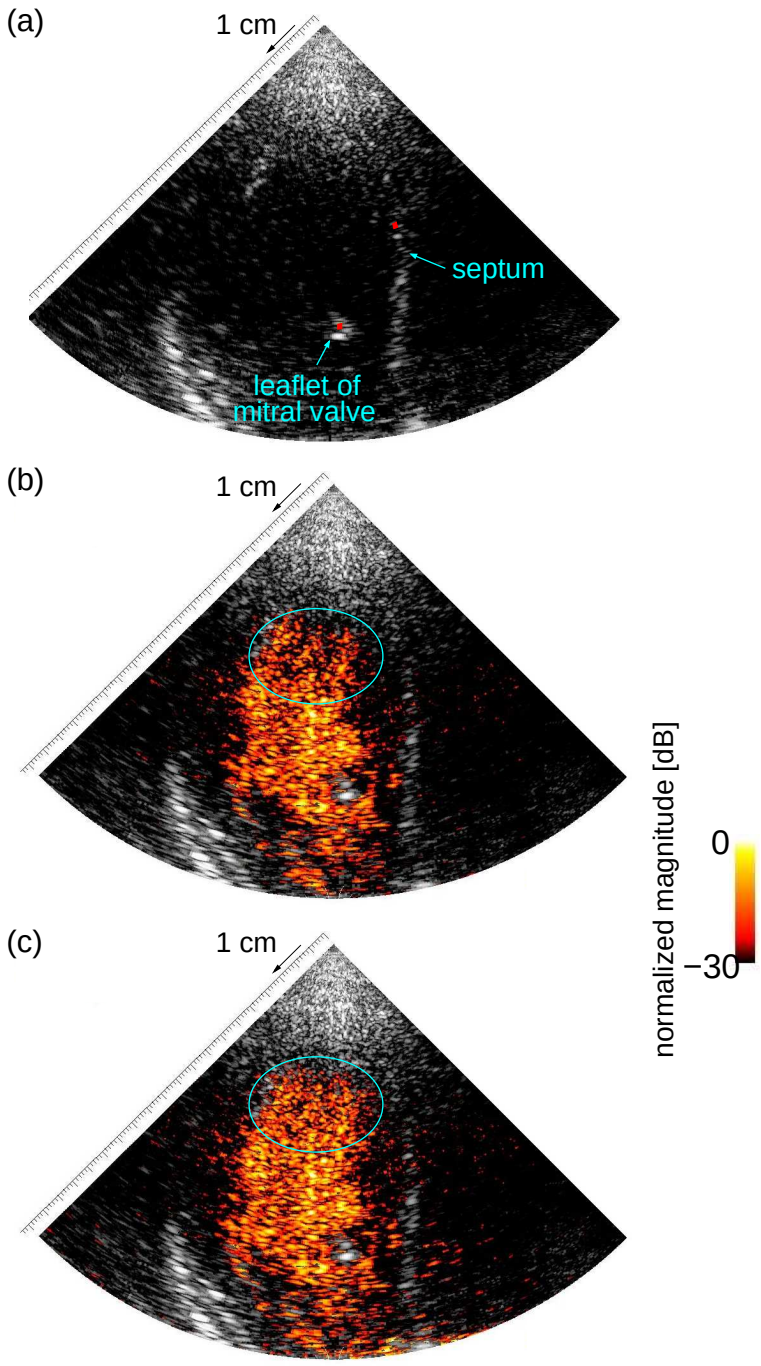

Figure 4.10: (a) Regions assigned for evaluation of mean frequencies and for determination of cutoff frequencies. Echoes in the regions on the septum and the leaflet filled in red were used. Blood echo images obtained by the cutoff frequencies determined using echoes from (b) the leaflet and (c) the septum.

4.4.3 Sequence of echo acquisition for finer B-mode imaging

In this study, the weighting by PCF-SB was used to improve the quality of the B-mode image degraded due to a single transmission of unfocused ultrasound. A case of requiring B-mode image with a better quality is conceivable when an operator desires to observe motions of the heart walls more accurately. A procedure for acquisition of a finer B-mode image is discussed in this section.

To acquire a B-mode image with a better image-quality, a large number of steered diverging beams for compounded B-mode imaging were interleaved before every transmitting event for estimation of blood velocity vector. Hence, the transmission sequence comprised transmissions of steered diverging beams for acquisition of compounded B-mode images and a single non-steered diverging beam per frame for estimation of velocity vector of blood flow as illustrated in Fig. 4.11(a). In the transmission event for B-mode imaging, 15 diverging beams with angular intervals of 6 degrees were transmitted and the corresponding beamformed signals were compounded to produce a B-mode image with a better image quality as shown in Fig. 4.11(b). On the other hand, in the transmission event for blood vector acquisition, a single non-steered diverging beam is transmitted and the beamformed signals is generated without compounding as shown in Fig. 4.11(c). This diverging beam is transmitted to the same direction in 40 frames for a robust estimation of velocity vector by averaging 2D correlation functions. Consequently, the acquisition frame rate FR of the B-mode image with the distribution of blood velocity vector is defined as:

$$FR = \frac{PRF}{N_{\mathrm{tx1}} + N_{\mathrm{tx2}}}, \tag{4.1}$$

where PRF, N_{tx1}, and N_{tx2} are the pulse repetition frequency, the number of steered diverging beam transmission for B-mode imaging, and the number of transmissions of

the non-steered diverging beam for blood velocity vector estimation, respectively. In the present study, PRF, N_{tx1}, and N_{tx2} were set at 6024 Hz, 15, and 40, respectively; therefore, the eventual frame rate was 109 Hz.

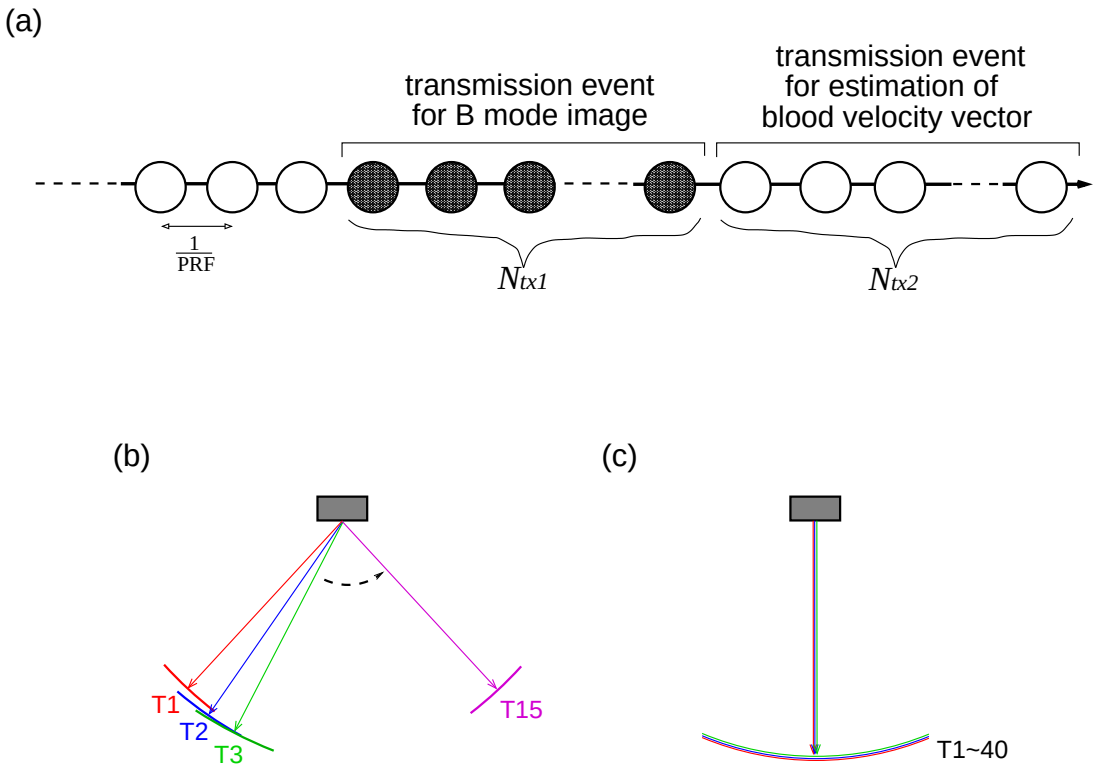

Figure 4.11: Sequence of transmissions of diverging waves for simultaneous acquisition of compounded B-mode image and 2D velocity vectors of blood flow inside cardiac chamber.

The virtual point sources used for B-mode and blood velocity vector imaging were located at 100 and 50 mm behind the array surface. Figures 4.12(a)-4.12(c) show the obtained distributions of 2D blood velocity vectors with compounded B-mode images in frames in early systole, early diastole, and mid diastole, respectively. The mitral valve and the aortic valve were located in the basal side of the left ventricle. As shown in Figs. 4.12(a) and 4.12(b), the fluxes flowing into and out of the cardiac cavity were visualized by blood flow vectors in early systolic and early diastolic phases. In mid diastole, the vortex-

like flow appeared as shown in Fig. 4.12(c). The feasibility of simultaneous acquisition of the fine B-mode image and the 2D velocity vector image by the proposed procedure was shown.

The multiple transmissions of diverging waves with different steered angles were interleaved for compounded B-mode imaging. Hence, the proposed procedure compromised to visualize dynamic motions of echoes from flowing blood cells due to a low frame rate. Nevertheless, the frame rate of the procedure is comparable to that of several tens hertz of conventional CDI, and the blood velocity vector in the cardiac lumen can be estimated, which is the technical merit of the proposed procedure.

4.5 Conclusion

Blood flow inside the left ventricular cavity of a healthy volunteer were visualized by the proposed method. First, the effect of adaptive MTI filtering was verified. Although the effect in rapid filling phase was imperfect, a better visualization of vortex flow in mid diastole was achieved by the proposed adaptive MTI filtering. Then, 2D velocity vectors estimated by speckle tracking with averaging 2D correlation functions were mapped in the cardiac cavity. The vortex-like blood flow was visualized in mid diastole. Such *in vivo* experimental results showed that visualization of blood flow patterns in the cardiac lumen with the proposed method was feasible.

On the other hand, to obtain finer B-mode images and 2D velocity vectors simultaneously, an alternative procedure of transmission of diverging beams was proposed, and its feasibility was also shown through an *in vivo* measurement.

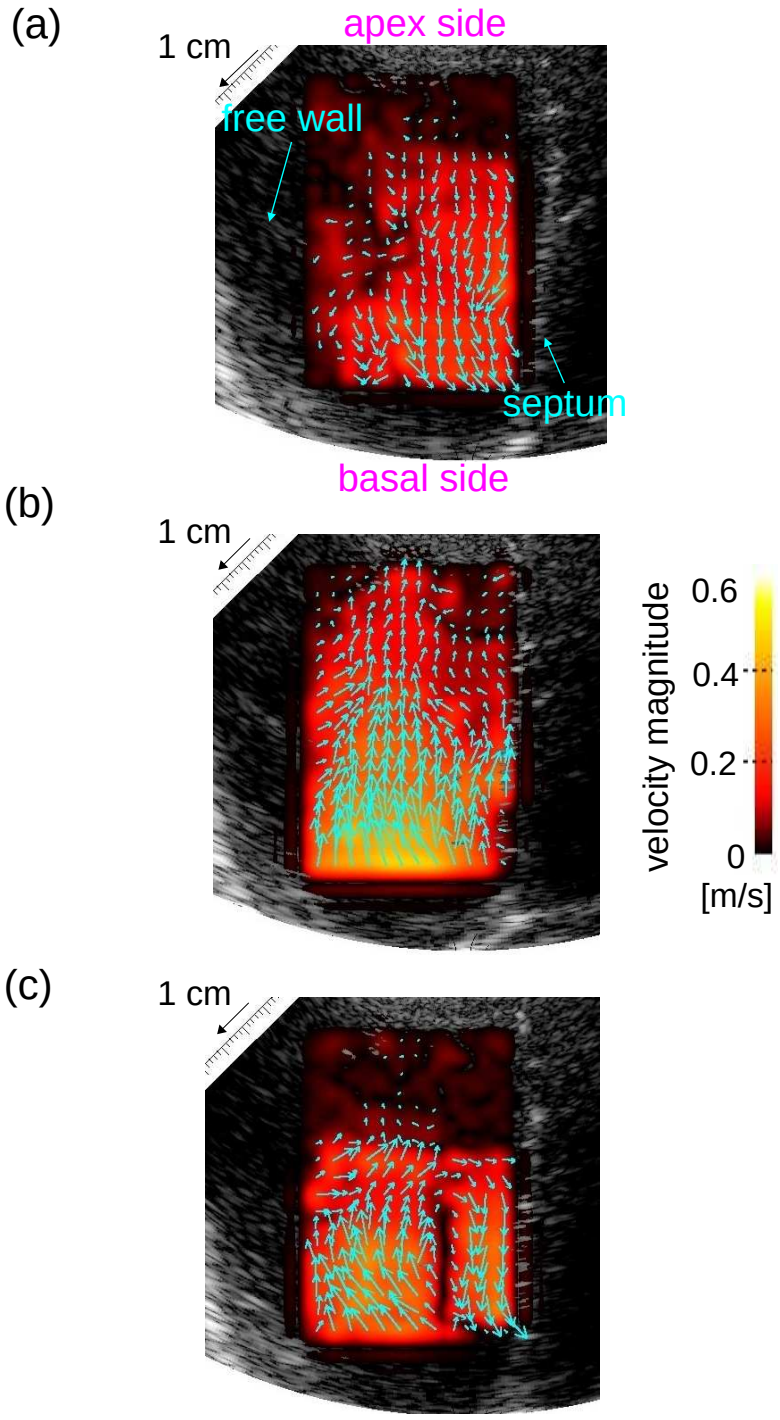

Figure 4.12: Velocity vector images of the cardiac lumen obtained by sequence of transmissions of diverging waves for acquiring compounded B-mode image and 2D velocity vectors of blood flows in the frames for (a) systole, (b) early diastole, and (c) mid diastole.

Chapter 5

Overall conclusion

In this thesis, a method of high-frame-rate imaging of echoes from blood cells was studied for visualization of complex behaviors of blood flow in the cardiac cavity. An imaging technique of echoes from blood cells at a better quality with high-frame-rate echocardiography was proposed. The blood echo image allowed the human eyes to perceive flow directions through motions of echoes from flowing blood cells. A finer estimator of the 2D blood velocity vector was proposed and its accuracy was evaluated through a phantom experiment. Chapters are concluded particularly in what follows.

Chapter 1 gives an introduction on a background, conventional methods, and research objective.

In Chapter 2, the strategy for imaging of echoes from blood cells with high-frame-rate echocardiography was described. Two different methods for improvement of the image-quality were presented; weighting techniques with coherence of changes in phases of echoes in the direction of frame and with PCF-SB using MTI-filtered echoes received by individual transducer element. In addition, a method for adaptive MTI filtering based on velocities

of heart walls was described.

In Chapter 3, a method of estimation of 2D blood velocity vector with speckle tracking was described. In the proposed method, 2D correlation functions were temporally averaged for a stable estimation of 2D velocity vector. The effect of the averaging process of 2D correlation functions was investigated through a steady flow experiment. The relationship between the duration for averaging of 2D correlation functions and the factors which improve the accuracy was examined. Moreover, the influence of the angle between the flow axis and the beam direction on the accuracy was examined.

In Chapter 4, flowing blood inside the cardiac cavity of a healthy human heart were visualized by the proposed method. Furthermore, the effect of adaptive MTI filtering was verified. The imaging of a vortex-like blood flow inside the cardiac cavity was achieved by the distribution of 2D velocity vectors. These *in vivo* experimental results showed that high-frame-rate imaging of blood flow patterns in the cardiac lumen was feasible. On the other hand, an alternative procedure of transmissions of diverging beams for acquisition of a fine B-mode image was proposed, and its feasibility was also shown through an *in vivo* measurement.

As described above, dynamic motions of echoes from blood cells could be perceived owing to ultrahigh-frame-rate measurement. Because real motions of flowing blood cells are visualized by the proposed method, the assessment of the cardiac pumping efficiency derived from complex flow structures would be possible by blood echo imaging.

Appendix A.

Effect of compounding technique on blood echo imaging

In high-frame-rate echocardiography, discontinuities of echo intensities occur in an ultrasound image because the transmit-receive directivity significantly changes due to the large interval between neighboring transmit beams. To compensate such blur, compounding (averaging) echo signals obtained by transmissions at different steering angles is effective [60]. In the compounding technique, individual beamformed RF signals are obtained by transmitting unfocused waves with different steering angles and, then, these RF signals at the same spatial point are averaged in different transmissions. It has been also shown that the compounding technique by tilted plane wave transmissions with a linear array transducer contributes to improve the image quality [66]. The effect of the compounding technique on the blood echo imaging is examined in what follows.

The effect of compounding technique on imaging of heart walls has been examined in the cited study [60]. Our objective is to visualize echoes from flowing blood cells at a high frame rate. However, coherent compounding is difficult when the phase of the echo signals from fast moving objects differs significantly among emissions [73]. The compounding technique weakens echoes from blood particles if done incoherently. Therefore, the difference of

velocities between heart walls and blood flow is considerable for fine blood echo imaging without incoherent compounding. Let me assume that the pulse repetition frequency is 160 μs and the velocity of blood flow is 1 m/s. Under these conditions, the movement between transmissions can be calculated as 160 μm. An wavelength of ultrasound is assumed to be 408 μm at a frequency of 3.75 MHz and a propagation velocity of 1530 m/s. Under such assumptions, flowing blood cells can move at the distance of a half of wavelength. Therefore, it is possible to compensate echoes from blood particles by the compounding procedure.

The effect of incoherent compounding for flowing scatterers was examined through a steady flow measurement. The spherically diverging wave was transmitted in three directions and steered at -10, 0, and $+10$ degrees. Echo signals were MTI-filtered to enhance echoes from flowing particles. The cutoff frequency of the MTI filter was set at 500 Hz, corresponding to a velocity of 0.1 m/s at a ultrasound frequency of 3.75 MHz. The envelope signals were detected from high-pass-filtered RF signals in each transmission to remove the phase information. In this experiment, the envelope signals of high-pass-filtered RF signals in each transmission were compounded (summed) to avoid the incoherent compensation by removing the phase information. At first, the MTI filtering was applied to beamformed RF signals obtained from each transmission. Then, envelopes of filtered RF signals of individual transmission were detected and these envelope signals at the same spatial point were compounded (averaged). To examine the effect of incoherent sum in the conventional compounding method, the accuracy of velocity vector estimation with the conventional compounding (i.e., RF compounding) and the envelope compounding was evaluated as described subsequently.

A blood-mimicking fluid (Shelly Medical Imaging Technologies US model) steadily

flowed through a cylindrical tube was measured by ultrasound. The internal and external diameters of the tube made of urethane rubber were 8 and 12 mm, respectively. The distance between the outer surface of the tube anterior wall and the probe surface was set at 5 cm. The angle between the probe surface and the tube was maintained at 15°. The tube contained 5% carbon powder (by weight) to obtain sufficient scattering from the wall for the identification of the walls, between which the blood-mimicking fluid flowed. The Reynolds number reached up to 1070 under the experimental conditions.

The velocity vector of the flow was estimated by applying speckle tracking to the distributions of envelope signals in two successive frames. Here, the envelope signals were obtained through envelope compounding or envelope detection after RF compounding. The kernel sizes in the lateral and axial directions in speckle tracking were set to 9 degrees and 4.6 mm, respectively. To estimate small displacements, the cross correlation function was up-sampled [77] by factors of 120 and 10 in the lateral and axial directions, respectively. The velocity vectors of the fluid inside the tube were estimated at 0.5 mm intervals along the manually assigned line. The velocity components along the direction of the flow axis were averaged as follows:

$$V = \frac{1}{N_j} \sum_{j=0}^{N_j-1} \boldsymbol{v}_j \cdot \boldsymbol{n}_f, \tag{1}$$

where A, $\boldsymbol{v}_j$, and $\boldsymbol{n}_f$ denote the cross-sectional area where the blood-mimicking fluid flowed, the estimated velocity vector at the j-th spatial point, and the unit vector parallel to the flow axis, respectively.

Figure A1 shows averaged velocities along the flow axis obtained by the RF compounding and the envelope compounding, respectively. As shown in Fig. AA1, although the differences between estimates and the true velocities appeared, the accuracy of velocity estimation with envelope compounding became much higher than that with RF compound-

ing. The low accuracy of velocity estimation with RF compounding would be caused by compensation among echoes from mimicking particles. Hence, it was verified that the conventional compounding procedure was unsuited for the blood echo imaging.

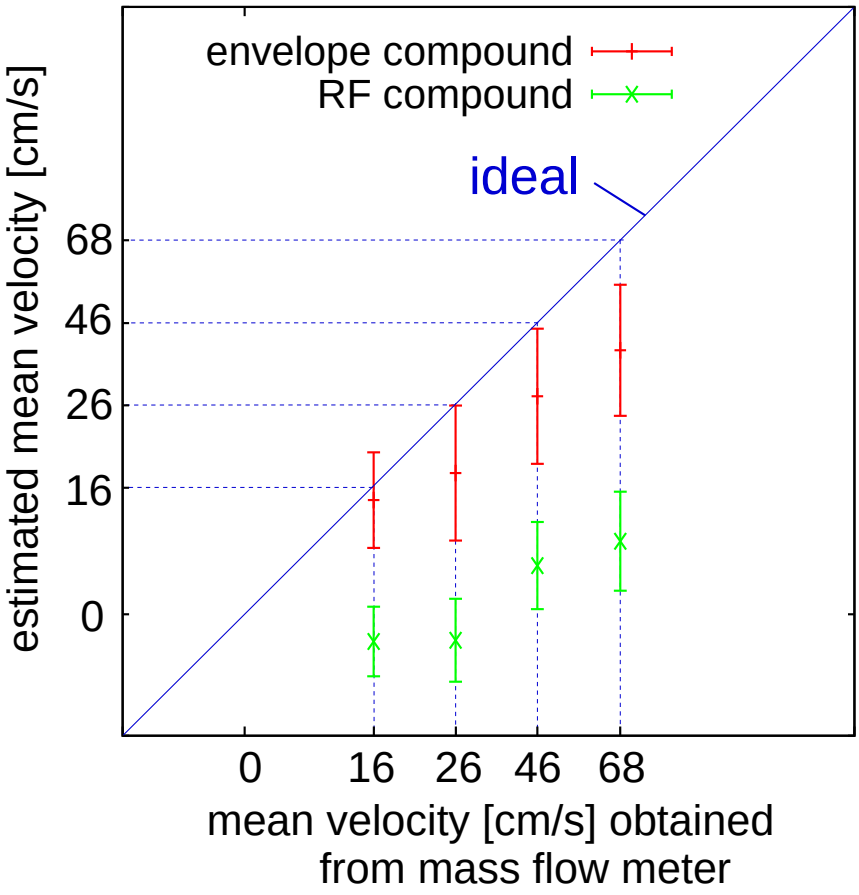

Figure A1: Averaged velocities along the flow axis obtained by the RF compounding and the envelope compounding.

Appendix B.

Estimation of streamline of blood flow

As for PC-MRI and E-PIV, visualization of streamline and pathline (time-resolved path) line have been performed. Streamline and pathline are useful tools for understanding fields of flow vectors by the human eyes. Streamline is defined as a trajectory of a particle flowing in a constant flow field, which is calculated by accumulating velocity vectors. These velocity vectors are assumed to be constant for the computation. On the other hand, pathline is defined as a trajectory of a particle flowing over time. Velocity vectors are accumulated for estimation of pathlines as well, but each particle is followed over time (i.e. in the direction of frame). In other words, streamline estimation is an Euler method and, on the other hand, pathline estimation is a Lagrange method.

Computation of streamline or pathline on a 2D ultrasonic image is theoretically impossible because the radical 3D motion of a particle cannot be computed using 2D velocity vectors which are obtained on a 2D plane. Here, streamlines of cardiac blood flow on a 2D ultrasound image was estimated with an assumption in which out of plane velocity from the image plane is zero. Note that streamlines obtained by this method are pseudo due to such assumption. Such pseudo streamline was computed by the 4th-order Runge-

Kutta method [80] with the distribution of velocity vectors. The feasibility of estimation of pseudo streamline using 2D velocity vectors obtained by the proposed method was examined through an *in vivo* experiment.

As described in Chapter 4, the distribution of velocity vectors estimated by speckle tracking with 2D correlation function averaging were interpolated with a reconstructive interpolation [77] to obtain the densely-mapped velocity vectors. The flow streamline was estimated by recursively computing the approximation of the 4th-order Runge-Kutta method defined as [80]

$$\begin{aligned}
\mathbf{p}_{n+1} &= \mathbf{p}_n + \frac{\Delta t}{6}\left(\mathbf{k}_1 + 2\mathbf{k}_2 + 2\mathbf{k}_3 + \mathbf{k}_4\right), \\
\mathbf{k}_1 &= \mathbf{f}\left(\mathbf{p}_n\right), \\
\mathbf{k}_2 &= \mathbf{f}\left(\mathbf{p}_n + \frac{\Delta t}{2}\mathbf{k}_1\right), \\
\mathbf{k}_3 &= \mathbf{f}\left(\mathbf{p}_n + \frac{\Delta t}{2}\mathbf{k}_2\right), \\
\mathbf{k}_4 &= \mathbf{f}\left(\mathbf{p}_n + \Delta t\mathbf{k}_3\right), \\
\mathbf{p}_n &\approx \mathbf{p}\left(\tau_0 + n\Delta t\right), \qquad (2)
\end{aligned}$$

where, $\mathbf{p}$, Δt, and $\mathbf{f}(\mathbf{p})$ denote the position, the step size (set to 1 ms), and the velocity vector at $\mathbf{p}$, respectively. The velocity vector in Eq. (2) was assumed to be constant; therefore, the velocity vector field in a frame was used for calculation of streamlines. Figure B1 illustrates a streamline computed using a 2D velocity vector field. As shown in Fig. B1, the streamline was computed recursively by increasing a variable n (advancing the virtual clock time $\tau = \tau_0 + n\Delta t$). The pseudo streamline can be calculated by accumulating 2D velocity vectors from an initial point in a frame.

Figure B2 shows pseudo streamlines in the cardiac cavity of a healthy volunteer obtained by the proposed method in rapid filling phase. Departure and terminal points of a stream-

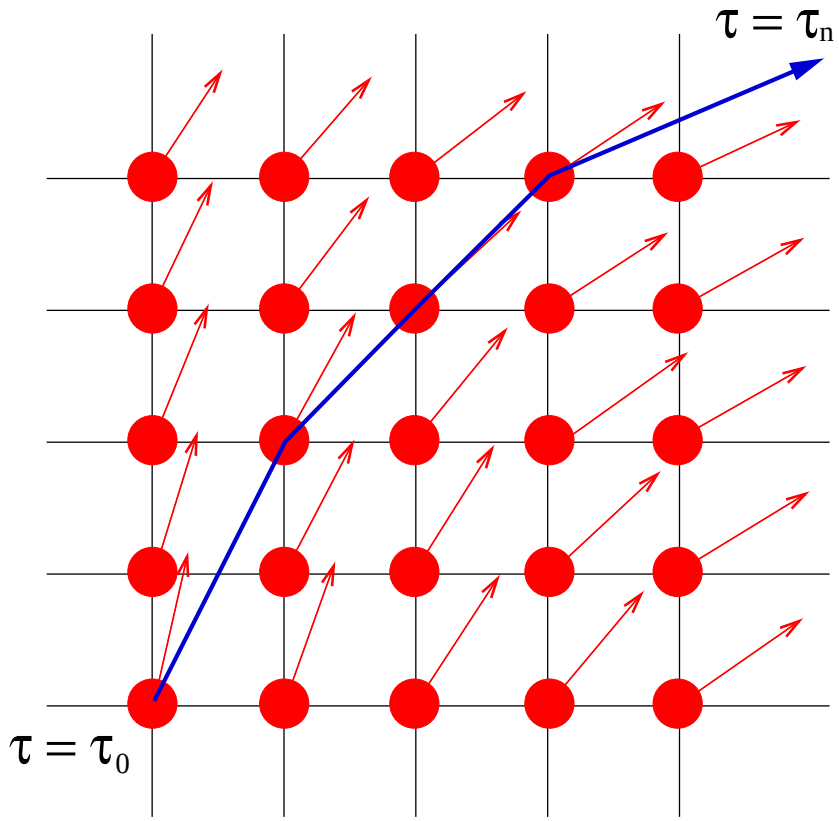

Figure B1: Illustration of streamline obtained from 2D velocity vector field. Blue and red colored arrows denote streamline and 2D velocity vector. Red colored circles represent pixel positions.

line were denoted by green and blue squares. The initial point $\mathbf{p}_0$ in Eq. (2) was manually assigned, which corresponds to the departure point in Fig. B2. To obtain a more stable distribution of velocity vectors, N_{cf} was set to 28 frames in estimation of streamlines. The blood flow toward the apex side of the heart was visualized by the obtained streamline in rapid filling phase.

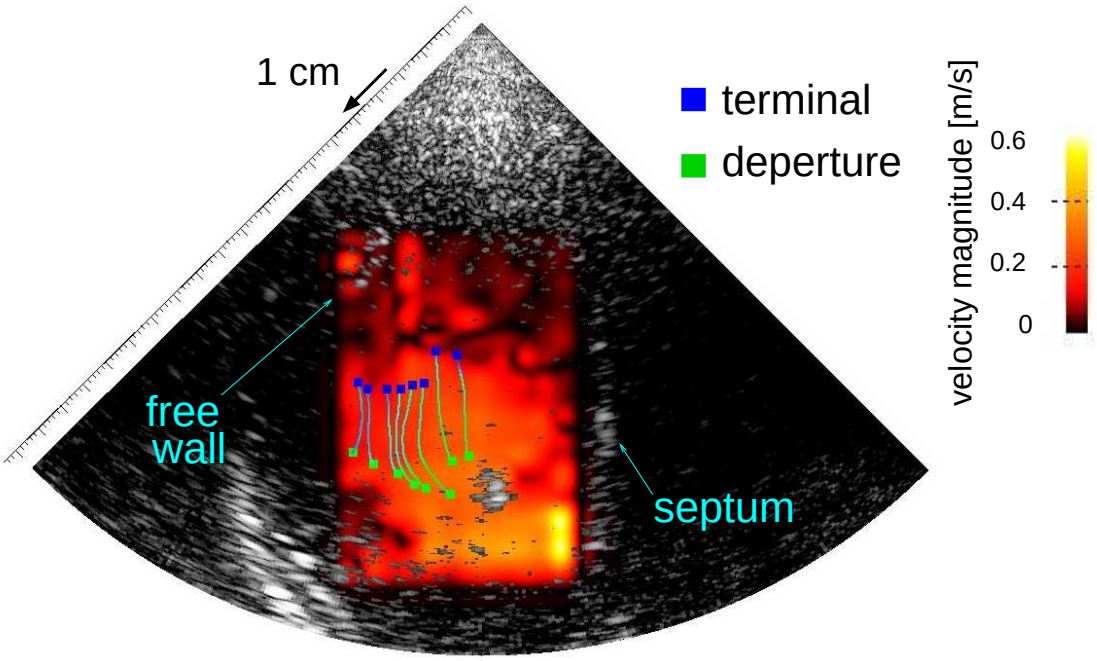

Figure B2: Pseudo streamlines of left ventricular blood flow with B-mode image during rapid filling phase.

List of peer reviewed papers

1. H. Takahashi, H. Hasegawa, and H. Kanai, "Identification of Heart Wall Based on Coherence among Ultrasonic RF Echoes," *Japanese Journal of Ultrasonics*, Vol. 36, No. 6, pp. 679-681 (November 2009) [in Japanese].

2. H. Takahashi, H. Hasegawa, and H. Kanai, "Automated Identification of the Heart Wall Throughout the Entire Cardiac Cycle Using Optimal Cardiac Phase for Extracted Features," *Japanese Journal of Applied Physics*, Vol. 50, No. 7, pp. 07HF16-1-07HF16-9 (July 2011).

3. H. Takahashi, H. Hasegawa, and H. Kanai, "Improvement of Automated Identification of the Heart Wall in Echocardiography by Suppressing Clutter Component," *Japanese Journal of Applied Physics*, Vol. 52, No. 7, pp. 07HF17-1-07HF17-7 (July 2013).

4. H. Takahashi, H. Hasegawa, and H. Kanai, "Echo Speckle Imaging of Blood Particles with High-Frame-Rate Echocardiography," *Japanese Journal of Applied Physics*, Vol. 53, No. 7, pp. 07KF08-1-07KF08-7 (June 2014).

5. H. Takahashi, H. Hasegawa, and H. Kanai, "Temporal Averaging of Two Dimensional Correlation Functions for Velocity Vector Imaging of Cardiac Blood Flow," *Journal of Medical Ultrasonics* (in press).

List of international conference papers

1. H. Takahashi, H. Hasegawa, and H. Kanai, "Automated Identification of the Heart Wall Region on Echocardiogram Using Classification of RF Signals," 5th International Symposium on Medical, Bio- and Nano-Electronics in Sendai P-24, pp. 141-42 (February 24-25, 2010, Sendai, Japan).

2. H. Takahashi, H. Hasegawa, and H. Kanai, "Automated Identification of the Heart Wall in Echocardiographic Images Throughout a Cardiac Cycle," SICE Annual Conference 2012, pp. 1171-76 (August 20-23, 2012, Akita, Japan).

3. H. Takahashi, H. Hasegawa, and H. Kanai, "Automated Identification of the Heart Wall on Echocardiogram Throughout a Cardiac Cycle," Medicinteknikdagarna, p. 83 (October 2-3, 2012, Lund, Sweden).

4. H. Takahashi, H. Hasegawa, and H. Kanai, "Fast Cardiac Blood Flow Imaging by Visualization of Ultrasonic Echoes from Blood Particles," 32nd International Acoustical Imaging Symposium (AI32), p. 34 (April 29 - May 1, 2013, Singapore).

5. H. Takahashi, H. Hasegawa, and H. Kanai, "High Frame Rate Blood Flow Imaging by Visualization of Ultrasonic Echoes from Blood Particles in Echocardiography," 2013 International Congress on Ultrasonics (ICU2013), pp. 581-85 (May 2-5, 2013,

Singapore).

6. H. Takahashi, H. Hasegawa, and H. Kanai, "Speckle-Enhanced Cardiac Blood Flow Imaging with High Frame Rate Ultrasound, 2013 Joint UFFC, EFTF and PFM Symposium, pp. 2030-33 (July 21-25, 2013, Prague, Czech Republic).

7. H. Takahashi, H. Hasegawa, and H. Kanai, "High Frame Rate Imaging of Cardiac Blood Flow by Visualization of Echoes from Blood Particles," 7th World Congress of Biomechanics, 8-19. Image-based Measurements, (July 6-11, 2014, Boston, USA).

8. H. Takahashi, H. Hasegawa, and H. Kanai, "Intraventricular Blood Flow Vector and Streamline Imaging Using High Frame Rate Cardiac Ultrasound," 2014 IEEE International Ultrasonics Symposium Proceedings, pp. 341-44 (September 3-6, 2014, Chicago, USA).

List of domestic conference papers

1. H. Takahashi, H. Hasegawa, and H. Kanai, "Automatic Identification of the Heart Walls Using Multiple Features Extracted from Ultrasonic RF Echoes," 2009 Tohoku-section Joint Convention record of Institutes of Electrical and Information Engineers 1E03, p. 137 (August 20-21, 2009, Sendai) [in Japanese].

2. H. Takahashi, H. Hasegawa, and H. Kanai, "Automatic Identification of the Wall Region in Echocardiography," The 38th Scientific Meeting of Tohoku-section of the Japan Society of Ultrasonics in Medicine 38-24, p. 14 (September 6, 2009, Fukushima) [in Japanese].

3. H. Takahashi, H. Hasegawa, and H. Kanai, "Automatic Identification of the Heart Wall Region Using Classification of Feature Vector of Ultrasonic RF Echoes," The 43rd Conference of Tohoku-section of Japanese Society for Medical and Biological Engineering A1-2, p. 9 (November 21, 2009, Fukushima) [in Japanese].

4. H. Takahashi, H. Hasegawa, and H. Kanai, "Automated Identification of Heart Wall by Classification of Ultrasonic RF Echoes in Feature Space," The Institute of Electronics, Information and Communication Engineers (IEICE) Technical Report, Ultrasonics, Vol. 109, No. 388, US2009-103, pp. 87-92 (January 25-26, 2010, Osaka) [in Japanese].

5. H. Takahashi, H. Hasegawa, and H. Kanai, "Automated Identification of Heart Wall

on Ultrasonic RF Echoes Using Classification Method in 2-D Feature Space," Reports of the 2010 Spring Meeting of the Acoustical Society of Japan 1-2-7, pp. 1427-1428 (March 8-10, 2010, Tokyo) [in Japanese].

6. H. Takahashi, H. Hasegawa, and H. Kanai, "Examination of Optimum Cardiac Phase for Feature Extraction of Ultrasonic RF Echoes Toward Automatic Identification of the Heart Walls," The 64th Ultrasonics Electronics Meeting 64-6 (June 10, 2010, Sendai) [in Japanese].

7. H. Takahashi, H. Hasegawa, and H. Kanai, "Determination of Optimum Cardiac Phase in Feature Extraction of Ultrasonics RF Echo Signals for Automated Identification of the Cardiac Walls," 2010 Tohoku-section Joint Convention record of Institutes of Electrical and Information Engineers 2F21, p. 215 (August 26-27, 2010, Hachinohe) [in Japanese].

8. H. Takahashi, H. Hasegawa, and H. Kanai, "Automatic Identification of the Heart Walls using Multiple Features of Ultrasonic Backscattering Echoes," The 66th Ultrasonics Electronics Meeting 66-2 (November 18, 2010, Sendai) [in Japanese].

9. H. Takahashi, H. Hasegawa, and H. Kanai, "Determination of Optimal Cardiac Phase for Automated Identification of the Heart Wall Region Using Multiple Features of RF Echoes," Proceeding of the 31st Symposium on Ultrasonic Electronics (USE 2010) 1Pa-53, Vol. 31, pp. 121-122 (December 6-8, 2010, Tokyo).

10. H. Takahashi, K. Nakahara, H. Hasegawa, and H. Kanai, "Heart Wall Region Automatically Identified Using Features Extracted from Ultrasonic RF signal," The 84th Scientific Meeting of the Japan Society of Ultrasonics in Medicine 84-基-031, p. S321 (May 27-29, 2011, Tokyo) [in Japanese].

11. H. Takahashi, H. Hasegawa, and H. Kanai, "Improvement of Automated Identification of the Heart wall by Reducing Stationary Clutter in Ultrasonic Echoes," Proceeding of the 33rd Symposium on Ultrasonic Electronics (USE 2012) 1J5-5, pp. 133-134 (November 13-15, 2012, Chiba).

12. H. Takahashi, H. Hasegawa, and H. Kanai, "Basic Examination of Enhancement of Echoes from Blood Particles for Noninvasive Ultrasonic Imaging of Cardiac Blood Flow," The 45th Scientific Meeting of Tohoku-section of the Japan Society of Ultrasonics in Medicine 45-6, p. 4 (March 10, 2013, Sendai) [in Japanese].

13. H. Takahashi, H. Hasegawa, and H. Kanai, "Noninvasive Measurement and Visualization of Cardiac Blood Flow Using High Frame Rate Ultrasonic Imaging," Reports of the 2013 Spring Meeting of the Acoustical Society of Japan 3-5-1, pp. 1467-1468 (March 13-15, 2013, Tokyo) [in Japanese].

14. H. Takahashi, H. Hasegawa, and H. Kanai, "High Frame Rate Imaging of Cardiac Blood Flow by Visualization of Ultrasonic Echoes," The 86th Scientific Meeting of the Japan Society of Ultrasonics in Medicine 86-奨-基 4, p. 406 (May 24-26, 2013, Osaka) [in Japanese].

15. H. Takahashi, H. Hasegawa, and H. Kanai, "Transthoracic Speckle Motion Imaging of Blood Flow in Left Ventricular Cavity with High Frame Rate Ultrasound," Proceeding of the 34th Symposium on Ultrasonic Electronics (USE 2013) 2E5-1, Vol. 34, pp. 183-184 (November 20-22, 2013, Kyoto).

16. H. Takahashi, H. Hasegawa, and H. Kanai, "Fast Ultrasonic Imaging of Echo Speckle from Blood Particle for Visualization of Cardiac Blood Flow Pattern," Proceeding of the 26th Bioengineering Conference, 2014 Annual Meeting of BED/JSME 2B-43,

p. 10 (January 11-12, 2014, Sendai) [in Japanese].

17. H. Takahashi, H. Hasegawa, and H. Kanai, "Cardiac Blood Flow Imaging with High Frame Rate Ultrasound by Improvement of Signal-to-Noise Ratios of Echoes from Blood Particles," Reports of the 2014 Spring Meeting of the Acoustical Society of Japan, p. 130 (March 10-12, 2014, Tokyo) [in Japanese].

18. H. Takahashi, H. Hasegawa, and H. Kanai, "Fast Ultrasonic Imaging of Cardiac Blood Flow by Improvement of Signal to Noise Ratios of Echoes from Blood Particles," The 87th Scientific Meeting of the Japan Society of Ultrasonics in Medicine 87-基-032, p. 479 (May 9-11, 2014, Tokyo) [in Japanese].

19. H. Takahashi, H. Hasegawa, and H. Kanai, "Speckle Imaging of Intracardiac Blood Flow with Suppression of Motion Artifact," Proceeding of the 35th Symposium on Ultrasonic Electronics (USE 2014) 3P5-12, Vol. 35, pp. 531-532 (December 3-5, 2014, Tokyo).

Bibliography

[1] A. S. Go, D. Mozaffarian, V. L. Roger, E. J. Benjamin, J. D. Berry, M. J. Blaha, S. Dai, E. S. Ford, C. S. Fox, S. Franco, H. J. Fullerton, C. Gillespie, S. M. Hailpern, J. A. Heit, V. J. Howard, M. D. Huffman, S. E. Judd, B. M. Kissela, S. J. Kittner, D. T. Lackland, J. H. Lichtman, L. D. Lisabeth, R. H. Mackey, D. J. Magid, G. M. Marcus, A. Marelli, D. B. Matchar, D. K. McGuire, E. R. Mohler III, C. S. Moy, M. E. Mussolino, R. W. Neumar, G. Nichol, D. K. Pandey, N. P. Paynter, M. J. Reeves, P. D. Sorlie, J. Stein, A. Towfighi, T. N. Turan, S. S. Virani, N. D. Wong, D. Woo, M. B. Turner, on behalf of the American Heart Association Statistics Committee and Stroke Statistics Subcommittee, "Heart Disease and Stroke Statistics—2014 Update: A Report From the American Heart Association," *Circulation*, Vol. 129, No. 3, pp. e28-e292, 2014.

[2] P. A. Heidenreich, J. G. Trogdon, O. A. Khavjou, J. Butler, K. Dracup, M. D. Ezekowitz, E. A. Finkelstein, Y. Hong, S. C. Johnston, A. Khera, D. M. Lloyd-Jones, S. A. Nelson, G. Nichol, D. Orenstein, P. W.F. Wilson and Y. J. Woo, "Forecasting the Future of Cardiovascular Disease in the United States: A Policy Statement From the American Heart Association," *Circulation*, Vol. 123, No. 8, pp. 933-944, 2011.

[3] A. M. Katz, *Physiology of the Heart: Third Edition* (Lippincott Williams & Wilkins, Philadelphia, PA, 2001) Chap. 2 and 17.

[4] P. P. Sengupta, G. Pedrizzetti, P. J. Kilner, A. Kheradvar, T. Ebbers, G. Tonti, A. G. Fraser, and J. Narula, "Emerging Trends in CV Flow Visualization," *Journal of the American College of Cardiology: Cardiovascular Imaging*, Vol. 5, No. 3, pp. 305-16, 2012.

[5] StudyBlue, Madison, WI, USA,
http://www.studyblue.com

[6] J. J. Charonko, R. Kumar, K. Stewart, W. C. Little, and P. P. Vlachos, "Vortices Formed on the Mitral Valve Tips Aid Normal Left Ventricular Filling," *Annals of Biomedical Engineering*, Vol. 41, No. 5, pp. 1049-61, 2013.

[7] W. Y. Kim, P. G. Walker, E. M. Pedersen, J. K. Poulsen, S. Oyre, K. Houlind, and A. P. Yoganathan, "Left Ventricular Blood Flow Patterns in Normal Subjects: a Quantitative Analysis by Three-Dimensional Magnetic Resonance Velocity Mapping," *Journal of the American College of Cardiology*, Vol. 26, No. 1, pp. 224—38, 1995.

[8] A. F. Bolger, E. Heiberg, M. Karlsson, L. Wigstrom, J. Engvall, A. Sigfridsson, T. Ebbers, J. P. Kvitting, C. J. Carlhall, and B. Wranne, "Transit of Blood Flow Through the Human Left Ventricle Mapped by Cardiovascular Magnetic Resonance," *Journal Cardiovascular Magnetic Resonance*, Vol. 9, No. 5, pp. 741-7, 2007.

[9] J. Eriksson, P. Dyverfeldt, J. Engvall, A. F. Bolger, T. Ebbers, and C. J. Carlhall, "Quantification of Presystolic Blood Flow Organization and Energetics in the Human Left Ventricle," *American Journal of Physiology - Heart and Circulatory Physiology*, Vol. 300, No. 6, pp. H2135-41, 2011.

[10] G. Nucifora, V. Delgado, M. Bertini, N. A. Marsan, N. R. V. de Veire, A. C.T. Ng, H. M. J. Siebelink, M. J. Schalij, E. R. Holman, P. P. Sengupta, and J. J. Bax, "Left

Ventricular Muscle and Fluid Mechanics in Acute Myocardial Infarction," *American Journal of Cardiology*, Vol. 106, No. 10, pp. 1404-9, 2010.

[11] P. R. Moran, "A Flow Velocity Zeugmatographic Interlace for NMR Imaging in Humans," *Magnetic Resonance Imaging*, Vol. 1, No. 4, pp. 197-203, 1982.

[12] D. Bryant, J. Payne, D. Firmin, and D. Longmore, "Measurement of Flow with NMR Imaging Using a Gradient Pulse and Phase Difference Technique," *Journal of Computer Assisted Tomography*, Vol. 8, No. 4, pp. 588-93, 1984.

[13] A. Harloff, J. Simon, S. Brendecke, D. Assefa, T. Helbing, A. Frydrychowicz, J. Weber, M. Olschewski, C. Strecker, J. Hennig, C. Weiller, and M. Markl, "Complex Plaques in the Proximal Descending Aorta: an Underestimated Embolic Source of Stroke," *Stroke*, Vol. 41, No. 6, pp. 1145-50, 2010.

[14] L. Wigstrom, L. Sjoqvist, and B. Wranne, "Temporally Resolved 3D Phase-Contrast Imaging," *Magnetic Resonance in Medicine*, Vol. 36, No. 5, pp. 800-3, 1996.

[15] T. Ebbers, "Flow Imaging: Cardiac Applications of 3D Cine Phase-Contrast MRI," *Current Cardiovascular Imaging Reports*, Vol. 4, No. 2, pp. 127-33, 2011.

[16] S. Napel, D. H. Lee, R. Frayne, and B. K. Rutt, "Visualizing Three-Dimensional Flow with Simulated Streamlines and Three-Dimensional Phase-Contrast MR Imaging," *Journal of Magnetic Resonance Imaging*, Vol. 2, No. 2, pp. 143-53, 1992.

[17] M. H. Buonocore, "Visualizing Blood Flow Patterns Using Streamlines, Arrows, and Particle Paths," *Magnetic Resonance in Medicine*, Vol. 40, No. 2, pp. 210-26, 1998.

[18] C. Kasai, K. Namekawa, A. Koyano, and R. Omoto, "Real-Time Two-Dimensional Blood Flow Imaging Using an Autocorrelation Technique," *IEEE Transactions on Sonics and Ultrasonics*, Vol. SU-32, No. 3, pp. 458-464, 1985.

[19] H. Torp, K. Kristoffersen, and B. A. J. Angelsen, "Autocorrelation Techniques in Color Flow Imaging: Signal Model and Statistical Properties of the Autocorrelation Estimates," *IEEE Transactions on Ultrasonics, Ferroelectrics, and Frequency Control*, Vol. 41, No. 5, pp. 604-12, 1994.

[20] H. Torp, "Clutter Rejection Filters in Color Flow Imaging: A Theoretical Approach," *IEEE Transactions on Ultrasonics, Ferroelectrics, and Frequency Control*, Vol. 44, No. 2, pp. 417-24, 1997.

[21] T. D. Fredriksen, I. K. Ekroll, L. Løvstakken, and H. Torp, "2-D Tracking Doppler: A New Method to Limit Spectral Broadening in Pulsed Wave Doppler," *IEEE Transactions on Ultrasonics, Ferroelectrics and Frequency Control*, Vol. 60, No. 9, pp. 1896-905, 2013.

[22] D. H. Evans, W. N. McDicken, R. Skidmore, and J. P. Woodcock, *Doppler Ultrasound, Physics, Instrumentation, and Clinical Applications* (John Wiley & Sons, New-York, NY, 1989).

[23] J. A. Jensen, *Estimation of Blood Velocities Using Ultrasound: A Signal Processing Approach* (Cambridge University Press, New-York, NY, 1996).

[24] D. H. Evans and W. N. McDicken, *Doppler Ultrasound, Physics, Instrumentation, and Signal Processing* (John Wiley & Sons, New-York, NY, 2000).

[25] J. A. Jensen, S. I. Nikolov, J. Udesen, P. Munk, K. L. Hansen, M. M. Pedersen, P. M. Hansen, M. B. Nielsen, N. Oddershede, J. Kortbek, M. J. Pihl, and L. Ye, "Recent Advances in Blood Flow Vector Velocity Imaging," *2010 IEEE International Ultrasonics Symposium Proceedings*, pp. 261-271, 2010.

[26] M. D. Fox, "Multiple Crossed-Beam Ultrasound Doppler Velocimetry," *IEEE Transactions on Sonics Ultrasonics*, Vol. 25, No. 5, pp. 281-286, 1978.

[27] L. Capineri, M. Scabia, and L. Marco, "Doppler System for Dynamic Vector Velocity Maps," *Ultrasound in Medicine and Biology*, Vol. 28, No. 28, pp. 237-48, 2002.

[28] P. Tortoli, G. Guidi, and P. Pignoli, "Transverse Doppler Spectral Analysis for a Correct Interpretation of Flow Sonograms," *Ultrasound in Medicine and Biology*, Vol. 28, No. 2, pp. 115-121, 1993,

[29] P. Tortoli, A. Dallai, E. Boni, L. Francalanci, and S. Ricci, "An Automatic Angle Tracking Procedure for Feasible Vector Doppler Blood Velocity Measurements," *Ultrasound in Medicine and Biology*, Vol. 28, No. 3, pp. 488-496, 2010.

[30] I. K. Ekroll, A. Swillens, P. Segars, T. Dahl, H. Torp, and L. Løvstakken, "Simultaneous Quantification of Flow and Tissue Velocities Based on Multi-Angle Plane Wave Imaging," *IEEE Transactions on Ultrasonics, Ferroelectrics, and Frequency Control*, Vol. 60, No. 4, pp. 727-38, 2013.

[31] S. Ricci, L. Bassi, and P. Tortoli, "Real Time Vector Velocity Assessment Through Multigate Doppler and Plane Waves," *IEEE Transactions on Ultrasonics, Ferroelectrics, and Frequency Control*, Vol. 61, No. 2, pp. 314-324, 2014.

[32] A. Swillens, P. Segers, and L. Løvstakken, "A Combined Speckle Tracking and Phase-shift Estimation Approach for 2D Blood Flow Imaging in the Carotid Bifurcation, *2010 IEEE International Ultrasonics Symposium Proceedings*, pp. 1072-75, 2010.

[33] H. Hasegawa and H. Kanai, "Displacement Estimation of Arterial Wall from Multiple Directions by Utilizing Diverging Transmit Beam for Synthetic Aperture Ultrasound Imaging," *2013 Joint UFFC, EFTF, and PFM Symposium*, pp. 1537-40, 2013.

[34] B. Y. S. Yiu, S. S. M. Lai, and A. C. H. Yu, "Vector Projectile Imaging: Time-Resolved Dynamic Visualization of Complex Flow Patterns," *Ultrasound in Medicine and Biology*, Vol. 40, No. 9, pp. 2295-309, 2014.

[35] S. Ohtsuki and M. Tanaka, "The Flow Velocity Distribution from the Doppler Information on a Plane in Three-Dimensional Flow," *Journal of Visualization*, Vol. 9, No. 1, pp. 69-82, 2006.

[36] D. Garcia, J. C. D. Álamo, D. Tanne, R. Yotti, C. Cortina, E. Bertrand, J. C. Antoranz, E. P. David, R. Rieu, F. F. Avilés, and J. Bermejo, "Two-Dimensional Intraventricular Flow Mapping by Digital Processing Conventional Color-Doppler Echocardiography Images," *IEEE Transactions on Medical Imaging*, Vol. 29, No. 10, pp. 1701-12, 2010.

[37] F. Mehregan, F. Tournoux, S. Muth, P. Pibarot, R. Rieu, G. Cloutier, and D. Garcia, "Doppler Vortography: A Color Doppler Approach to Quantification of Intraventricular Blood Flow Vortices," *Ultrasound in Medicine and Biology*, Vol. 40, No. 1, pp. 210—21, 2014.

[38] G. E. Trahey, J. W. Allison, and O. T. Von Ramm, "Angle Independent Ultrasonic Detection of Blood Flow," *IEEE Transactions on Bio-medical Engineering*, Vol. BME-34, No. 12, pp. 965—967, 1987.

[39] L. N. Bohs, B. J. Geiman, M. E. Anderson, S. C. Gebhart, and G. E. Trahey, "Speckle Tracking for Multi-Dimensional Flow Estimation," *Ultrasonics*, Vol. 38, No. 1-8, pp. 369-75, 2000.

[40] J. D'hooge, E. Konofagou, F. Jamal, A. Heimdal, L. Barrios, B. Bijnens, J. Thoen, F. van de Werf, G. R. Sutherland, and P. Suetens, "Two-Dimensional Ultrasonic Strain

Rate Measurement of the Human Heart *in vivo*," *IEEE Transactions on Ultrasonics, Ferroelectrics, and Frequency Control*, Vol. 49, No. 2, pp. 281-286, 2002.

[41] E. Konofagou, W. N. Lee, J. Luo, J. Provost, and J. Vappou, "Physiologic Cardiovascular Strain and Intrinsic Wave Imaging," *Annual Review of Biomedical Engineering*, Vol. 13, pp. 477-505, 2011.

[42] R. L. Maurice, J. Ohayon, Y. Frtigny, M. Bertrand, G. Soulez, and G. Cloutier, "Noninvasive Vascular Elastography: Theoretical framework," *IEEE Transactions on Medical Imaging*, Vol. 23, No. 2, pp. 164-80, 2004.

[43] H. Ribbers, S. Holewijn, J. D. Blankenstejin, and C. L. de Korte, "Non-Invasive Two Dimensional Elastography of the Carotid Artery," *2005 IEEE International Ultrasonics Symposium Proceedings*, pp. 1113-6, 2005.

[44] M. Cinthio, A. R. Ahlgren, T. Jansson, A. Eriksson, H. W. Persson, and K. Lindström, "Evaluation of an Ultrasonic Echo-tracking Method for Measurements of Arterial Wall Movements in Two Dimensions," *IEEE Transactions on Ultrasonics, Ferroelectrics, and Frequency Control*, Vol. 52, No. 8, pp. 1300-11, 2005.

[45] L. Løvstakken, S. Bjærum, D. Martens, and H. Torp, "Blood Flow Imaging-A New Real-Time, 2-D Flow Imaging Technique," *IEEE Transactions on Ultrasonics, Ferroelectrics, and Frequency Control*, Vol. 53, No. 2, pp. 289-299, 2006.

[46] R. Chiao, L. Mo, A. Hall, S. Miller, and K. Thomenius, "B-mode blood flow (B-flow) imaging," *2010 IEEE International Ultrasonics Symposium Proceedings*, pp. 1469—72, 2000.

[47] D. P. Shattuck, M. D. Weinshenker, and S. W. Smith, and O. T. von Ramm, "Explososcan: A Parallel Processing Technique for High Speed Ultrasound Imaging with

Linear Phased Arrays," *Journal of the Acoustical Society of America*, Vol. 75, No. 4, pp. 1273-82, 1984.

[48] M. Tanter, J. Bercoff, L. Sandrin, and M. Fink, "Ultrafast Compound Imaging for 2-D Motion Vector Estimation: Application to Transient Elastography," *IEEE Transactions on Ultrasonics, Ferroelectrics and Frequency Control*, Vol. 49, No. 10, pp. 1363-1374, 2002.

[49] S. Sasaki, R. Takagi, K. Matsuura, S. Yoshizawa, and S. Umemura, "Monitoring of High-Intensity Focused Ultrasound Lesion Formation Using Decorrelation between High-Speed Ultrasonic Images by Parallel Beamforming," *Japanese Journal of Applied Physics*, Vol. 53, No. 7, pp. 07KF10-1-07KF10-6, 2014.

[50] J. Udesen, F. Gran, K. L. Hansen, J. A. Jensen, C. Thomsen, and M. B. Nielsen, "High Frame-Rate Blood Vector Velocity Imaging Using Plane Waves: Simulations and Preliminary Experiments," *IEEE Transactions on Ultrasonics, Ferroelectrics, and Frequency Control*, Vol. 55, No. 8, pp. 1729-43, 2008.

[51] K. L. Hansen, J. Udesen, F. Gran, J. A. Jensen, and M. B. Nielsen, "In-Vivo Examples of Complex Flow Patterns with a Fast Vector Velocity Method," *Ultrasound in Medicine and Biology*, Vol. 30, No. 5, pp. 471—476, 2009.

[52] H. Hasegawa and H. Kanai, "Simultaneous Imaging of Artery-Wall Strain and Blood Flow by High Frame Rate Acquisition of RF Signals," *IEEE Transactions on Ultrasonics, Ferroelectrics, and Frequency Control*, Vol. 55, No. 12, pp. 2626-39, 2008.

[53] H. Hasegawa and H. Kanai, "Blood Flow Stream Line Imaging by Direct Visualization of Echo Trajectories," *2010 IEEE International Ultrasonics Symposium Proceedings*, pp. 1319-1322, 2010.

[54] M. Lenge, A. Ramalli, E. Boni, H. Liebgott, C. Cachard, and P. Tortoli, "High-Frame-Rate 2-D Vector Blood Flow Imaging in the Frequency Domain," *IEEE Transactions on Ultrasonics, Ferroelectrics, and Frequency Control*, Vol. 61, No. 9, pp. 1504-14, 2014.

[55] B. F. Osmanski, M. Pernot, G. Montaldo, A. Bel, E. Messas, and M. Tanter, "Ultrafast Doppler Imaging of Blood Flow Dynamics in the Myocardium," *IEEE Transactions on Medical Imaging*, Vol. 31, No. 8, pp. 1661-8, 2012.

[56] G. R. Hong, G. Pedrizzentti, G. Tonti, P. Li, Z. Wei, J. K. Kim, A. Baweja, S. Liu, N. Chung, H. Houle, J. Narula, and M. A. Vannan, "Characterization and Quantification of Vortex Flow in the Human Left Ventricle by Contrast Echocardiography Using Vector Particle Image Velocimetry," *Journal of the American College of Cardiology: Cardiovascular Imaging*, Vol. 1, No. 6, pp. 705-17, 2008.

[57] R. Faludi, M. Szulik, J. D'hooge, P. Herijgers, F. Rademakers, G. Pedrizzetti, and J. U. Voigt, "Left Ventricular Flow Patterns in Healthy Subjects and Patients with Prosthetic Mitral Valves: An In Vivo Study Using Echocardiographic Particle Image Velocimetry," *Journal of Thoracic and Cardiovascular Surgery*, Vol. 139, No. 6, pp. 1501-1510, 2010.

[58] A. Kheradvar, H. Houle, G. Pedrizzetti, G. Tonti, T. Belcik, M. Ashraf, J. R. Lindner, M. Gharib, and D. Sahn, "Echocardiographic Particle Image Velocimetry: A Novel Technique for Quantification of Left Ventricular Blood Vorticity Pattern," *Journal of the American Society of Echocardiography*, Vol. 23, No. 1, pp. 86-94, 2010.

[59] C. Prinz, R. Faludi, A. Walker, M. Amzulescu, H. Gao, T. Uejima, A. G. Fraser, and J. U. Voigt, "Can Echocardiographic Particle Image Velocimetry Correctly Detect

Motion Patterns as They Occur in Blood inside Heart Chambers? A Validation Study Using Moving Phantoms," *Cardiovascular Ultrasound*, Vol. 10, No. 24, pp. 24-33, 2012.

[60] H. Hasegawa and H. Kanai, "High-frame-rate Echocardiography Using Diverging Transmit Beams and Parallel Receive Beamforming," *Journal of Medical Ultrasonics*, Vol. 38, No. 3, pp. 129-40, 2011.

[61] H. Hasegawa and H. Kanai, "High Frame Rate Echocardiography With Reduced Sidelobe Level," *IEEE Transactions on Ultrasonics, Ferroelectrics, and Frequency Control*, Vol. 59, No. 11, pp. 2569-75, 2012.

[62] H. Hasegawa and H. Kanai, "Comparison of Spatial Resolutions of Parallel Beamforming and Diffraction Tomography in High Frame Rate Echocardiography," *Japanese Journal of Applied Physics*, Vol. 53, No. 7, pp. 07KF02-1-07KF02-3, 2014.

[63] H. Takahashi, H. Hasegawa, and H. Kanai, "Echo Speckle Imaging of Blood Particles with High-Frame-Rate Echocardiography," *Japanese Journal of Applied Physics*, Vol. 53, No. 7, pp. 07KF08-1-07KF08-7, 2014.

[64] H. Takahashi, H. Hasegawa, and H. Kanai, "Intraventricular Blood Flow Vector and Streamline Imaging Using High Frame Rate Cardiac Ultrasound," *2014 IEEE International Ultrasonics Symposium Proceedings*, pp. 341-44, 2014.

[65] H. Hasegawa and H. Kanai, "Effect of Subaperture Beamforming on Phase Coherence Imaging," *IEEE Transactions on Ultrasonics, Ferroelectrics, and Frequency Control*, Vol. 61, No. 11, pp. 1779-90, 2014.

[66] G. Montaldo, M. Tanter, J. Bercoff, N. Benech, and M. Fink, "Coherent Plane Wave Compounding for Very High Frame Rate Ultrasonography and Transient Elastog-

raphy," *IEEE Transactions on Ultrasonics, Ferroelectrics, and Frequency Control*, Vol. 56, No. 3, pp. 489—506, 2009.

[67] D. Ensminger and L. J. Bond, *Ultrasonics: Fundamentals, Technologies, and Applications, Third Edition* (CRC Press, Boca Raton, FL, 2011).

[68] A. Koriyama, W. Yasuhara, and H. Hachiya, "Experimental Evaluation of Quantitative Diagnosis Technique for Hepatic Fibrosis Using Ultrasonic Phantom," *Japanese Journal of Applied Physics*, Vol. 51, No. 7S, pp. 07GF09, 2012.

[69] T. Higuchi, S. Hirata, T. Yamaguchi, and H. Hachiya, "Quantitative Evaluation of Liver Fibrosis Using Multi-Rayleigh Model with Hypoechoic Component," *Japanese Journal of Applied Physics*, Vol. 52, No. 7S, pp. 07HF19, 2013.

[70] J. Ophir, I. Cespedes, H. Ponnekanti, Y. Yazdi, and X. Li, "Elastography: A Quantitative Method for Imaging the Elasticity of Biological Tissues," *Ultrasonic Imaging*, Vol. 13, No. 2, pp. 111-134, 1991.

[71] K. R. Nightingale, P. J. Kornguth, and G. E. Trahey, "The Use of Acoustic Streaming in Breast Lesion Diagnosis: a Clinical Study," *Ultrasound in Medicine and Biology*, Vol. 25, No. 1, pp. 75—87, 1999.

[72] A. Tanaka and Y. Saijo, "Blood Flow Visualization of Left Atrial Spontaneous Echo Contrast (SEC) Using Gradient Based Optical Flow Estimation," *The 29th Annual International Conference of the IEEE EMBS Proceeding*, pp. 4500-3, 2007.

[73] J. A. Jensen and S. I. Nikolov, "Directional Synthetic Aperture Flow Imaging," *IEEE Transactions on Ultrasonics, Ferroelectrics, and Frequency Control*, Vol. 51, No. 9, pp. 1107-1118, 2004.

[74] M. Karaman, P. C. Li, and M. O'Donnell, "Synthetic Aperture Imaging for Small Scale Systems," *IEEE Transactions on Ultrasonics, Ferroelectrics, and Frequency Control*, Vol. 42, No. 3, pp. 429-442, 1995.

[75] T. L. Szabo, *Diagnostic Ultrasound Imaging: Inside Out* (Academic Press, Waltham, MA, 2004) Chap. 8.2.

[76] C. M. Bishop, *Pattern Recognition and Machine Learning* (Springer, Berlin, 2006) Chap. 9.1.

[77] I. Cespedes, Y. Huang, J. Ophir, and S. Sprat, "Methods for Estimation of Subsample Time Delays of Digitized Echo Signals," *Ultrasonic Imaging*, Vol. 17, No. 2, pp. 142-71, 1995.

[78] H. Takahashi, H. Hasegawa, and H. Kanai, "Improvement of Automated Identification of the Heart Wall in Echocardiography by Suppressing Clutter Component," *Japanese Journal of Applied Physics*, Vol. 52, No. 7, pp. 07HF017-1-07HF017-7, 2013.

[79] K. Nakahara, H. Hasegawa, and H. Kanai, "Optimization of Feature Extraction for Automated Identification of Heart Wall Regions in Different Cross Sections," *Japanese Journal of Applied Physics*, Vol. 53, No. 7, pp. 07KF09-1-07KF09-9, 2014.

[80] W. H. Press, S. A. Teukolsky, W. T. Vetterling, and B. P. Flannery, *Numerical Recipes 3rd Edition: The Art of Scientific Computing* (Cambridge University Press, NY, 2007).